Nickel isotope fractionation during adsorption on the calcite surface and coprecipitation with calcite.

Maria Cristina Castillo Alvarez

Université Fédérale
Toulouse Midi-Pyrénées

THÈSE

En vue de l'obtention du

DOCTORAT DE L'UNIVERSITÉ DE TOULOUSE

Délivré par l'Université Toulouse 3 - Paul Sabatier

Présentée et soutenue par

Maria Cristina CASTILLO ALVAREZ

Le 31 janvier 2019

Fractionnement des isotopes de nickel lors de l'adsorption à la surface de la calcite et coprécipitation avec la calcite

Ecole doctorale : **SDU2E - Sciences de l'Univers, de l'Environnement et de l'Espace**

Spécialité : **Sciences de la Terre et des Planètes Solides**

Unité de recherche :
GET - Geosciences Environnement Toulouse

Thèse dirigée par
Eric OELKERS, Ghylaine QUITTE-LEVASSEUR et Jacques SCHOTT

Jury
Mme Rachel James, Rapporteur
M. Olivier Rouxel, Rapporteur
M. Marc Benedetti, Rapporteur
M. François Chabaux, Examinateur
M. Eric Oelkers, Directeur de thèse
Mme Ghylaine Quitte, Co-directeur de thèse
M. Jacques Schott, Co-directeur de thèse

Nickel isotope fractionation during adsorption on the calcite surface and coprecipitation with calcite

Abstract

The chemical and isotopic compositions of trace elements in calcite are the basis for most past temperature, atmospheric CO_2, and ocean pH paleo reconstructions. The isotope compositions of divalent metals incorporated into the calcite structure also have the ability to record valuable information that reflects the geochemical conditions of formation (Galy et al., 2002; Chang et al., 2004; Beard et al., 2012; Mavromatis et al., 2013; Fantle and Tipper, 2014; Mavromatis et al., 2015; Mavromatis et al., 2019). Moreover, as the equilibrium and kinetic partition of divalent metals between calcite and fluid exhibit contrasting behaviors, it can be expected that their isotope composition in calcite exhibits distinct trends (Schott et al., 2014).

Because Ni aqueous speciation strongly depends on fluid pH and alkalinity, the isotopic composition of Ni adsorbed on calcite surface and/or incorporated into the calcite lattice could provide information on the chemical environment in which this mineral originally formed. To calibrate this potentially useful tool, experiments were performed at 25°C to determine Ni isotope fractionation during 1) Ni adsorption on calcite surface as a function of solution pH (from 7.5 to 8.7) and 2) Ni coprecipitation with calcite at pH = 6.2, pCO_2 = 1 atm as a function of calcite growth rates (ranging from $10^{-8.2}$ to $10^{-7.3}$ mol m^{-2} s^{-1}).

Results show that the equilibrium fractionation factor, $\Delta^{60}Ni_{solid\text{-}solution}$, for Ni adsorption on calcite is equal to -0.49 ± 0.16‰ and is pH – independent. Light Ni isotopes are also preferentially incorporated in calcite during its coprecipitation. The extent of Ni isotope fractionation decreases from -0.3 to -1 ‰ as the calcite precipitation rate increases from $10^{-8.2}$ to $10^{-7.3}$ ·mol m^{-2} s^{-1}. This behavior, due to the strong hydration of the Ni^{2+} aqua ion, may serve to approximate calcite precipitation rates and pCO_2 in past oceans.

Résumé

Les compositions chimiques et isotopiques traces des métaux de traces dans la calcite sont à la base de la plupart des reconstructions de températures passées, de CO_2 atmosphérique et de pH océanique. Les compositions isotopiques des métaux divalents incorporées dans la structure de calcite ont également la capacité d'enregistrer des informations précieuses reflétant les conditions géochimiques de la formation. (Galy et al., 2002; Chang et al., 2004; Beard et al., 2012; Mavromatis et al., 2013; Fantle and Tipper, 2014; Mavromatis et al., 2015; Mavromatis et al., 2019). De plus, comme la répartition à l'équilibre et la cinétique des métaux divalents entre la calcite et le fluide présentent des comportements contrastés, on peut s'attendre à ce que leur composition isotopique dans la calcite présente des tendances distinctes (Schott et al., 2014).

Comme la spéciation aqueuse de Ni dépend fortement du pH et de l'alcalinité, la composition isotopique de Ni adsorbée à la surface de la calcite et / ou incorporée dans le réseau de calcite pourrait fournir des informations précieuses sur l'environnement chimique dans lequel ce minéral s'est formé à l'origine. Pour calibrer cet outil potentiellement utile, des expériences ont été effectuées à 25 ° C pour déterminer le fractionnement isotopique du Ni pendant 1) l'adsorption de Ni à la surface de la calcite en fonction du pH de la solution (de 7,5 à 8,7) et 2) la coprécipitation de Ni avec de la calcite à pH 6,2, pCO_2 = 1 atm en fonction de taux de croissance de la calcite allant de $10^{-8,2}$ à $10^{-7,3}$ mol m^{-2} s^{-1}.

Les résultats montrent que le facteur de fractionnement à l'équilibre, solution $\Delta^{60}Ni_{solid\text{-}solution}$, pour l'adsorption de Ni sur la calcite est égal à -0,49 ± 0,16 et indépendant du pH. Les isotopes de Ni léger sont également incorporés de manière préférentielle dans la calcite pendant sa coprécipitation. L'ampleur du fractionnement isotopique du Ni diminue de -0.3 and -1 lorsque le taux de précipitation de la calcite augmente de $10^{-8,2}$ à $10^{-7,3}$ mol m^{-2} s^{-1}. Ce comportement, dû à la forte hydratation de l'ion aqueux Ni^{2+}, peut servir à estimer les taux de précipitation de la calcite et la pCO_2 dans les océans du passé.

Preface

This PhD study has been carried out at the Geosciences Environnement Toulouse (GET) laboratory at the Centre National de la Recherche Scientifique (CNRS) in Toulouse, France. This thesis consists of two chapters that are versions of manuscripts that have been prepared for submission to peer-reviewed academic journals (chapters 3 and 4), as well as a general introduction to the topic (chapter 1) a methodology section (chapter 2) and general conclusions of this work (chapter 5).

- Chapter 1 is a general introduction to the thesis that presents an overview of calcite precipitation kinetics, the interaction of calcite with divalent metals, particularly Ni, and how isotope fractionation is driven by mineral growth and metal incorporation. This chapter also includes a summary of the experimental studies comprised in this thesis.
- Chapter 2 presents a detailed description of the experiments and analytical techniques used during this thesis. This chapter details the steps undertaken to optimize previously published experimental protocols for isotope analysis. Notably, this chapter recounts the determination of the best choice of materials, reagents and initial conditions, as identified through preliminary tests and thermodynamic models. All the details of the experimental design are explained as well as the sample treatment prior to measurements and the principle of analytical techniques used for chemical and isotopic analysis used during this work.
- Chapter 3 presents the results of a study of Ni isotope fractionation during its adsorption onto the calcite surface. In this chapter, the experiments of adsorption as a function of time and pH and the Ni isotope fractionation occurring during them are explained in detail. The main results of this chapter were submitted to *Geochimica et Cosmochimica Acta* on the 24th September 2018 as a manuscript titled "Experimental determination of Ni isotope fractionation during Ni adsorption from an aqueous fluid onto calcite surfaces" that is found as annex 1 of this thesis. It is authored by Cristina Castillo Alvarez, Ghylaine Quitté, Jacques Schott and Eric H. Oelkers. The experimental and analytical work was performed

by myself, with suggestions of Jacques Schott. Measurements on the Neptune MC-ICP-MS were carried out in collaboration with Ghylaine Quitté. Data evaluation and interpretation was performed by myself, with aid from Jacques Schott and Eric H. Oelkers. The manuscript was written by myself and the co-authors.

- Chapter 4 presents the results of a study of Ni isotope fractionation during its coprecipitation with calcite as a function of precipitation rate. The experiments were designed and performed by myself with suggestions from Jacques Schott and Martin Voigt. Analytical work was performed by myself. Measurements on the Neptune MC-ICP-MS were carried out in collaboration with Ghylaine Quitté. Data evaluation and interpretation was performed by myself, with aid from Jacques Schott and Eric H. Oelkers.
- Chapter 5 includes a summary of this thesis, the general conclusions, and potential directions that this research can take in the future.

Table of contents

List of figures

List of tables

Nomenclature

Abbreviations

AAS	Atomic Absorption Spectrometry
CPES	Calcite pre equilibrated solutions
IEC	Ion Exchange Chromatography
ICP-OES	Inductively Coupled Plasma Optic Emission Spectrometry
KIE	Kinetic Isotope Effect
MC-ICPMS	Multi Collector- Inductively Coupled Plasma Mass Spectrometry
LOD	Limit of Detection
Me^{2+}	Divalent metals
PE	Polyethylene
PP	Polypropylene
PTFE	Polytetrafluoroethylene
PZC	Point of zero charge
XRD	X-Ray Diffraction
SCM	Surface complexation Modelling
SD	Standard Deviation
SEM	Scanning Electron Microscopy
SE	Standard Error
SI	Saturation Index
SS	Steady State

Symbols

α	Activity coefficient
Å	Armstrong
δ	delta
Δ	fractionation factor
Ω	saturation state
I	Ionic strength
K_{SP}	Solubility product
D	Partition coefficient
S	Specific surface area
T	Temperature
t	Time
K_{wex}	water exchange rate
K_{ex}	exchange rate
R_p	Precipitation rate
X_i	Mole fraction of species i
k_d	partition coefficient

Chapter 1. Introduction

1.1 Carbonates and their role in regulating ocean pH.

1.1.1 CO_2 and the carbonic acid system in the ocean

Currently, a prevalent environmental issue is the increase in atmospheric carbon dioxide (CO_2) due to the burning of fossil fuels. Throughout geologic time atmospheric CO_2 concentrations have fluctuated significantly; however, these concentrations have recently gained significant attention due to the sharp increase in CO_2 release since the dawn of the industrial revolution in 1800. Since then, more than 500pg of anthropogenic carbon have been released into the atmosphere. Oceans have taken up about 48% of these emissions (Sabine et al., 2004; Mackenzie and Lerman, 2006) resulting in a shift in average pH of surface seawater from 8.2 to just under 8.1. This shift affects the carbonic acid system in seawater and ultimately affects marine carbonates. Thus, carbonate-water interactions are an essential component of climate regulation and the fate of fossil fuel derived CO_2.

Oceans can absorb CO_2 due to the fast exchange rate at the gas-liquid interface thereby influencing atmospheric CO_2 content and in turn Earth's climate (Broecker, 2012). As atmospheric CO_2 concentration increases so does the amount of dissolved CO_2 in seawater. This is observable in data from the atmospheric observation station in Mauna Loa, Hawaii, where a correlation exists between atmospheric CO_2 concentration and seawater pH (Fig. 1). Increasing dissolved CO_2 in the ocean changes the ratio of CO_2 dissociated products and results in the formation of carbonic acid (H_2CO_3); carbonic acid generation results in increased bicarbonate (HCO_3^-) and H^+ ion concentrations and decreased carbonate (CO_3^{2-}) ion concentrations. This decrease in CO_3^{2-} ion concentrations changes its saturation state with respect to calcium carbonate ($CaCO_3$) and subsequently the precipitation rate of marine carbonates.

It is essential to understand the thermodynamic and kinetic factors controlling carbonate-water interactions in order to better understand their role in climate regulation. These factors play a major role in regulating the chemical composition of oceans (Van Cappellen et al., 1993) and are crucial in modeling geochemical processes that can be used to predict future environmental conditions (Morse and Mackenzie, 1990; Morse et al., 2007). However, a major problem in calibrating climate models is the need for information on past climate conditions. These data can be obtained through proxy reconstructions. Proxies provide a better understanding of past climates

and allow model sensitivity to be tested, thereby improving our ability to predict future climate change.

In proxy reconstructions, past climatic conditions that cannot be directly measured are correlated with another variable (Clarke and Wheeler, 1922). For example, correlations between seawater and atmospheric CO_2 concentrations (as in Fig. 1) can be extended into the past through combination with data obtained from air bubbles trapped in ice cores. Since atmospheric CO_2 is related to oceanic pH past values for atmospheric CO_2 can be inferred by using oceanic pH as a proxy.

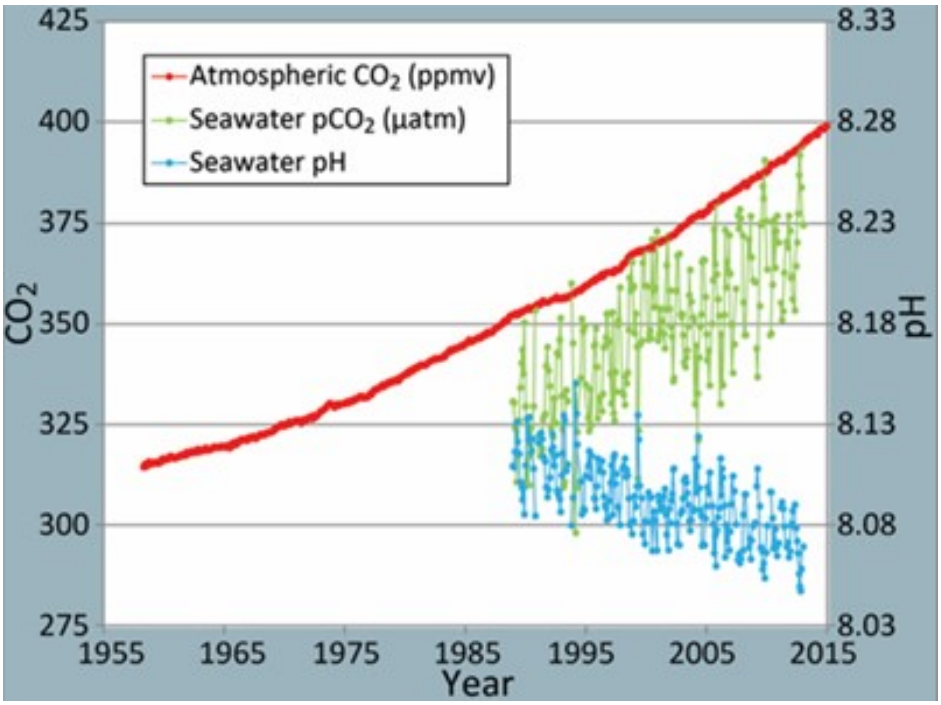

Figure 1. correlation between atmospheric CO_2, oceanic pH, and oceanic pCO_2 from NOAA: Modified after R. A. Feely, Bulletin of the American Meteorological Society, July 2008. Source: NOAA PMEL graphic. Data: Mauna Loa Observatory and Station Aloha.

1.1.2 Determination of seawater conditions in the past through proxies

Carbonate sediments precipitated in the ocean preserve a number of elemental and isotopic proxies that are used to determine past oceanic temperatures and seawater conditions (Lea, 2013). The most studied paleo oceanographic conditions for which proxies are used are temperature,

salinity, primary productivity, nutrient content, and surface-water carbon dioxide concentrations; all are examined through the use of elemental and isotope ratios (Goldstein and Hemming, 2013).

The most used elemental proxies include Sr/Ca and Mg/Ca ratios of biologically precipitated carbonates for temperature (Marshall and McCulloch, 2002; Cléroux et al., 2008; Flannery and Poore, 2013), Cd/Ca ratios for nutrient utilization (Bryan and Marchitto, 2010), Ba/Ca ratios for alkalinity (Lea and Boyle, 1990), and Zn/Cd ratios in foraminifera shells for carbonate ion concentration (Marchitto, 2011). For isotopic ratios, the most commonly used include the stable carbon isotope composition of bulk organic matter or individual marine organic components as a proxy for past surface-water CO_2 conditions (Tipple et al., 2010), the amount of $\delta^{18}O$ in foraminifera and corals to assess temperature fluctuations (Grossman and Ku, 1986), and B isotope ratios ($\delta^{11}B$) to determine changes in oceanic pH and alkalinity (Sanyal et al., 1996). There are inherent issues with using these proxies to reconstruct paleo oceanographic conditions, these include poor resolution of proxy data as well as uncertainties related to the proxy itself. Therefore, efforts are focused towards the development of new and more robust paleo-proxy tools, such as the trace metal incorporation in marine sediments.

1.2 Calcite growth from solution

1.2.1 Calcite

Carbonates are sedimentary rocks found in essentially all marine systems and are characterized by the presence of the carbonate ion (CO_3^{2-}) in their structure. Calcium carbonate ($CaCO_3$) is the most abundant carbonate and it possesses 2 main polymorphs: calcite and aragonite. These polymorphs differ mainly in their systematic crystalline structure; calcite is rhombohedral and aragonite is orthorhombic. Calcite and aragonite solubility product (K_{sp}) are also different from one another. K_{sp} is a thermodynamic constant that determines if a mineral and the coexisting aqueous solution are at chemical equilibrium. In the case of $CaCO_3$, the solubility product can be described by the equation

$$k_{sp} = \alpha(Ca^{2+})_{eq} * \alpha(CO_3^{2-})_{eq} \quad (1)$$

where *a(i)* represents the activity of the *ith* aqueous species.

At 25 ºC and standard atmospheric pressure, K_{sp} of calcite and aragonite were experimentally determined to be $10^{-8.48}$ and $10^{-8.34}$, respectively (Plummer and Busenberg, 1982). Calcite's lower K_{sp} value means it is more stable than aragonite (Mucci, 1983; Morse and Mackenzie, 1990). It also means that in oceans, the zone where aragonite can be found will be closer to the surface and more susceptible to changes in seawater chemistry. Because the product $a(Ca^{2+}) * a(CO_3^{2-})$ decreases with increasing oceanic depth, almost all deep sea carbon rich sediments are depleted in aragonite (Morse and Mackenzie, 1990).

1.2.2 Thermodynamic principles of mineral formation

Crystallization from solution is a fundamental process for mineral formation. According to classic crystallization theory, the process begins with a spontaneous clustering of ions or molecules leading to nucleation once a free energy barrier has been overcome for a critical cluster size. These clusters then grow by incorporation of ions/molecules resulting in the formation of crystals and minimization of system free energy (Meldrum and Cölfen, 2008; De Yoreo et al., 2015).

$CaCO_3$ precipitation from aqueous solution is dominated by the reaction $Ca^{2+} + CO_3^{2-} \rightleftharpoons CaCO3$, which is the result of simultaneous precipitation (forward) and dissolution (backwards) reactions of the mineral occurring at the solid-water interface (Plummer and Busenberg, 1982; Chou et al., 1989; Wollast, 1990). At equilibrium these rates are identical and one can write:

$$\frac{a(Ca^{2+}) * a(CO_3^{2-})}{k_{sp}} = \Omega = 1 \qquad (2)$$

where *a(i)* represents the activity of the *ith* aqueous species, and Ω stands for the solution saturation state with respect to the considered solid phase.

Ω <1 means that a solution is undersaturated and dissolution will tend to take place; alternatively, Ω >1 means a solution is oversaturated and the mineral may precipitate. In order for nucleation to take place, the saturation state commonly needs to be significantly higher than 1.

The attachment of ions to a mineral surface from an aqueous solution happens in steps. As oversaturation increases the spacing of the steps decreases and the step velocities increase causing a more rapid growth rate. The velocity and spacing of these steps and density of kink sites on the crystal surface determine the mineral growth rate (De Yoreo and Vekilov, 2003; Joswiak et al., 2018). The rate at which minerals grow can be described in terms of Ω by the equation:

$$R = k * (\Omega - 1)^n \quad (3)$$

where R is the precipitation rate (normalized to the reacting surface area) k is the rate constant, and n is the order of the overall reaction obtained from fitting the experimental data to the equation.

1.2.3 Reactions at the calcite surface

Three steps are required for crystal growth from solution: 1) diffusion of ions to the mineral-fluid interface, 2) adsorption on the surface of the mineral, and 3) incorporation into the bulk structure. The exchange of ions between mineral and fluid occurs at the mineral-fluid interface which occupies the outermost few monolayers of a surface. Composition of this interface can be different from that of the bulk lattice as has been shown by high-resolution X-ray reflectivity measurements (P. Fenter et al., 2000; P Fenter et al., 2000; Schlegel et al., 2002).

The speciation and charge at the mineral surface can be described using surface complexation models (SCM) that use thermodynamics to describe the formation of hydrolyzed species on the calcite surface (fig.2, Van Cappellen et al. 1993; Pokrovsky et al. 2000). Formation of surface species depends on aqueous solution pH. There is a point at which the total net charge at the calcite surface is 0, (usually around 8.3) termed the point of zero charge (PZC). In more acidic solutions the surface is positively charged and dominated by protonated surface species; contrastingly, in alkaline solutions, it is dominated by negatively charged surface species (Hohl et al., 1980; Davis and Kent, 1990; Pokrovsky and Schott, 2002).

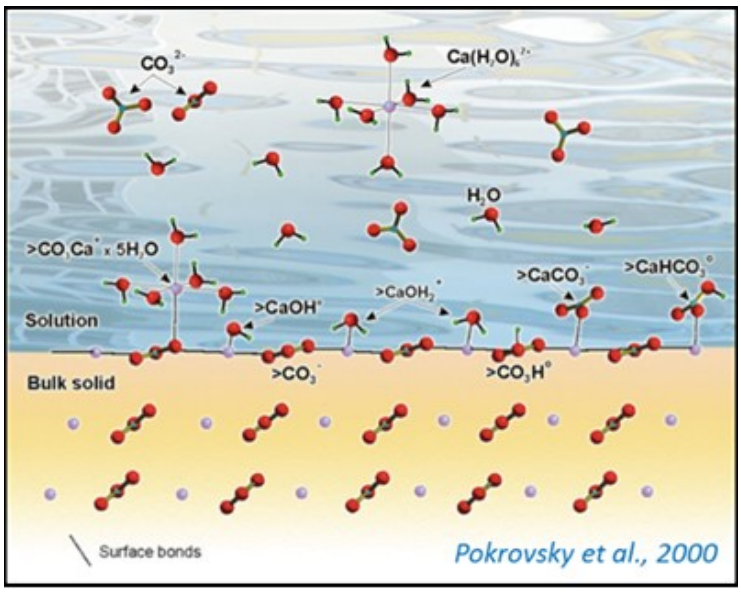

Figure 2. Speciation at the calcite-fluid interface. Figure taken from Pokrovsky et al.(2000).

Surface complexation models (SCM) developed by Van Cappellen et al. (1993), Pokrovsky et al., (2000), and Pokrovsky and Schott (2002) assume there are two primary hydration sites on the calcite surface: $>CaOH^0$ and $>CO_3H^0$ (where > represents a surface species). Each of these primary hydration sites has 1:1 stoichiometry. These sites are assigned a +1 or −1 charge in $>Ca^{1+}$ and $>CO_3^{1-}$ since the charges are partially satisfied by bonds to the underlying bulk structure. Consequently, hydration and adsorption of calcite constituent ions (Ca^{2+} and CO_3^{2-}) from the aqueous solution result in the formation of the following surface species: $>CO_3H^0$, $>CO^{-3}>CaCO_3^-$, $>CaOH^{2+}$, $>CaO^-$, and $CaHCO_3^0$. The existence of such species has been demonstrated using spectroscopic methods (Stipp and Hochella, 1991). In calcite supersaturated aqueous solutions, the successive protonation/deprotonation of these sites and reactions with ions leads to precipitation.

1.2.4 Mechanism of divalent metal incorporation

Calcite has a high affinity for divalent metals (Me^{2+}; Davis et al. 1987; Zachara et al. 1991; Lakshtanov and Stipp 2007), which are incorporated in the calcite lattice by substituting for a Ca^{2+} ion. This makes calcite a significant sink for elements such as Ca, Mg, and Sr (Wilkinson and Algeo 1989; Tipper et al. 2006; Krabbenhöft et al. 2010; Pearce et al. 2015). Thus, calcite has an important impact on the mobility and geochemical cycles of trace metals in aquatic environments

(Van Cappellen et al., 1993; Gaskova et al., 2009; Villegas-Jiménez et al., 2009). The adsorption of Me^{2+} on the calcite surface can also affect the mineral growth rate and growth mechanism (Katz, 1973; Meyer, 1984; Davis et al., 1987; Freund et al., 2001; Wasylenki et al., 2005).

The main ways in which calcite interacts with metals is through adsorption on the calcite surface and incorporation into the bulk structure. The sorption and incorporation processes are tightly interrelated since adsorption is a necessary intermediate step for all incorporation reactions and both mechanisms are controlled by the same chemical factors (Curti, 1999).

1.2.4.1 Adsorption

Adsorption is the surface-limited accumulation of an adsorbate as a surface complex without the development of a three-dimensional structural arrangement (Sposito, 2009). It is attained via complexation on the hydrated surface (Zachara et al., 1991; Pokrovsky et al., 2000; Lakshtanov and Stipp, 2007). The main factor affecting the adsorption of ions on calcite is the pH of the calcite containing aqueous solution; this affects both the surface speciation of calcite (Fig. 3) and the aqueous speciation of the Me^{2+}. For this reason, most of the studies on Me^{2+} adsorption are conducted as a function of pH of the reactive aqueous fluid.

The pH dependence of surface-exchange reactions is consistent with the adsorption behavior of Me^{2+} on calcite (Fig. 4). The sorption of divalent metals generally increases with increasing pH (Zachara et al., 1991; Hoffmann and Stipp, 2001; Lakshtanov and Stipp, 2007; Belova et al., 2014; Pokrovsky et al., 2014) and mass of the solid (Belova et al., 2014) and decreases with ionic strength (Lamana, 2010).

Various studies have suggested that the surface of calcite is in exchange equilibrium with major and minor solutes in the aqueous phase (Möller and Sastri, 1974; Mucci and Morse, 1985; Villegas-Jiménez et al., 2009). Competition with such cations is another factor which affects the sorption behavior of metals. In the case of Ca, studies by Kornicker et al. (1985) and Zachara et al. (1991) determined that the increase in sorption caused a decrease in the aqueous concentration of Ca maintained by calcite solubility.

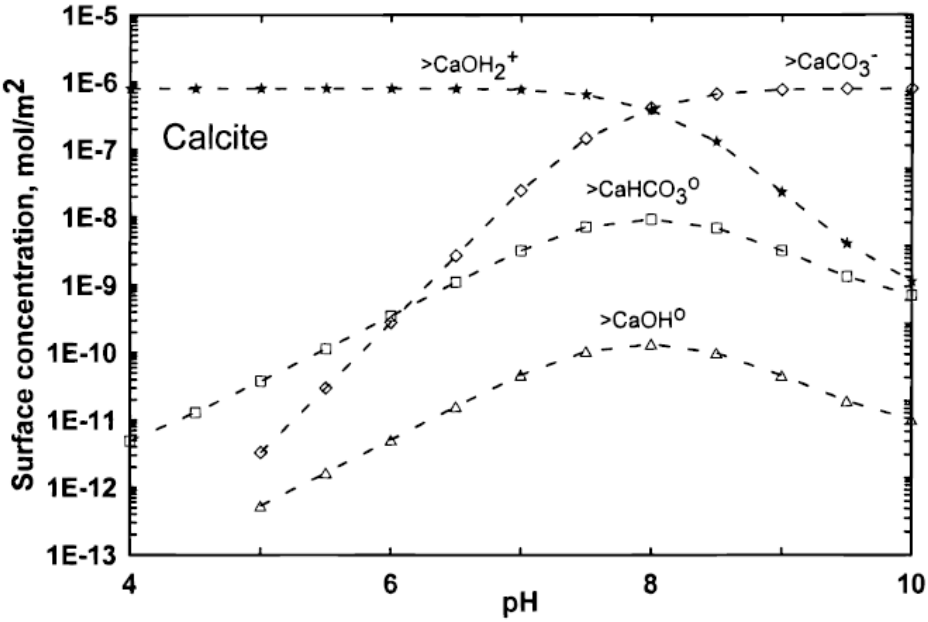

Figure 3. Effect of pH on the distribution of Ca species. (Pokrovsky et al., 2002a)

The higher affinity that some Me^{2+} show for the calcite surface can be correlated to the difference between the ionic radii of the metals and that of calcium. In particular, Me^{2+} with ionic radii smaller than calcite easily substitute into cation sites in bulk calcite (Reeder and Ribbe, 1983). The smaller the difference in size between the metal and Ca, the smaller the disruption to the atomic structure and the affinity of the Me^{2+} for calcite. For cations larger than Ca, only a certain fraction can be tolerated before aragonite becomes the stable phase, so their fractional sorption is much smaller (Zachara et al., 1991).

Sorption is quantified using the distribution coefficient K_d, which is defined as the ratio of the concentration of the metal sorbed on the solid to the metal in the aqueous solution in equilibrium with calcite (Jenne et al., 1979; Gomes et al., 2001):

$$k_d = \frac{[Me]_{adsorbed}}{[Me]_{solution}} \tag{4}$$

where $[i]$ stands for the concentration of the *ith* species

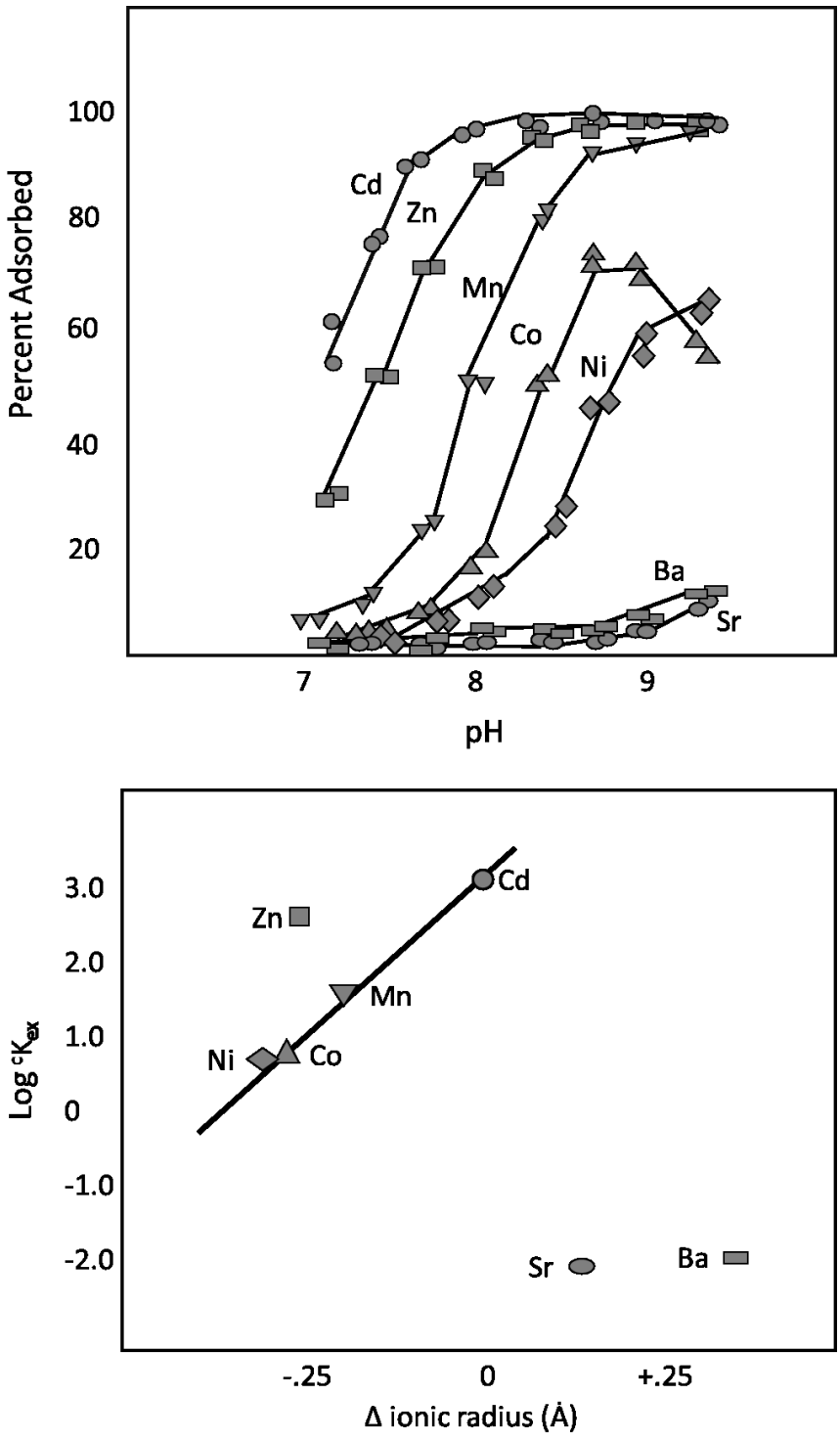

Figure 4. Adsorption of divalent cations on calcite (top) and the relationship between the difference in ionic radius between the Me^{2+} *and calcite and their conditional equilibrium constant (bottom) from* (Zachara et al., 1991)

The desorption of Me^{2+} correlates well with its hydration energy. Metals that dehydrate soon after adsorption create a local structure similar to a surface precipitate while those with high hydration energies remain hydrated until their incorporation into the structure. The more strongly hydrated metals are also the most desorbable (Zachara et al., 1991).

1.2.4.2 Coprecipitation

Coprecipitation occurs whenever foreign species are trapped in the body of a precipitating solid (Curti, 1977). In the case of Me^{2+} coprecipitation with calcite, it entails its incorporation into the bulk solid by replacing a Ca^{2+} cation with a Me^{2+} ion (Lakshtanov and Stipp, 2007). Coprecipitation is a more permanent removal of metal cations from the fluid than adsorption since they will remain in the solid until it dissolves (Román-Ross et al., 2006).

The affinity of a Me^{2+} for the solid is measured by the partition coefficient (D_{Me}). The partitioning of elements between calcite and the reactive fluid is commonly described using thermodynamics by the Henderson and Kracek (1927) :

$$D_{Me} = \frac{X_{Me}}{X_{Ca}} \frac{[Ca]}{[Me]} \quad (5)$$

where X_i represents the mole fraction of the *ith* species in the solid and $[i]$ stands for the concentrations of the ion in aqueous solution.

The higher the D_{Me}, the more the metal tends to go into the solid. However, if crystal growth is rapid, adsorbed ions may be buried into the freshly precipitated material resulting in solid concentrations that deviate substantially from those predicted for equilibrium partitioning between the crystal and its surroundings (Hofmann et al., 2012). The effectiveness of this entrapment process depends on the interaction between the growth rate of the crystal and the diffusivity at the boundary layer. It follows that the partition coefficient depends on the precipitation rate and approaches 1 with increasing precipitation rate (Lakshtanov and Stipp, 2007).

1.2.4.3 Coupled adsorption/precipitation models

Two models involving coupled adsorption/precipitation processes describe the sorption behavior of metal ions on carbonate surfaces (Comans and Middleburg, 1987; Davis et al., 1987). Both models postulate that metal ions first bind to the calcite surface through an adsorption reaction and then dehydrate to create a surface co-precipitate. These models differ in their conceptual view of the coprecipitation reaction.

During fast crystal growth, the adsorption process is often controlled by aqueous diffusion. At high precipitation rates, a growing crystal may trap species at the ratio of their diffusivities in the bulk aqueous solution. The effectiveness of this entrapment process is determined by the growth rate of the crystal and diffusivity in the boundary layer of the crystal (Wang and Xu, 2001). During slow precipitation, when diffusion is not limiting, adsorption is nearly at equilibrium and D_{Me} approaches its equilibrium value.

1.3 Isotope fractionation during mineral growth

1.3.1 Isotope notation

Equilibrium, in terms of isotope fractionation, is parallel to the concept of chemical equilibrium and requires that the forward and backward reaction between two phases occur simultaneously and at the same rate. Therefore, the same equations that can be used to describe a chemical reaction can be used to describe isotope exchange reactions. However, it should be noted that the time required to reach isotopic equilibrium can differ from that required to reach chemical equilibrium (Blanchard et al., 2017).

Isotope exchange in carbonates can be described by:

$$MeCO_3 + Me^{2+}* \leftrightarrow MeCO_3* + Me^{2+} \quad (6)$$

where * denotes the component enriched in the heavy isotopes

The equivalent of K_{eq}, the equilibrium constant of a chemical reaction, is the equilibrium fractionation factor α, so that

$$\alpha_{A-B} = \frac{R_A}{R_B} \tag{7}$$

where *R* is the ratio of heavy to light isotope in substance *A* or *B*

Kinetic fractionation occurs in an incomplete process where the light isotopes exhibit faster reaction rates than the heavy isotopes. For example, during diffusion, the molecules containing lighter isotopes will move and potentially react faster. They can be described by first order kinetics for two competing isotope reactions:

$$A \overset{k}{\rightarrow} B \tag{8}$$

$$A^* \overset{k*}{\rightarrow} B^* \tag{9}$$

where *A* and *B* are the light or heavy (*) isotopes of substance *A* and *B*, and *k* corresponds to the rate constants for the light (*k)* and heavy (*k**) isotopes

Then the fractionation factor α corresponds to the ratio of the rate constants as defined by:

$$\alpha_{A-B} = \frac{k}{k^*} \tag{10}$$

In the conventional delta notation (Urey 1950), the isotope composition of component A (or B) is expressed relative to that of a standard as per mil deviation (‰):

$$\delta_A = \left[\left(\frac{R_{A\ sample}}{R_{A\ standard}}\right) - 1\right] * 1000 \tag{11}$$

So that

$$\Delta_{A-B} = \delta_A - \delta_B \quad (12)$$

The fractionation factor can be evaluated via abinitio calculations from reduced partition fraction ratios (RPFR) β of the considered phase so that:

$$\Delta_{A-B} = 1000(Ln\beta_B - Ln\beta_A) \quad (13)$$

1.3.2 Isotope fractionation

The isotopic composition of elements incorporated into minerals provides information on the mechanisms of chemical reactions and their rates in geochemical processes such as redox transformations, sorption, complexation, and dissolution and precipitation. These processes cause a modification in the relative abundance of the isotopes of an element within reactants and products (Urey, 1947).

Fractionation of stable isotopes between two phases can be attributed to a small difference in masses of the isotopes resulting in small variations in their thermodynamic and kinetic properties; therefore, it can be dominated by either equilibrium (thermodynamic) or kinetic factors (Urey, 1947; Bigeleisen, 1965; Criss, 1999; Schauble, 2004). In general, isotope fractionation between any two phases or compounds within a phase can be attributed to some combination of mass dependence of equilibrium partition coefficients, diffusion coefficients, and reaction rate constants (Watkins and Watson, 2017).

1.3.3 Equilibrium fractionation

During equilibrium fractionation, it is expected that both the forward and backward reaction rates are greater for the lighter isotopes because the zero-point vibrational energy and the mean molecular velocity of light isotopes are higher than those of heavy isotopes (e.g. Bigeleisen 1965; O'Neil 1986; Criss 1999). In addition, heavier isotopes form molecules with higher bonding energies which are more difficult to break. In general, the main processes responsible for thermodynamically driven fractionation of metal isotopes could change oxidation state and/or

differentiate in coordination number or bonding geometry since they can modify the bond vibrational frequencies of atoms (Bigeleisen, 1949; Schauble, 2004).

Isotope partitioning at thermodynamic equilibrium depends only on temperature and the identity and composition of the phases. It reflects the slight change of free energy between two phases containing different isotopes of the same chemical element. Since it is crucial that the precipitation reaction rate exceeds the dissolution reaction rate for mineral growth to occur, it is only possible to observe *equilibrium* isotope fractionation if the reaction is slow enough so that there are no ionic transport limitations to the surface and the rate of species attachment to advancing steps is slow.

1.3.4 Equilibrium isotope fractionation during adsorption

Analyzing metal isotope ratios in solution and of sorbed species allows for the determination of the fractionation factor (Δ) associated with sorption (Wiederhold, 2015). Fractionation during sorption is mostly governed by differences in the environment of the sorbed species compared to its aqueous counterpart.

Theoretical and experimental calculations have shown isotope fractionation within aqueous species is correlated to their bond length. Generally, chemical species that have lower coordination numbers have shorter bond lengths and preferentially incorporate the heavier isotopes of an element (Schauble, 2004; Zeebe, 2005; Bogatko et al., 2013; Colla et al., 2013; Huang et al., 2014). Isotope fractionation between the common species present in solution has also been investigated based on ab initio calculations and experimental measurements (Fujii et al., 2011; Fujii et al., 2014), and the isotopic fractionation between several aqueous species of a given metal have been calculated by Density Functional Theory (DFT).

1.3.5 Kinetic fractionation

Kinetic isotope effects are caused by the different reaction rates of light and heavy isotopes and are only preserved in incomplete processes. The influence of kinetic effects on the isotopic composition depends strongly on the relative extent of reaction progress (Wiederhold, 2015).

Kinetic processes have an important effect on the isotopic composition of an element during mineral precipitation and need to be accounted for to have a better understanding of its chemical and biochemical cycles (Anbar and Rouxel, 2007; Baskaran, 2011). Kinetic isotope effects may be

caused by diffusive transport to the mineral-fluid interface as well as the mass dependence on species attachment rate at the solid surface. DePaolo (2011) suggested different regimes of mineral precipitation (Fig. 5) based on the limiting step of the reaction. For regimes 2, 3, and 4, the kinetic effects caused by diffusion and rates of attachment to growth sites will play a role in the isotopic fractionation.

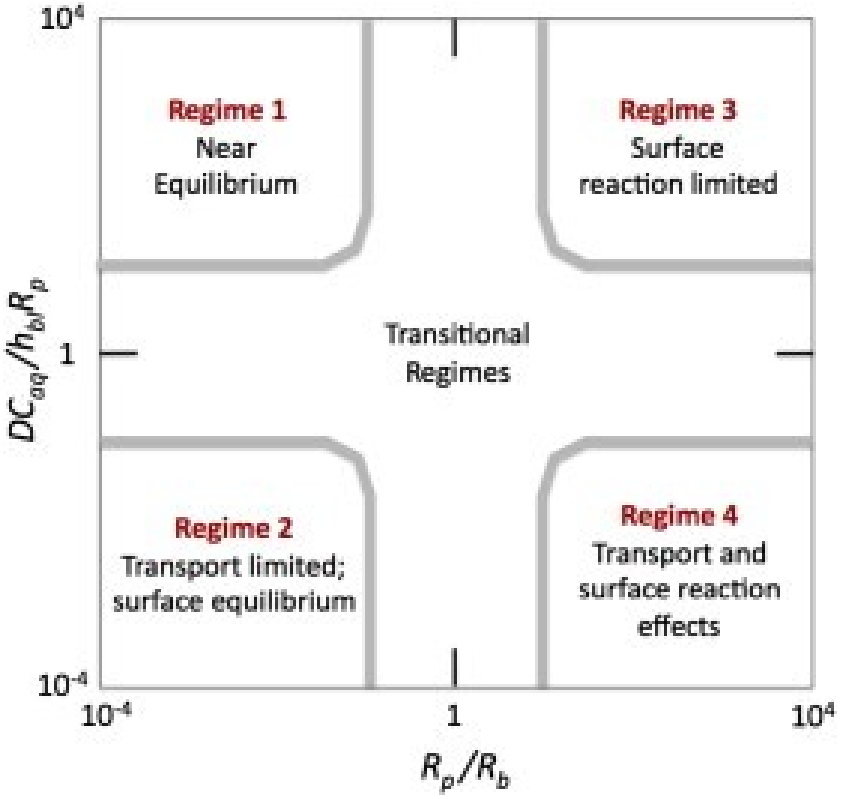

Figure 5. Different rates of precipitation regimes proposed by DePaolo (2011). The figure shows net precipitation rate over backward dissolution rate on the x axis and diffusion flux over precipitation flux on the y axis

1.3.6 Significance of the water exchange rate

The water exchange rate (k_{wex}) of an aqueous metal species measures the lifetimes of water molecules in its inner-coordination shell (Wang et al., 2007). It is equivalent to $1/\tau$, where τ is the residence time of water molecules in the first hydration sphere surrounding the cation (Bourg et al., 2010) so that a low k_{wex} implies that water molecules are more strongly attached to the cation. (Fig. 6) Water-exchange rates are key indicators of chemical reactivity in aqueous coordination compounds and are fundamental in understanding the reactivity of these ions in chemical and

biological systems; they are involved in phenomena such as adsorption, electron transfer, and surface charging (Helm and Merbach, 1999; Wang et al., 2007).

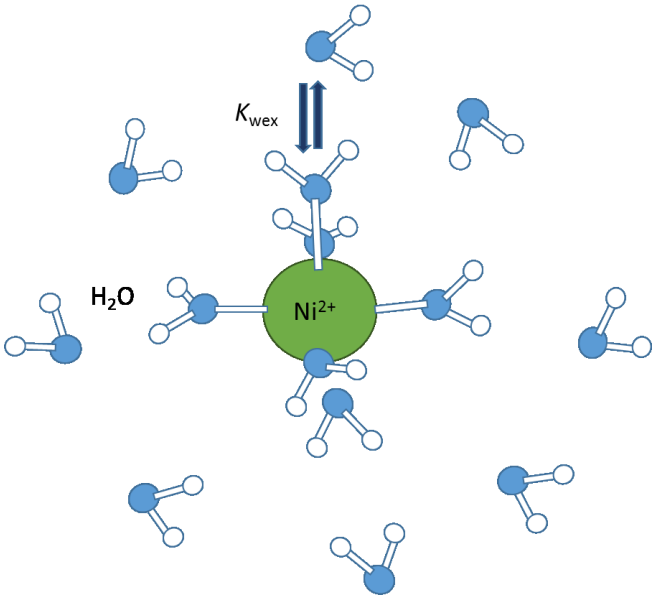

Figure 6. Sketch of the Ni^{2+} aqueous ion

Of the three steps required for crystal growth from solution (diffusion of ions to the mineral-fluid interface, adsorption on the mineral surface, and incorporation into the bulk structure), the last two require a progressive desolvation of the ions. While the origin of kinetic isotopic and trace element fractionation during calcite precipitation is not fully understood, several studies associate it with dehydration of dissolved ions during the incorporation step and rehydration during the coupled dissolution step. It has even been suggested that ion desolvation is the main mechanism causing fractionation of free aqueous metal cations with the rate of exchange of H_2O in the metal following an inverse power law mass dependence (Hofmann et al., 2012):

$$\frac{k_{wex.j}}{k_{wex,i}} = \left(\frac{m_i}{m_j}\right)^{-Y} \tag{14}$$

where Y is 0.05 ± 0.01 for investigated cations.

The rearrangement of the coordination shell necessary for the metal to have access to the calcite surface is not normally a rate limiting step because water exchange in the first hydration shells is usually fast. However, the Me^{2+} desolvation rates relative to Ca is critical; as the desolvation rate of Ca^{2+} is the rate limiting step for calcite growth, it would be difficult for metals such as Mg and Ni which desolvate at rates 3-5 orders of magnitude slower than Ca (Table 1) to get totally desolvated in bulk calcite except under very slow calcite precipitation rates (Mavromatis et al., 2013).

Table 1. Rate of exchange of water in the metal coordination sphere

Metal (Me^{2+})	log k_{wex} (s^{-1})
Cu	9.5
Ba	9.2
Sr	8.9
Ca	**8.8**
Cd	8.2
Zn	7.8
Mn	7.0
Fe	6.3
Co	5.8
Mg	**5.4**
Ni	**4.3**

In any reaction where a chemical bond must be broken, it is expected that the rate of bond breaking, and the rate of reaction, will be higher for the light isotopic species (Zeebe and Wolf-Gladrow, n.d.; Criss, 1999). Experimental (deBoer R. B., 1977; Mucci, 1983), theoretical (Pokrovsky and Schott, 2002; DePaolo, 2011; Hofmann et al., 2012), and molecular simulation studies suggest that the kinetics of Me^{2+} attachment/detachment to and from the calcite surface is related to the rate of exchange of water molecules.

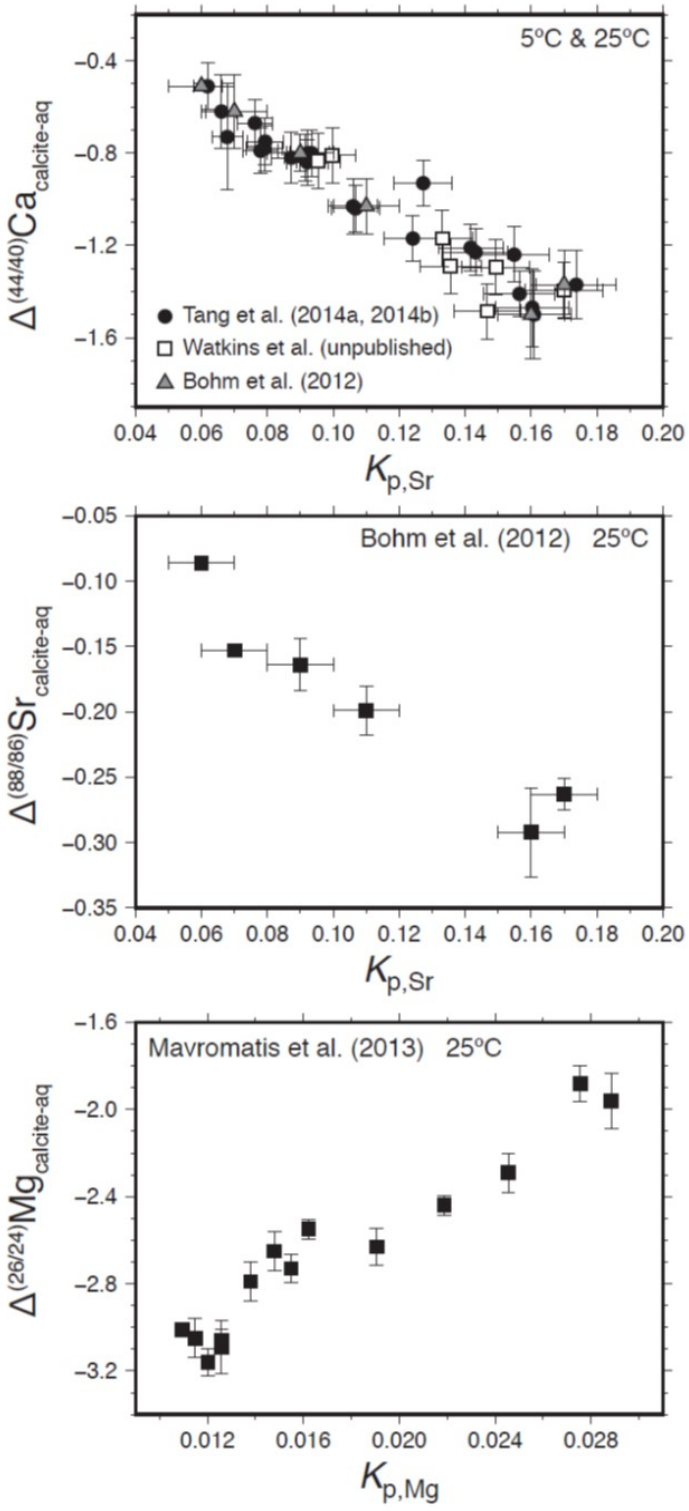

Figure 7. Stable isotope fractionation of a) Ca, b) Sr and c) Mg correlated with their partitioning between calcite and fluid. Watkins et al. (2017)

As an example, the extent of strontium isotope fractionation in calcite increases with calcite precipitation rate (Böhm et al., 2012) while the extent of magnesium isotope fractionation decreases with calcite precipitation rate (Mavromatis et al., 2013; Saenger and Wang, 2014). Fig. 7 shows the isotope fractionations of two trace metals (Sr and Mg) incorporated into inorganic calcite compared to that of Ca^{2+}. Its variation with growth rate leads to correlations between metal isotope fractionations and metal partitioning. The differences in the desolvation rates of these metals relative to Ca^{2+} may be the cause of such trends. For instance, Sr^{2+} has a desolvation rate similar to Ca whereas Mg^{2+} has a desolvation rate more than 3 orders of magnitude slower (Table 1, Nielsen 1984). Furthermore, infrared spectra of calcite grown at different rates confirm the incomplete desolvation of Mg^{2+} ions at higher growth rates based on the presence of water in the infrared spectra of fast-grown calcite (Mavromatis et al., 2013).

1.3.7 Implications for paleo reconstructions

Isotope exchange reactions between $CaCO_3$ and seawater are the basis for past temperature, atmospheric CO_2, and ocean pH paleo reconstructions; such reconstructions utilize oxygen, carbon, and boron isotopes, respectively. The isotopic compositions of Me^{2+} incorporated into the calcite structure also have the ability to record valuable information reflecting the geochemical conditions of formation(Galy et al., 2002; Chang et al., 2004; Mavromatis et al., 2013; Mavromatis et al., 2019) Moreover, as the equilibrium and kinetic partition of these elements between calcite and fluid exhibit contrasting behaviors, it can be expected that their isotope composition in calcite exhibits distinct trends (Schott et al., 2014).

Traditionally, temperature is considered to be the main factor controlling the degree of isotope fractionation (Emrich et al., 1970). However, it has been suggested that temperature plays only a secondary role in fractionation during mineral growth (Lemarchand et al., 2004). Several experimental studies show other processes such as the mineral growth rates (Mavromatis et al., 2013), mineralogy (Romanek et al., 1992), metal desolvation rates (DePaolo, 2011), biologically mediated effects (Pogge von Strandmann, 2008; Hippler et al., 2009), and fluid saturation state with respect to precipitating solid (Lemarchand et al., 2004) also have an important effect on isotope fractionation. These studies could provide important information on the geochemical conditions of mineral formation.

During mineral precipitation from solution at high precipitation rates, the system is not at isotopic equilibrium. The preferential incorporation of light isotopes combined with the precipitation rate dependence that has been shown in several studies (Böhm et al., 2012; Mavromatis et al., 2013) suggests that the fractionations are mostly kinetic in origin. These deviations from equilibrium fractionation could additionally provide information on geochemical processes and paleoenvironments. This thesis focuses on the incorporation of Ni in calcite. This element is of special interest due to the slow desolvation rate it exhibits; it demonstrates the slowest of desolvation rate of all Me^{2+} discussed in this chapter. Therefore, it has the potential to reveal valuable information on the precipitation rate of Ni bearing calcite.

1.4 Nickel

1.4.1 Nickel isotopes

Naturally occurring Ni is composed of five stable isotopes (58, 60, 61, 62, and 64) with ^{58}Ni being the most abundant (68.08%). Ni isotope compositions are conventionally reported relative to the U.S. National Institute of Standards and Technology Standard Reference Material 986 (NIST SRM 986) international standard. While most past work on Ni isotopes has centred on cosmochemistry, Ni isotope compositions for silicate Earth, sediments, and water samples have also been characterized. This study focuses on existing oceanic Ni data.

1.4.2 Nickel in the ocean

Nickel in the ocean exhibits nutrient-like behavior as its dissolved concentration ranges from of 2 nmol/kg at the surface to 12 nmol/kg at greater depths with an estimated average of about 8 nmol/kg (Sohrin and Bruland, 2011). It is a bioessential trace metal, and 10–60% of Ni in coastal and open-ocean is complexed with organic ligands (Donat et al., 1994; Saito et al., 2004). In seawater, the dominant Ni species is Ni^{2+}, the only stable oxidation state over the pH range of most natural waters.

The global marine Ni budget is controlled by the input of dissolved Ni from river water, dissolution in the oceans of riverine and atmospheric transported particulate material, Ni scavenging by marine minerals sedimentation, and geothermal activity (Sclater et al., 1976; Li et al., 2003; Jeandel and Oelkers, 2015). The main sink of Ni in the ocean is ferromanganese crust.

The isotopic composition of seawater was determined by Cameron and Vance (2014) who reported values of $\delta^{60}Ni = 1.44 \pm 0.15$. Interestingly, the isotopic composition of Ni in the oceans is nearly homogeneous across all ocean basins. This can be explained by the significantly longer residence time of Ni, about 30,000 years (Cameron and Vance, 2014), compared to the mixing time for global oceans of about 2,000 years (Jenkins, 2003). Along different depths in a study of the Black Sea, variation in isotopic composition of Ni is very substantial, at about 1.5‰, requiring very large isotope effects associated with the sources and sinks of Ni (Vance et al., 2016).

Rivers, the main input of Ni into the ocean, are isotopically heavier than the crust from which they originated, meaning that light Ni isotopes are probably retained during soil formation (Ratié et al., 2015). They been determined to have an annual $\delta^{60}Ni$ average of +0.80‰ and to show significant seasonal variability between +0.29 and +1.34‰ (Cameron and Vance, 2014). It should be noted that while compared to the crust, rivers provide isotopically heavy inputs into oceans, Ni in oceans is about 0.6‰ heavier than Ni in rivers.

Table 2. Ni inputs and outputs into the ocean

	Ni content (moles)	$\delta^{60}Ni$ ‰
seawater	1.12×10^{13}	1.44
	Ni in/ out (mol per year)	$\delta^{60}Ni$ (‰)
Inputs		
river water	5.20×10^{8}	0.8
mineral dust	4.60×10^{8}	
cosmic dust	1.20×10^{7}	
volcanic emission	1.90×10^{8}	
benthic flux	3.40×10^{6}	
groundwater	1.20E $\times 10^{8}$	
hydrothermal fluid	3.30×10^{-8}	1.5
Outputs		
ferromanganese crust	5.10×10^{-8}	0.9-2.5

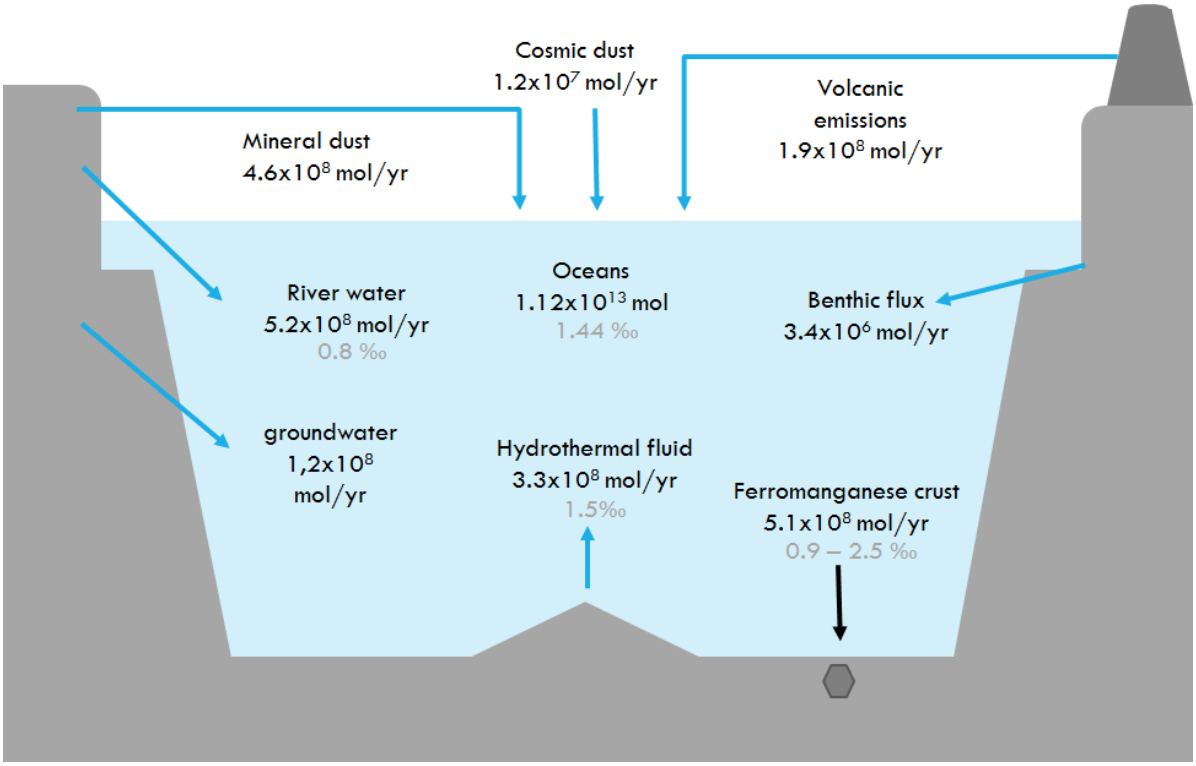

Figure 8. Ni budget in the ocean. Modified after Gall et al. (2013).

Based on isotopic mass balance considerations, a source of isotopically heavy Ni in modern oceans is missing. (Cameron and Vance, 2014). It has also been speculated that the effects of Ni sorption onto Fe/Mn oxide surfaces, which is a major sink of Ni in the ocean (Peacock and Sherman, 2007), could explain, at least in part, the isotopic composition of seawater since it favors enrichment of lighter isotopes (Wasylenki et al., 2015; Gueguen et al., 2018). Alternatively, the source of heavy Ni could be balanced by an oceanic sink enriched in light Ni isotopes. It has been suggested that this sink could be sulfides associated with anoxic or suboxic marine sediments that are enriched in organic matter (Gueguen et al., 2013; Hofmann et al., 2014). However, the role of organic-rich sediments in Ni isotope mass balance is unclear at this time as the bulk δ^{60}Ni of organic-rich sediments displays a large range from 0.28‰ to 2.5‰ (Porter et al., 2014).

Table 2 shows a compilation of the data on Ni fluxes into and out of the ocean from with the addition of Ni isotope data from several publications. These data, which represents the known information on the Ni budget in the ocean is schematically represented in Figure 8.

1.4.3 The motivation for studying Ni isotopic fractionation during its interactions with calcite

Isotope exchange reactions between calcium carbonates and seawater are important in paleo-reconstructions including determination of past temperature, atmospheric CO_2, and oceanic pH from oxygen, carbon, and boron isotopes, respectively. In paleo oceanographic research proxies are continuously evolving and improving. Simultaneously new proxies are being studied and developed through water column analysis, surface sediment analysis, and through laboratory experimentation. When Ni substitutes for Ca^{2+} in calcite as octahedral Ni^{2+} the Ni isotopic composition (in sedimentary calcite) can provide valuable information on the chemical composition, pH, and pCO_2.

If the removal of Ni from the dissolved phase in the surface ocean is associated with isotopic fractionation, then Ni isotopes may be able to yield constraints on precise biogeochemical processes involved at the time of mineral formation. This is due to its strong complexation with organic ligands and its slow water exchange rate (table 1); out of the first row transition metals, Ni has the most inhibiting enthalpy of dehydration at -513 kcal/mol (Baes and Mesmer, 1976).

Another advantage of Ni over other divalent metals is that during its incorporation in calcite it undergoes fewer processes that cause fractionation (i.e. redox or change of coordination number) and thus the main mechanism causing fractionation will be the distribution within species. This distribution within species will reflect in the Ni^{2+} composition since it is the only species of Ni that can exchange into the calcite lattice. The isotope fractionation among aqueous species will, therefore, be reflected in the composition of free Ni and consequently in the fractionation between Ni in the solid and the reactive fluid.

The speciation of a metal in solution affects its kinetic and thermodynamic properties. It also affects the isotopic composition of the aqueous metal and the metal incorporated from the solution into a solid. This study provides new insights into the parameters controlling isotope fractionation of Ni during its interactions with calcite and provides new tools to reconstruct paleo-environmental conditions based on the composition of the Ni isotopes recorded in carbonate sediments.

1.5 Scope of this thesis

Only a few experiments have investigated the adsorption of Ni on the calcite surface and its coprecipitation with this mineral. However, to our knowledge, no isotope data has been published on Ni isotope fractionation that is linked to these processes. The aim of this thesis is to fill this gap and also characterize the mechanisms controlling Ni isotope fractionation that are driven by interactions of this element with calcite. It is expected that the extent of adsorption of Ni on calcite and coprecipitation with calcite can reveal information on the chemical composition of the reactive fluid from which Ni came into contact with this mineral. Results of this thesis will provide important insight into several key questions:

- Does the speciation of the solution affect the fractionation of Ni during adsorption on calcite?
- What is the mechanistic cause of Ni isotope fractionation during adsorption and coprecipitation on/with calcite?
- Is there a link between calcite precipitation rate and the extent of Ni isotope fractionation?
- Can Ni incorporated into calcite be used as a proxy for paleo oceanic conditions?
- Does Ni incorporated in calcite play a significant role in the oceanic Ni isotope budget?

In an attempt to answer these questions, two experimental studies have taken place. Each is presented in a different chapter of this thesis. The first study (chapter 3) is devoted to the investigation of Ni isotope fractionation during adsorption on the calcite surface as a function of pH. This study was motivated by the search for a heavy source or light sink of Ni in the ocean in order to better constrain the Ni global oceanic isotope budget. The second study (chapter 4) investigates Ni isotope fractionation associated with its coprecipitation with calcite. The aim of this study is the development of a new proxy to determine paleo oceanic chemical composition (pH, pCO_2, saturation state with respect to calcite). To evaluate this new proxy, experiments were designed to quantify Ni isotope fractionation as a function of the precipitation rate of calcite at 1 atm pCO_2 and 25ºC.

Chapitre 1b. Introduction générale

Les carbonates sont des roches sédimentaires trouvées dans pratiquement tous les systèmes marins et caractérisés par la présence de l'ion carbonate (CO_3^{2-}) dans leur structure. Le carbonate de calcium ($CaCO_3$) est le carbonate le plus abondant à la surface de la Terre, avec deux polymorphes principaux, la calcite et l'aragonite. La calcite a une forte affinité pour les métaux divalents (Davis et al., 1987; Zachara et al. 1991; Lakshtanov et Stipp, 2007). Les principales voies d'interaction des métaux avec la calcite sont leur adsorption à la surface du minéral et leur incorporation dans le réseau cristallin. Les processus de sorption et d'incorporation sont étroitement liés puisque l'adsorption est une étape intermédiaire nécessaire pour toutes les réactions d'incorporation et que les deux mécanismes sont contrôlés par les mêmes facteurs chimiques (Curti, 1999). Cela fait de la calcite un puits pour des éléments divalents tels que Cd, Zn, Mn, Fe, Cd, Mg et Sr. (Wilkinson et Algeo, 1989; Tipper et al., 2006; Krabbenhöft et al., 2010; Pearce et al., 2015) qui peut avoir un impact important sur la mobilité et les cycles géochimiques des métaux traces dans les milieux aquatiques (Van Capellen, 1993; Villegas-Jimenez, 2009; Martin-Garin et al., 2003).

La composition isotopique des éléments incorporés dans les minéraux fournit des informations sur les mécanismes des réactions chimiques et leurs vitesses dans les processus géochimiques tels que les transformations redox, la sorption, la complexation, la dissolution et la précipitation. Ces processus modifient l'abondance relative des isotopes d'un élément dans les réactifs et les produits (Urey, 1946). Le fractionnement des isotopes stables entre deux phases peut être attribué à la faible différence de masse des isotopes entraînant de petites variations de leurs propriétés thermodynamiques et cinétiques. Il peut donc être dominé par des facteurs d'équilibre (thermodynamiques) ou cinétiques (Urey, 1947; Bigeleisen, 1965; Schauble, 2004). En général, le fractionnement isotopique entre deux phases ou composés au sein d'une phase peut être attribué à une certaine combinaison de coefficients de partage à l'équilibre, coefficients de diffusion et constantes de vitesse de réaction (Watkins, 2017).

Les réactions d'échange d'isotopes entre les carbonates de calcium et l'eau de mer peuvent servir comme témoins ou proxys des conditions physico-chimiques passées à la surface de la terre et sont à la base de paléo-reconstructions concernant, notamment, la température, la teneur de l'atmosphère en CO_2 et le pH des océans à partir des isotopes de l'oxygène, du carbone et du bore, respectivement. En paléo-océanographie, les proxys évoluent et s'améliorent continuellement, tandis que de nouvelles méthodes se développent grâce à l'analyse des sédiments et à des

expériences en laboratoire. Ainsi le remplacement de Ca^{2+} par Ni^{2+} dans le réseau de la calcite et le fractionnement isotopique du Ni qui devrait en résulter, pourrait permettre à la composition isotopique de Ni dans les calcites sédimentaires de fournir des informations sur la composition chimique, le pH et la pCO_2 des océans dans le passé.

Si la migration de Ni de la phase dissoute dans l'océan vers la calcite est associée à un fractionnement isotopique, les isotopes de nickel peuvent alors être en mesure de créer des contraintes sur les processus biogéochimiques précis mis en œuvre au moment de la formation de ce minéral. La composition isotopique des métaux divalents incorporés dans la calcite dépend fortement de la vitesse de précipitation de ce minéral (DePaolo, 2011 ; Mavromatis et al., 2013). Si ce fractionnement cinétique est aussi observé pour le nickel, la composition isotopique de cet élément dans les calcaires sédimentaires pourrait devenir un nouvel indicateur de l'état de saturation des océans par rapport à la calcite et ainsi de la teneur en CO_2 des océans au moment de la précipitation de ces minéraux.

Un autre avantage du nickel par rapport à d'autres métaux divalents est que lors de son incorporation dans la calcite il ne subit pas de changement redox ou de son nombre de coordination, deux processus qui pourraient impacter sa composition isotopique. Par conséquent, les principaux paramètres susceptibles de contrôler le fractionnement isotopique de cet élément seront i) la distribution des espèces du nickel en solution qui sont peuvent modifier la composition isotopique de Ni^{2+}(aq) et ainsi celle de Ni^{2+} incorporé dans le réseau de la calcite et, ii) la vitesse de précipitation de la calcite susceptible d'induire un fractionnement isotopique de Ni lié aux différents coefficients de diffusion et vitesses de désolvatation des isotopes du nickel.

Le but de cette étude est donc de quantifier le fractionnement isotopique de Ni et de fournir de nouvelles informations sur les paramètres contrôlant ce fractionnement isotopique lors de des interactions de ce métal avec la calcite et ainsi de proposer de nouveaux outils pour reconstruire les conditions paléo-environnementales à partir des compositions des isotopes de Ni enregistrées dans les sédiments carbonatés.

Un petit nombre de travaux ont examiné l'adsorption de Ni sur la surface de la calcite et sa coprécipitation avec ce minéral, mais à notre connaissance, aucune donnée n'a encore été publié sur les fractionnements isotopiques du Ni liés à ces processus. Le but de cette thèse est de combler cette lacune. Il s'agit également de caractériser les mécanismes contrôlant le fractionnement des isotopes du Ni induits par les interactions de cet élément avec la calcite. On peut s'attendre à ce que

les coefficients de partage et de fractionnement isotopique mesurés lors ' de l'adsorption du nickel sur la calcite et de sa coprécipitation avec ce minéral puissent révéler des informations sur la composition chimique du fluide à partir duquel Ni a interagi avec ce minéral. Les résultats de cette thèse doivent fournir les clefs pour pouvoir répondre à plusieurs questions:

- La spéciation de la solution affecte-t-elle le fractionnement isotopique de Ni lors de son adsorption sur la calcite ?
- Quelles sont les causes mécanistes des fractionnements isotopiques du nickel lors de son adsorption et de sa coprécipitation sur / avec la calcite ?
- Existe-t-il un lien entre la vitesse de précipitation de la calcite et l'étendue du fractionnement des isotopes du nickel entre calcite et fluide ?
- La composition isotopique du nickel incorporé dans la calcite peut-il servir de proxy des paramètres physico-chimiques du fluide à partir duquel il s'est formé ?

Deux études expérimentales ont été réalisées pour tenter de répondre à ces questions. La première étude, qui est présentée au chapitre 3, est consacrée à l'étude du fractionnement isotopique du Ni lors de son adsorption sur la surface de la calcite en fonction du pH. Cette étude a été motivée par la recherche d'une source de nickel lourd ou d'un puits de nickel léger afin de mieux équilibrer le budget isotopique du Ni dans l'océan. Dans la seconde étude, rapportée au chapitre 4, on étudie le fractionnement isotopique du Ni associé à sa coprécipitation avec la calcite. L'objectif est de développer un nouveau proxy de la composition chimique de l'eau de mer dans le passée (pH, pCO_2, état de saturation par rapport à la calcite). Pour évaluer ce nouveau proxy, des expériences ont été conçues afin de quantifier le fractionnement des isotopes du Ni en fonction du taux de précipitation de la calcite à 25°C et sous une pression de CO_2 de 1 atm.

Chapter 2. Experimental and analytical methods

This chapter presents the experimental design as well as the sample treatment prior to measurements and the principle analytical techniques used for chemical and isotopic analysis. Section 2.1 describes in detail the experimental conditions and choice of materials, their characteristics, and their treatment prior to the experiments along with the preliminary tests performed to select the best materials and reagents for this study. Section 2.2 shows the initial conditions of the experiments, identified through preliminary tests and thermodynamic models, and the details of the experimental design including the steps undertaken to optimize the experiments for run duration and to be suitable for isotope analysis. Section 2.3 describes the experimental protocol used for Ni adsorption on calcite and Ni coprecipitation with calcite experiments. Section 2.4 describes the preparation of samples prior to measurements and analytical techniques used during this thesis. It also describes in detail the ion exchange chromatography process used to separate Ni from the matrix elements and the Ni isotope measurements.

2.1 Starting materials

2.1.1 Reagents

Research in this thesis is centered on aqueous solution calcite interactions. All aqueous solutions used during this thesis were prepared using high purity (>99 %) reagents and deionized MQ water (resistivity 18.2 MΩ) from a Millipore system. All acids used during the experiments were doubly distilled, and commercial reagents were either of suprapure (NaOH, $Ni(NO_3)_2$) or normapure ($CaCO_3$, $CaCl_2$, Na_2CO_3, NaCl) grade.

For work performed inside the clean lab, reagents were of suprapure (HF) or trace metal grade (NH_4OH and H_2O_2). The HNO_3 and HCl were purified once or twice through sub-boiling distillation. The aqueous citric acid solution was prepared from 99.5% $C_6H_8O_7*H_2O$ purchased from Acros Organics and cleaned using Bio-Rad AG1-X8 resin. The aqueous NH_4OH solution was either trace grade or purified by evaporating and equilibrating suprapure ammonia with MQ H_2O for a few days in a closed container.

2.1.2 Calcite

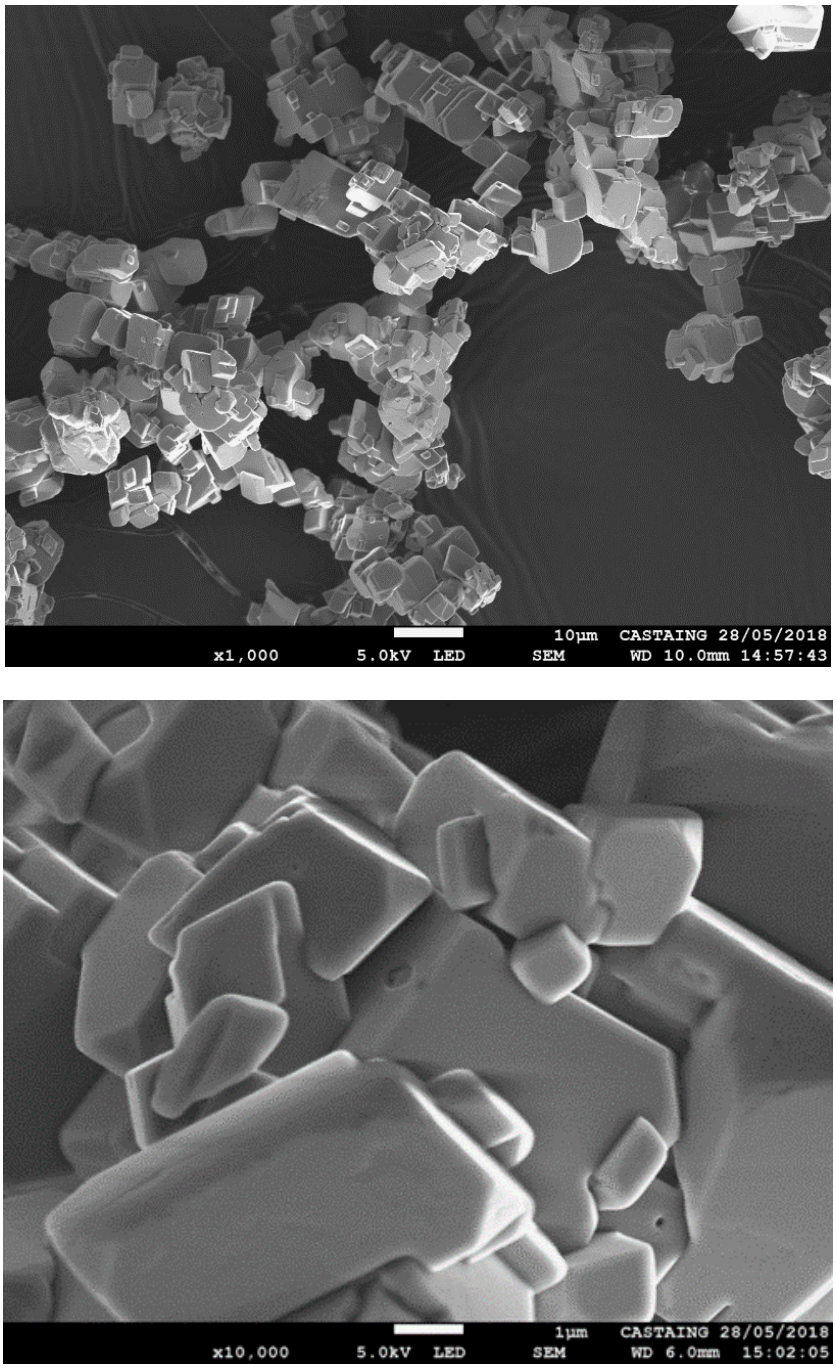

Figure 9. SEM images of the synthetic calcite used in this study.

Synthetic high purity Merck MESURE® calcite was used for all experiments in this thesis. It was shown to be 100% calcite by X-ray diffraction (XRD). XRD analyses were performed using an INEL CPS-120 diffractometer with Co Kα-radiation having a detection limit of ~5%. The

obtained diffraction patterns were compared to the characteristic profile for calcite taken from the RRUFF database (Lafuente et al., 2016). The surface area of the calcite crystals was determined to be 0.31 m^2/g as measured by triple-point krypton adsorption using the Brunauer–Emmett–Teller (BET) method (Brunauer et al., 1938). Scanning Electron Microscope (SEM) images of the calcite were obtained at the Raimond Castaing center for microcharacterization in Toulouse using a JEOL JSM 6700F SEM. These images show the calcite crystals with rhombohedral morphology with intergrowths and agglomerations. These images were also used to estimate the average length of the calcite crystals (about 6 μm; see Fig. 9).

2.1.3 Aqueous Nickel stock solution

A 10,000 ppm aqueous nickel stock solution was prepared from a nickel nitrate ($Ni(NO_3)_2$) (Sigma-Aldrich, 99.99 %, trace metal basis) salt. This salt was dissolved into deionized MQ water (resistivity 18.2 MΩ). For the adsorption experiments that required a diluted solution, a fresh 6 ppm Ni solution was prepared for every set of experiments starting from the 10,000 ppm stock solution.

Two aqueous Ni stock solutions were used during this study. The isotopic composition of the first Ni stock solution was measured repeatedly during this study and was determined to be -0.52 ± 0.17‰ (average of all measurements; Fig. 10). A second Ni stock solution was prepared after depletion of the first. It was prepared in the same way but from a different $Ni(NO_3)_2$ salt. This solution was used for the last set of experiments and its composition, measured during a single mass spectrometry session, was -0.63 ± 0.07‰. The differences in isotopic composition could be explained by heterogeneities of the $Ni(NO_3)_2$ salt.

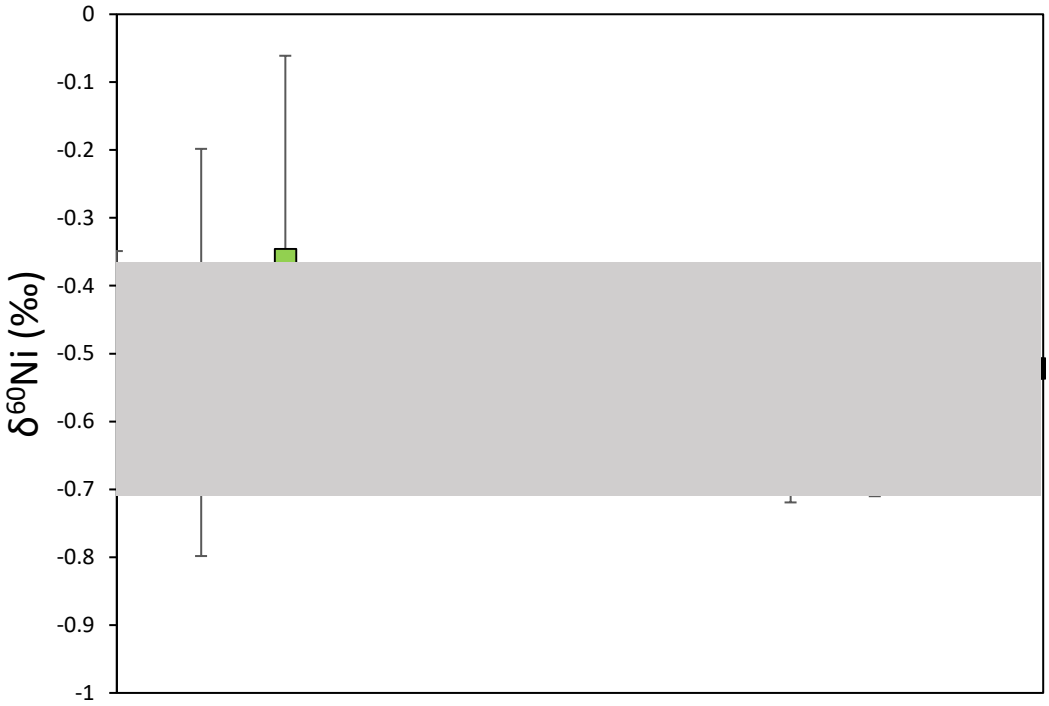

Figure 10. Isotopic composition of the first aqueous Ni stock solution. Each black square represents a measurement of the Ni stock solution and the grey line represents the average of measurements determined to be -0.52 ± .17 ‰

2.2 Experimental methods

2.2.1 Reactors

Reactor vessels can leach contaminants or adsorb metals to their walls. Notably, glass and polypropylene tend to sorb cations and this effect increases as pH increases (Struempler, 1973). Although these effects are small at room temperature, the loss of Ni due to adsorption on the reactor vessels can be important due to the low concentration used in the experiments.

Polyethylene (PE), polycarbonate (PC), and polypropylene (PP) centrifuge tubes were tested for their suitability for this project by storing an aqueous solution containing 80 ppb Ni for 24 hours. Solutions were prepared by adding HCl or NaOH to MQ water to approach a pH of 7 or 9; these values mark pH limits of solutions used for the adsorption experiments (see chapter 3). After 24 hours the solutions were recovered from these tubes, filtered, acidified to a pH of 2 using HNO_3, and then analyzed using the AAS furnace. This test determined that PC adsorbed

the least Ni at 1.5% while PP and PE adsorbed 3% and 5%, respectively (Table 2). PC was selected for use as the best plasticware option for adsorption experimentation given the minimal loss of material that was within the 2% uncertainty of AAS measurements. Thus, 50mL Nalgene centrifuge tubes were used for adsorption experiments. Later 1L PC vials with PP lids were used in coprecipitation experiments (see chapter 4). Prior to their use, all reactors were cleaned with 1 M HCl solution for 24 hours then rinsed several times with MQ H_2O and air dried.

Table 3. Percentage of Ni recovered in different material reactor vessels during tube adsorption preliminary testing.

material	percentage recovered	
	pH 7	pH 9
PE	92.3	96.8
PC	97.6	98.4
PP	95.3	97.5

2.2.2 Thermodynamic calculations

All aqueous species distribution, fluid saturation states, and chemical activities were calculated using the thermodynamic modeling computer code PHREEQC (Parkhurst and Appelo 2013) along with the minteq.v4 database. In some speciation calculations, the stability constants of $NiCO_3^0$ and $NiHCO_3^+$ in the database were replaced with those published by Baeyens et al (2003). This information allowed for the prediction of experimental initial conditions such as Ni concentration and pH of solutions that were used for models and calculations.

2.2.3 Adsorption Experiments

A total of 9 sets of experiments (briefly described in Table 3) were conducted during this study. The name series shows a number representing the chronological order of the experiment and a letter representing the type of experiment [P for pH dependent, K for kinetics, and I for adsorption isotherm]. Series 1P, 2P and 4P were used to determine the background electrolyte to

be used for the remainder of the experiments and is further discussed in this chapter. Results of 3K, 8K, 6P, 7P and 9P in the adsorption section (chapter 3).

Table 4. Summary of adsorption experiments.

Series	variable	electrolyte	duration (days)	Ni conc. (ppb)
1P	pH	NH_4Cl	1	80
2P	pH	$NaNO_3$	1	80
3K	time	NaCl	1	80
4P	pH	NaCl	1	80
5I	[Ni]	NaCl	1	70-130
6P	pH	NaCl	1	100
7P	pH	NaCl	1	100
8K	time	NaCl	0.125 to 7	100
9P	pH	NaCl	3	100

2.2.3.1 Background electrolyte

Experimental series 1P, 2P, and 4P aimed to select the best background electrolyte for use in the remainder of experiments. The initial goal was to avoid the addition of sodium to the aqueous solution since the elution profile of Ni and Na are too close to obtain a full separation during ion exchange chromatography. Three different background electrolytes were tested to determine the best option (Fig. 11). However, after tests were performed, it became apparent that using NaCl as a background electrolyte resulted in a better and more defined adsorption edge and it was therefore selected for use in all experiments.

For a first test, ammonium chloride (NH_4Cl) was used as a background electrolyte and ammonium hydroxide (NH_4OH) or HCl were used to adjust the pH of the aqueous solutions. Ionic strength was kept constant at 0.1 M. The same procedure was applied to sodium nitrate ($NaNO_3$) and sodium chloride (NaCl); the pH of sodium nitrate was adjusted using NaOH and HNO_3 and the pH of sodium chloride was adjusted using NaOH and HCl. It can be seen from the adsorption edge pattern described in Fig. 11 that about 30% of the Ni was removed from solution when the pH ranged from 7.5 to 9.5. This could be due to precipitation of Ni hydroxide and/or to the OH competition for adsorption sites. Both $NaNO_3$ and NaCl adsorption tests exhibit a typical pattern as

a function of pH, however, NaCl exhibits a better defined adsorption edge than the other electrolytes. For this reason, NaCl was used for all subsequent adsorption experiments performed.

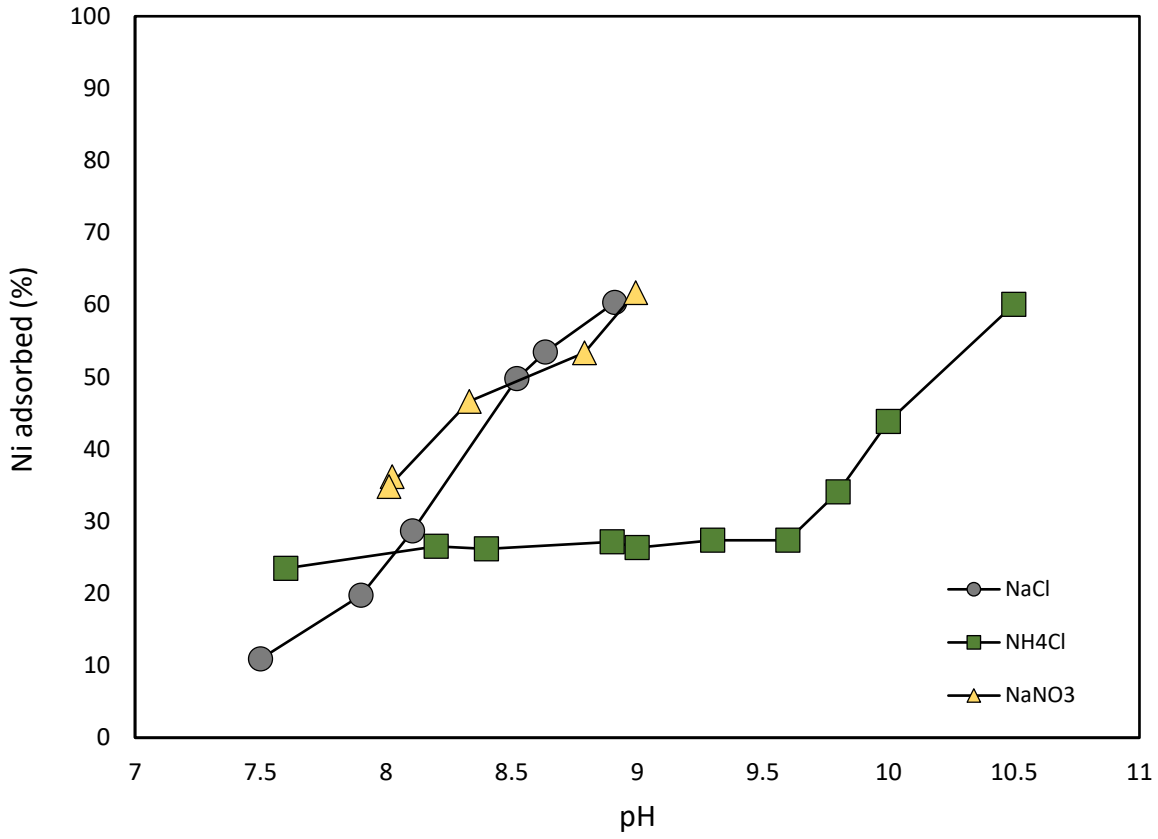

Figure 11. Effect of background electrolyte on the adsorption edge of Ni. The experiments shown were conducted using different background electrolytes: grey circles represent experiments where NaCl was used, green squares show experiments performed using NH_4Cl, and yellow triangles show experiments performed using $NaNO_3$ as a background electrolyte. All experiments were kept at 25°C, atmospheric pCO_2, and 0.1 ionic strength.

2.2.3.2 Ni concentration

An important parameter in the design of these experiments, especially for adsorption experiments, was the determination of the Ni concentration in experimental aqueous solutions. Isotope analyses require a minimum Ni concentration of 100 ppb, this requires 600 ng of Ni in total when taking into account the replicates. Adaptations had to be made relative to the Ni

concentration in the aqueous solution used in previous Ni adsorption studies to ensure having sufficient Ni for analysis.

To choose the best Ni concentration for these experiments, the saturation state of the solution with respect to Ni bearing solids (such as nickel hydroxide and nickel carbonate) were calculated using PHREEQC. According to these calculations, approximately 150 ppb of Ni in solution would be required to reach saturation of these Ni bearing solids. The results of these calculations were tested experimentally by adding different concentrations of Ni into the reactors and measuring the Ni concentration after 24 hours to assess the possible decrease in concentration by either adsorption on the reactor walls or precipitation of Ni complexes. The results of these tests are shown in Table 4.

At pH 8.5, no significant Ni precipitation occurred even with high Ni concentrations. However, at pH 9, only the lowest Ni concentration considered (100 ppb) showed a difference in the Ni concentration that was less than 2%. It is important to note the uncertainty on these measurements is ±2%. Based on the results from these tests, a Ni concentration of 100 ppb was selected for adsorption experiments (Chapter 3).

Table 5. Test of Ni precipitation due to supersaturation with respect to Ni-bearing solid phases.

pH	$[Ni]_{0\ solution}$ (ppb)	$[Ni]_{end\ solution}$ (ppb)	Difference (%)
8.5	98.4	97.6	0.8
8.5	142.5	139.4	2.2
8.5	193.6	184.3	4.8
9	100.1	98.9	1.2
9	142.5	132.3	7.2
9	190.6	178.2	6.5

2.2.4 Coprecipitation Experiments

2.2.4.1 Determining experimental conditions for coprecipitation experiments

A model of Ni coprecipitation with calcite was created to facilitate the determination of experimental conditions that would optimize these experiments, not only with respect to run duration but to also ensure the amount of Ni in the samples was sufficient for isotopic analysis and

within the range of AAS measurements to facilitate the concentration measurements. To find the precipitation rate, first the saturation state (Ω) of the solution with respect to calcite must be computed. It is found through:

$$\Omega = \frac{a_{Ca} * a_{CO3}}{K_{sp\ calcite}} \quad (15)$$

where $K_{sp\ calcite}$ is the solubility product of calcite ($10^{-8.48}$) and a_i is the activity of the *ith* ion calculated at a given time step according to the concentration of the ion of interest.

With this information, the precipitation rate at a given time step can be calculated from:

$$R = k * (\Omega - 1)^n \quad (16)$$

where k is the rate constant ($10^{-6.38}$ mol m^2 s^{-1}) and n is a reaction order determined by fitting experimental data to this equation.

After the amount of calcite precipitated is calculated, the new Ca and carbonate concentration in the solution can be determined and used as an initial concentration for the next time step. This process can be repeated until the aqueous fluid concentration remains constant, denoting the attainment of steady state (SS) conditions. The concentration of Ni in solution was then calculated using a partition coefficient D_{Ni} = 1 (Lakshtanov and Stipp, 2007) which determined the amount of Ni that gets incorporated into calcite and how much remains in solution. The Ni concentration corresponding to this SS was added to the reactor at the start of the experiment, just before pumping began, to decrease the time required to reach SS conditions.

2.2.4.2 Ni concentration in rectors

For coprecipitation experiments, the saturation state of the fluid with respect to Ni-bearing solids susceptible to precipitate was < 1 because these experiments were run at a lower pH (about 6.2) than the adsorption experiments. Note the solubility of $NiCO_3$ and NiOH increases with

decreasing pH of the solution. However, metals are known to inhibit the growth and dissolution rates of calcite (Meyer, 1984; Takasaki et al., 1994; Ghizellaoui and Euvrard, 2008), and for this reason, the concentration was kept as low as possible while taking into account requirements of the isotope measurements. Additionally, efforts were made to limit the concentration of Na in the aqueous fluids. A mass of more than 2.5 mg of a 0.2 M NaCl solution would exceed the resin capacity during ion exchange chromatography. Thus, 2.5 mg of solution must contain at least 600 ng of Ni.

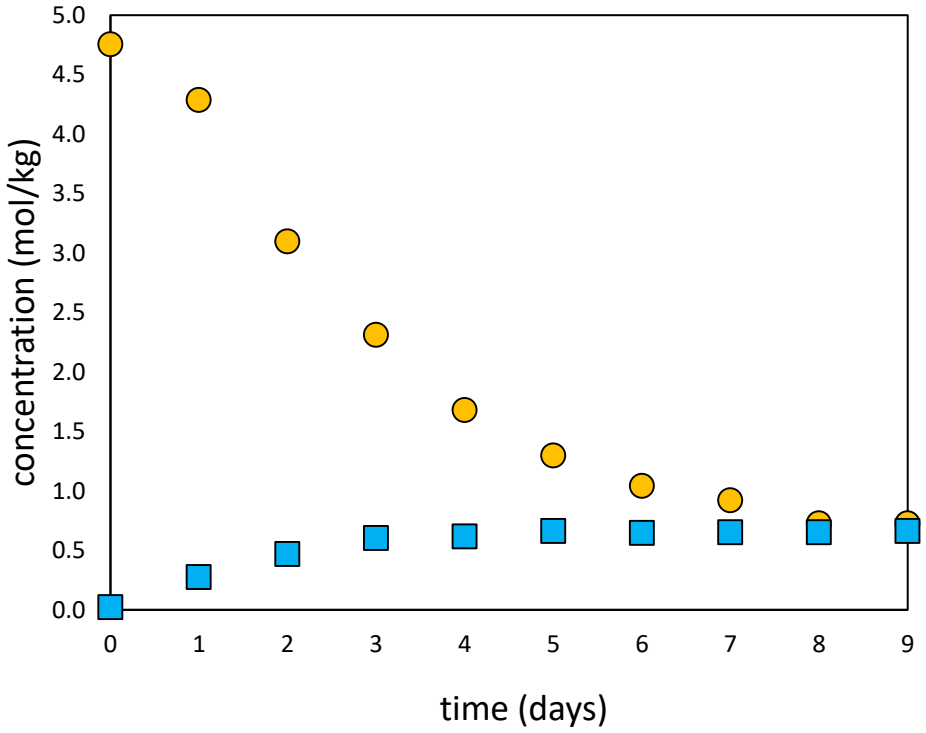

Figure 12. Results of C15 and C16 Ni co-precipitation experiments started without and with Ni in the reactor at the beginning of the experiment. Blue squares correspond to experiment C15 where no Ni was present in reactors at the beginning of the run. Orange circles represent experiment C16 where Ni was added to the reactor prior to the beginning of the run.

Another consideration is the time required to reach SS with respect to the aqueous Ni concentration. The experimental run time is controlled by the difference between starting Ni concentration and SS concentration and the precipitation rate of the solid. To decrease run time of experiments, a test was performed in order to study the effect of starting the experiments with Ni

in the reactor and time required to reach steady state as well as Ni isotopic composition at the end of experiments. Two parallel experiments were run under identical conditions, with the exception of the initial concentration of Ni in the reactor. Experiment C15 had no initial Ni while experiment C16 contained about 5 ppm Ni. The concentration of Ni in both cases evolved until reaching a final steady state value of about 0.7 ppm (Fig. 12). The difference observed between these two runs was that in the experiment where initial Ni concentration in the reactor was closer to the final concentration attained a steady state in a significantly smaller time. Experiment C15 which started with no Ni in the reactor attained steady state conditions in 4 days whereas experiment C16 which started at 4.7 ppm required 9 days.

From this data, it can be inferred that the steady state aqueous Ni concentrations are not affected by initial Ni conditions in the reactor. However, the time required to attain chemical SS is significantly influenced by Ni concentration at the start of experiments. As for isotopic composition, there is no difference, within uncertainty, between Ni isotope compositions of the aqueous fluids (Fig. 13) at the conclusion of the experiments.

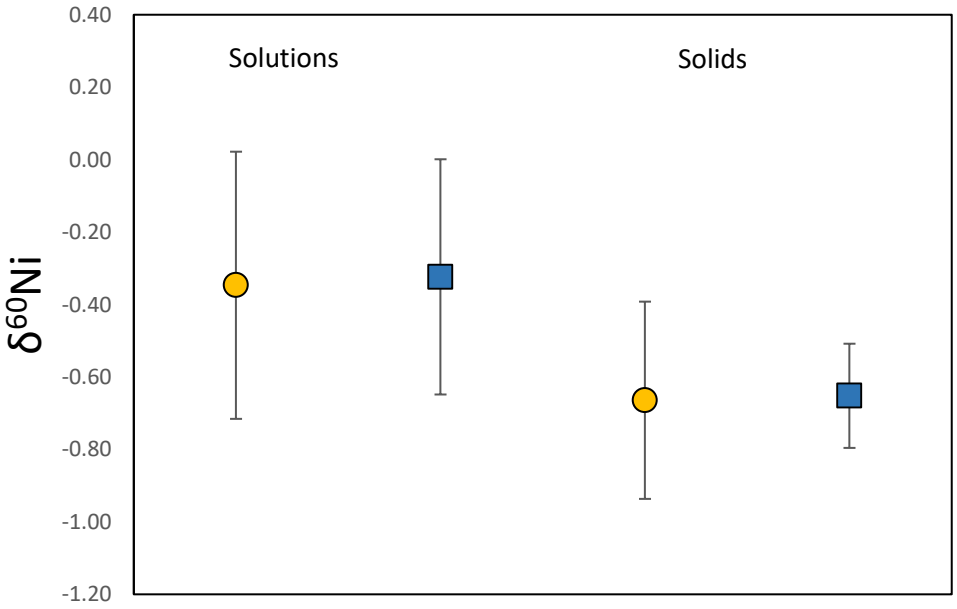

Figure 13. Comparison of isotopic compositions of solids and solutions recovered from coprecipitation experiments C15 and C16. Blue squares represent experiment C15 and orange circles represent C16.

The tests performed show that there is no significant effect of adsorption on calcite on the co-precipitation process when the experiments are started with Ni in the initial aqueous solution. Both the chemical and isotopic compositions of experiments C15 and C16 are essentially the same at the conclusion of these experiments. This suggests that experiments can start at near SS Ni concentrations to significantly reduce their duration. This was done for runs with calcite precipitation rates slower than $R_p = 9.80x10^{-9}$ mol m^2 s^{-1}. As an example, experiment C29 was started with 1 ppm Ni in the reactor and reached steady state conditions within 14 days. If it had been started without Ni, according to the modeled simulation (described in section 2.2.4.1) it would require more than 40 days to attain SS (Fig. 14).

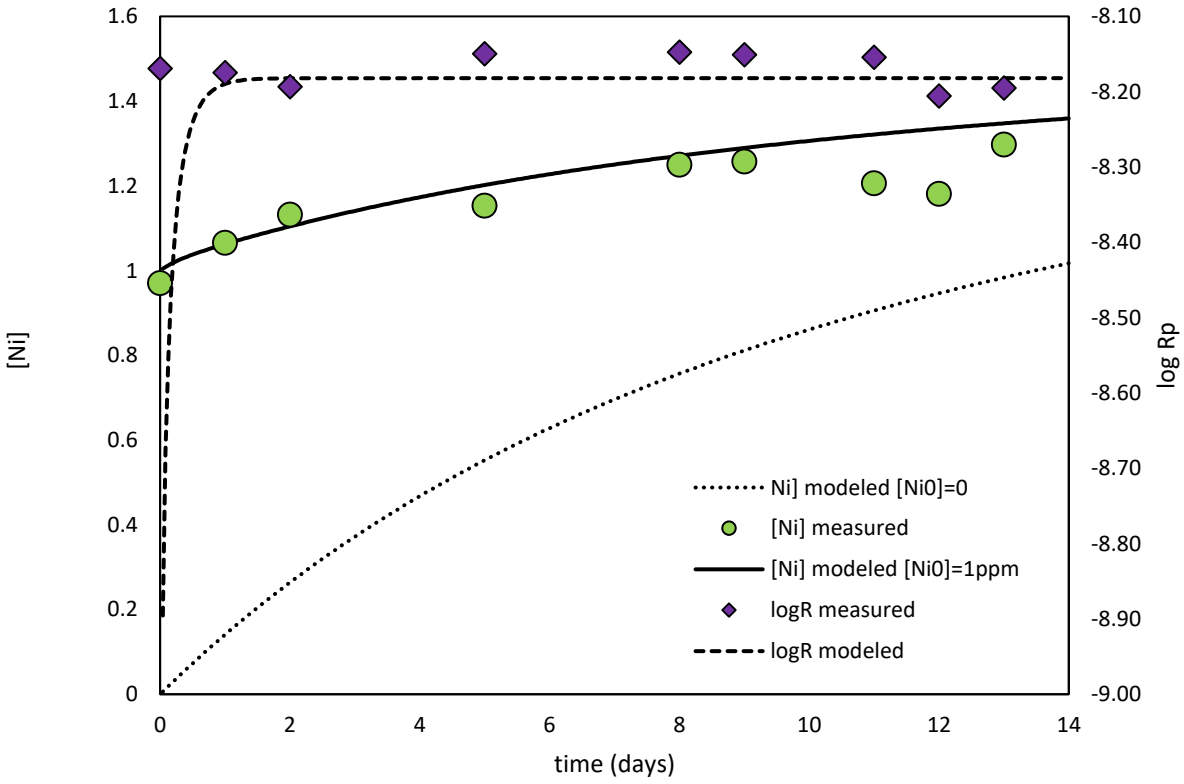

Figure 14. Comparison of results of coprecipitation models with experimental data obtained for experiment C29. The dashed line represents the modeled precipitation rate for experiment C29 and purple diamonds show measured precipitation rates. The modeled concentration of Ni in the reactor at a given time is shown by the a) the solid line when starting with 1 ppm Ni in the reactor and b) the dotted line if no Ni was

present in the reactor at the beginning of the experimental run. Green circles show measured Ni concentrations for experiment C29.

2.3 Experimental protocol

2.3.1 Adsorption experiments

Three series of adsorption experiments were performed in this study. Each series consisted of a set of individual batch reactors that were run with a selected set of fluid compositions (pH or Ni concentration) or time durations. Individual batch reactors were used so the complete fluid and solid could be sampled from the reactor at a selected time and analyzed for their compositions. The first series was carried out with constant pH and varying Ni concentrations to obtain a sorption isotherm. A second series was performed where pH and Ni concentration were kept constant and each reactor was sampled at a different time. A third series was carried out in which pH was varied at a constant Ni concentration. All experimental series consisted of individual experiments where 30 g of fluid and 1- 1.5 g calcite suspensions were kept at an ionic strength of 0.01M NaCl under atmospheric pCO_2 and a temperature of 25°C.

2.3.2 Coprecipitation experiments

Prior to the beginning of the experiments, the PC reactors, stirrers and any other plasticware used for coprecipitation experiments were cleaned with 1N HCl. The peristaltic pump tubes were cleaned by circulating HCl and then MQ H_2O in the system during a 24 hour period.

Ni coprecipitation with calcite experiments were performed in mixed flow rectors using the constant addition method described in Tesoriero and Pankow (1996) with a few adaptations. This technique involves the addition of 2 separate solutions; one solution contains aqueous Ni and Ca ions while the other solution contains carbonate ions. Mixing of the two solutions in the reactor leads to calcite supersaturation in the fluid and results in the growth of calcite. Precipitation rates were modified by varying the flow rate and molarities of the inlet solutions as well as the amount of calcite seed material.

The initial solution in the reactor was pre-equilibrated with calcite. Afterwards, this solution was added to the reactors along with the calcite seeds. This solution and the calcite were then

allowed to re-equilibrate overnight while bubbling CO_2 in the reactor. In some cases, right before the start of the experiment, a small aliquot of 10,000ppm Ni was added to reach the modeled steady state Ni concentration (see above).

The molar concentrations of the inlet solutions ($Ni/CaCl_2$ and $NaCO_3$) ranged from 0.06 to 0.2 mol/kg. The NaCl concentration of the inlet fluids was adjusted to maintain the ionic strength constant and equal to that of the original reactive fluid. The two inlet solutions were pumped at equal flow rates using the peristaltic pump.

The amount of aqueous solution in the reactor was kept constant by removing a volume equal to the one added since the last sampling occurred. Pumping of the input solution continued until steady state was reached. At that point, the addition of Ca and carbonate by pumping was the same that precipitated as calcite and therefore the composition of the aqueous solution in the reactor remained essentially constant. This was confirmed by regularly measuring pH, Ca, Ni, and alkalinity concentrations.

The temperature in the reactors was kept at 25ºC +/- 2ºC by immersing them in a Fisher thermostatic bath. The calcite powder was held in suspension using a Teflon floating stirrer to prevent grinding of the calcite against the bottom of the vessel. To minimize evaporation in long-term experiments, CO_2 gas was passed through a 0.2 M NaCl solution before bubbling it in the reactor.

2.3.2.1 Sampling

To minimize the removal of calcite from the system stirring was stopped a few minutes prior to aqueous fluid sampling in order to allow solid material to settle. pH was measured in situ with fluid filtered through a 0.22 µm Merck Millipore Teflon syringe filter. Three sub-samples were taken for alkalinity, dissolved element concentration, and isotopic compositional analysis. All fluid samples were acidified shortly after sampling using double distilled HNO_3 (for samples to be measured by AAS) or HCl (for samples to be prepared for isotopic analysis).

2.4 Chemical analysis

2.4.1 Alkalinity and pH

The alkalinity of the fluid samples was measured soon after sampling via 0.05 M HCl acidimetric titration using a Schott TA 10 plus volumetric automatic titrator. The measurements were performed following the Gran method (Stumm, 1996) and had an uncertainty of ±1% with a detection limit of 5×10^{-5} eq/l.

The pH of fluid samples was measured using a standard Mettler Toledo glass pH electrode calibrated before every measurement using Thermo Fisher buffers (pH=4.006, 6.865, and 9.183 at 25°C). In adsorption experiments, the pH was measured immediately after sampling while stirring the aliquot reserved for this purpose. In coprecipitation, experiments pH measurements were performed in situ. The buffers used for electrode calibration were kept in the same thermostat bath as the reactors to obtain a more accurate temperature correction.

2.4.2 Ca and Ni concentration measurement

2.4.2.1 Atomic absorption spectrometry

Calcium and nickel concentrations of fluids were measured by Atomic Absorption Spectroscopy (AAS). There are two types of AAS analysis depending on the method used for adding thermal energy to a sample: flame and graphite furnace. In flame AAS, the sample is absorbed by a nebulizer that transforms it into an aerosol. The flame generated by the combustion of air and acetylene atomizes elements contained in the aerosol. Excitation of the atoms is performed using a cathode lamp that contains the element and produces a luminous spectrum; light from this lamp is divided into a measurement and a reference beam. When a sample passes through the flame, the atoms of the analyzed element absorb the energy of the beam. This absorbance is the difference between the energy of the measurement beam and that of the reference beam. The absorbance is then converted into concentration by the Beer–Lambert–Bouguer law (Beer, 1852) that relates attenuation of light to properties of the material. In graphite furnace AAS, the process is similar but a graphite tube with a strong electric current is instead used to heat a sample.

The flame AAS has the advantage of being more rapid as the furnace can measure lower elemental concentrations. Additionally, modifiers can be added which react with an interfering substance in the sample to make it more volatile than the element to be analyzed. The volatile

component vaporizes at a relatively low temperature and is removed during low and medium temperature stages of the electrothermal atomization.

2.4.2.2 Ca and Ni concentrations for the coprecipitation experiments

Ca and Ni concentrations collected from the coprecipitation experiments were measured by flame AAS using a Perking Elmer AAnalyst 400. The uncertainty of these measurements is ±2%.and the detection limit is 7×10^{-7} mol/kg. Measurements were performed in the range of 0.5 to 5 ppm. Standards were prepared using a Ca standard at 1000 ppm and an aqueous 2% HNO_3 solution for dilution. This solution was also used to dilute the collected experimental samples so that their concentration fell within the measurement range. Since this required a sample dilution factor of 200, matrix effects became negligible. This was confirmed by measuring Ca solutions of a known concentration in the presence of all matrix elements and comparing them with a calibration made with standards prepared with only HNO_3 and Ca. Lanthanum oxide was added to samples and standards to reach a final concentration of 0.409g/L in order to avoid anionic chemical interferences.

Ni samples were diluted using 0.2 M NaCl diluted into 2% aqueous HNO_3. Standard solutions were prepared using the same matrix concentrations ranging from 0.2 to 2 ppm. The instrument used for all analyses was a Perking Elmer AAnalyst 400

2.4.2.3 Adsorption experiment Ni measurements

For adsorption experiments, an AAS graphite furnace was used to measure the lower Ni concentrations. Standards were prepared fresh prior to each measurement with a range of 10-100 ppb using an aqueous 5% HNO_3 solution as a matrix. For all of these measurements, samples were measured undiluted. An aqueous 0.05 M NH_4Cl solution was used as a matrix modifier to counter the effects of NaCl in samples.

2.4.3 Isotope analysis

2.4.3.1 Sample preparation

Liquid samples were prepared for purification by ion exchange chromatography by first evaporating them to dryness in perfluoroalkoxy alkanes (PFA) vials on hotplates. Next, the dry residuals were dissolved into in 2 M aqueous HCl. For solid samples, 2 subsamples were first taken for XRD and SEM analysis while remaining solids were dissolved in 4 M HCl to avoid possible Ni isotope heterogeneities.

For the solids, a calcium fluoride precipitation step was additionally performed. This step was necessary to reduce the mass of ions, and in particular, Ca loaded onto the columns and avoid surpassing the resin capacity. To remove these Ca cations, they were precipitated as CaF_2 by adding hydrofluoric acid (HF) to the fluids bearing the dissolved solid samples. To do this, chloride in the fluids was replaced by fluorides by taking up the sample in 5 mL 1 M HF, evaporating it, and then repeating this step. Samples were centrifuged for 10 minutes at 4500 rpm and afterwards, the supernatant was placed in a teflon beaker. Then, 2 mL of MQ water were added to centrifuge tubes and the centrifugation process was repeated, adding the supernatant to the same teflon beaker. Finally, samples were evaporated and taken up in 2 M HCl.

2.4.3.2 Sample purification

Nickel needs to be separated from most other matrix elements prior to isotope analysis. All Ni purification work was carried out in a clean lab environment under a laminar flow hood and high purity reagents were used. Nickel purification was performed using a 5 step procedure modified from that of Quitté and Oberli (2006) which is summarized in table 5. In ion exchange chromatography, a resin is used to remove dissolved ions from solution. This is a reversible reaction where ions attach to functional groups of the resin replacing those that have a lower affinity for these sites. This affinity for the resin depends on the partition coefficient of the compound in a given fluid.

Steps 1 and 2 require the anion exchange resin AG 1-X8 (from Bio-Rad). During these steps, Fe and Zn, the main isobaric interferences for Ni, are removed. The removal of Fe and Zn can be performed in a single step; however, it is necessary to perform the separation in 2 steps in order to optimize the separation of such elements since maximal values for the distribution coefficients of Fe and Zn correspond to different HCl concentrations (Quitté and Oberli, 2006).

Step 3 is performed using a Triskem Nickel specific resin which is based on the complexation of Ni with Dimethylglyoxime (DMG) in order to form Ni-DMG. Step 4 uses the cation exchange resin AG50W-X8 (Bio-Rad) to purify the sample. Step 5, the final step, uses the AG1-X8 anion exchange resin to remove Fe introduced during the separation process, including the use of the Nickel specific resin from the 3rd step.

In more detail, columns were prepared for the step 1 by adding 1.8 mL of pre-cleaned chloride form (200–400 mesh) 1.8 mL AG1-X8 anion resin to an acid-cleaned 10 mL polypropylene column (from Bio-Rad). The resin was then cleaned with alternating between 6 N HCl and MQ water and then conditioned with 10 mL of 9 M HCl. Samples were loaded in 2 mL 9M HCl. In HCl media, Ni elutes immediately while Fe is retained. Ni is recovered in Teflon beakers and 4 more mL of 9 M HCl are used to assure complete recovery. The recovered elution fractions were then evaporated and taken up in 2 mL 2 M HCl. It should be noted that step 2 entails the same procedure as step 1 but replaces 9 M HCl with 2 M HCl.

Step 3 requires a Triskem Nickel specific resin that is based on the formation of Ni-DMG. Since DMG elutes in acids, it is compulsory to ensure that all reagents introduced in the columns have a pH between 8 and 9. For this same reason, the Ni- specific resin must be discarded at the end of the procedure, after the resin is exposed to nitric acid.. 2mL of this resin are placed in 10 mL Bio-Rad columns and washed with 10 mL H_2O and 10 mL of ammonium citrate ($(NH_4)_3C_6H_8O_7$). Next, it is conditioned using 5 mL 0.2 M $(NH_4)_3C_6H_8O_7$. The sample is then loaded into 1 mL 1 M $(NH_4)_3C_6H_8O_7$ and 5 mL 1 M HCl. The resin is washed with 20 mL 0.2M $(NH_4)_3C_6H_8O_7$ and Ni is finally recovered using 12 mL 3 M HNO_3. In order to break the DMG complex, a few drops of perchloric acid are added into recovered Ni and then it is evaporated. Afterwards, 1-2 oxidation steps take place using 1 mL HNO_3 and 1 mL H_2O_2. The purpose of this step is to get rid of organic matter.

Step 4 is a purification step. It requires 0.15 mL of the Bio-Rad AG50W-X8 anion resin. The resin is washed with H_2O and conditioned using 0.7mL of H_2O. The sample is then loaded in 0.2 mL H_2O and afterwards, the resin is cleaned with 2.5mL of 0.2 M HCl. The elution of Ni takes place with the addition of 0.5 mL 3 M HCl.

Step 5 is necessary to remove Fe introduced during the Ni specific step (step 3) and it follows the same procedure as described in step 1. The only difference from step 1 is that the

molarity of HCl used for conditioning the resin, loading the sample, and Ni elution was 6 M instead of 9 M. At the end of this step, samples were evaporated to dryness and then stored in Teflon beakers until they were ready for analysis.

Table 6. Summary of the Ni purification process

	reagent	volume (mL)
Col. 1		
resin	AG1-X8	2
condition	2M HCl	10
load	2M HCl *	2
Ni elution	2M HCl	4 (+2)
Col. 2		
resin	AG1-X8	2
condition	9M HCl	10
load	9M HCl *	2
Ni elution	9M HCl	4 (+2)
Col. 3		
resin	Nickel specific	2
condition	0.2M $(NH_4)_3C_6H_8O_7$	5
load	1M $(NH_4)_3C_6H_8O_7$ +1M HCl	1+5
clean matrix	0.2M $(NH_4)_3C_6H_8O_7$	20
Ni elution	3M HNO_3	12
Col. 4		
resin	AG50W-X8	0.15
condition	H_2O	0.7
load	H_2O	0.2
clean matrix	0.2M HCl	2.5
Ni elution	3M HCl	0.5
Col. 5		
resin	AG1-X8	2
condition	6M HCl	10
load	2M HCl *	2
Ni elution	2M HCl	4 (+2)

* Ni elutes during this step

2.4.3.3 Measurements

Nickel isotope measurements were performed in collaboration with Dr Ghylaine Quitté at the Observatoire Midi-Pyrénées (OMP) analytical platform in Toulouse using a Thermo-Fischer Neptune multi-collector inductively coupled plasma mass spectrometer (MC-ICPMS) and at École Normale Supérieure (ENS) in Lyon using a Thermo-Fischer Neptune Plus MC-ICPMS.

In MC-ICPMS analysis, samples are introduced into the inductively coupled plasma as a fine aerosol. This can be achieved by nebulization of a solution or by laser ablation of a solid. The plasma then strips off their electrons to create positively charged ions. These ions are accelerated across an electrical potential gradient and focused into a beam through a series of slits and electrostatically charged plates. After it passes through an energy filter it results in an energy spectrum in the ion beam and then travels through a magnetic field where ions are separated according to their mass to charge ratio. These mass-resolved beams are then directed into collectors where ions are converted into voltage and then isotopic ratios are calculated by comparing the voltage measured in different selected collectors.

The sample residue from the ion exchange chromatography was taken up in 0.1 M HCl before passing through the mass spectrometer. Samples were measured in medium resolution mode which allows for full resolution of interferences such as $^{40}Ar^{18}O^{+}$ on mass 58 and $^{40}Ar^{20}Ne^{+}$ or $^{38}Ar^{22}Ne^{+}$ on mass 60. Measurements were performed using the sample-standard bracketing technique and Cu doping. Sample-standard bracketing allows normalization of the measurements to that of a δ-zero standard so that the relative difference between solutions can be obtained. Cu doping is used to correct for instrumental mass fractionation. Since Cu and Ni behave similarly, the deviation from the true isotopic composition of Cu can be calculated and it can be assumed to be the same as for Ni and therefore the same correction can be applied to the Ni values.

The concentration of the measured samples varied between 50 and 200 ppb, and the Cu concentration was kept at half that of Ni. The concentration of Ni and Cu in the standard matched that of the sample. Samples were measured in 2 cycles. During the 1st cycle, Ni isotope masses were measured (58, 60, 61, 62 and 64) along with masses 57 and 66 which are used for correcting for possible isobaric interference from ^{58}Fe and ^{64}Zn, respectively. During the 2nd cycle, Cu isotopes were measured and used to correct for instrumental mass bias.

2.4.3.4 Validation of the chemical separation procedure

Standards were processed with every batch of samples to ensure that no fractionation occurred during the Ni separation process. Two standards were used for this purpose, a Sigma Aldrich Ni standard that was also used as a bracketing standard and an ICP mono element standard solution. Their original composition is plotted next to the average composition of processed standards in Fig. 15. Standards were processed and measured in the same way as the samples. The

Sigma Aldrich standard was also added to a 0.01 M $CaCO_3$ saturated solution and the 0.2 M NaCl matrix to replicate the experimental matrix and ensure the proper separation of Ni from matrix elements. This was particularly important for Na, used as a background electrolyte, since the elution profile of Ni and Na are very close.

A blank for the ion exchange chromatography was prepared for every set of samples processed. They were measured using an Agilent 7700 quadrupole ICP-MS. The analytical error associated with these measurements is estimated to be ± 5%. The measured blanks vary between 0.85 and 1.93 ng of Ni, which is negligible compared to the samples which contained at least 600 ng.

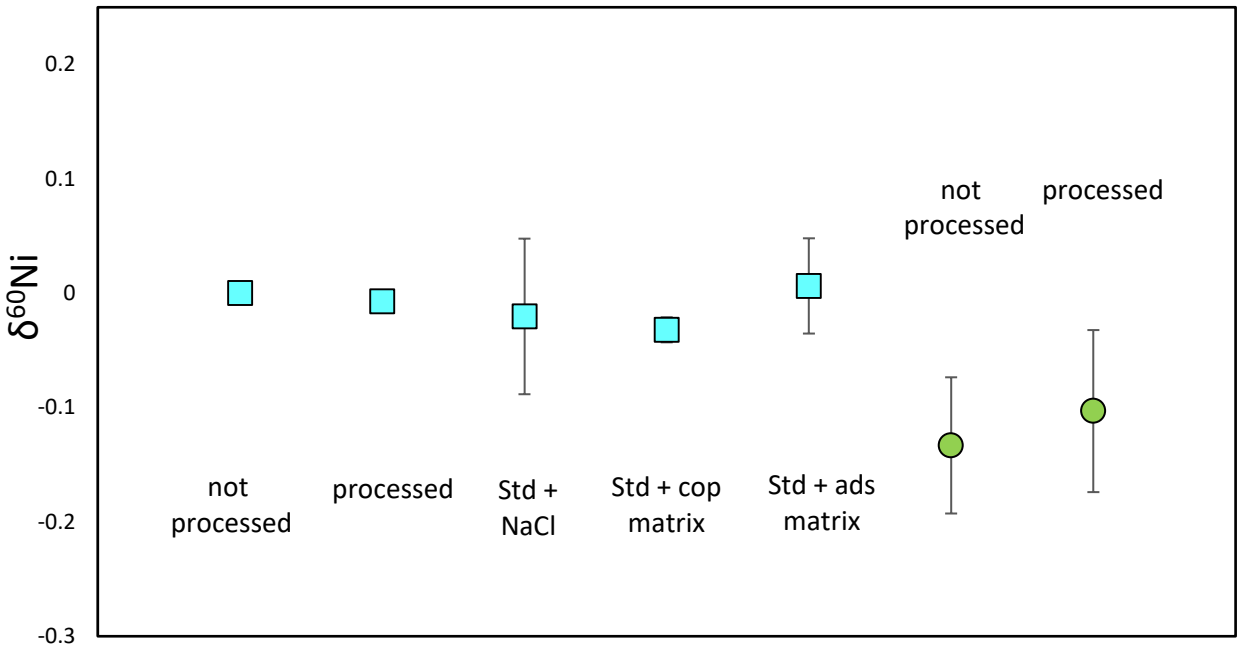

Figure 15. Ni standards. Unprocessed standards were directly measured while the processed standards were treated via the ion exchange chromatography process (without the addition of an experimental matrix). 'NaCl processed' represents the standard processed with the addition of NaCl. 'ads processed' refers to the standard processed with the addition of the matrix used in adsorption experiments. 'cop' exhibits the standards run during measurement of the coprecipitation experiments. A second standard is represented by the green circles, showing the composition of processed and not processed standards.

Chapter 3. Ni isotope fractionation during adsorption on the calcite surface

3.1 Introduction

3.1.1 Ni isotope imbalance in the ocean

Input sources of Ni into the ocean are continental river water and atmospherically transported dust dissolution. The major Ni sink in oceans is particle scavenging—the adsorption of an element onto particles and eventual burial (Goldberg, 1954), sedimentation, and geothermal activity. (Sclater et al., 1976; Jeandel and Oelkers, 2015)

The oceanic Ni isotope budget is not yet well constrained. Rivers are the main input of Ni into the ocean. Rivers have a composition of + 0.80‰ while the composition of seawater is 1.44 ± 0.15‰ (Cameron and Vance, 2014). This shows seawater is more enriched in the heavier Ni isotopes than river water and suggests a missing source for heavy nickel isotopes or a missing sink of light Ni isotopes.

It has been speculated that, since they are a major sink for Ni in the ocean (Peacock and Sherman 2007), Ni onto Fe/Mn oxide surfaces may affect seawater isotopic composition. Experimental work documents that Ni sorption onto ferrihydrite favors uptake of its lighter isotopes (Wasylenki et al., 2015; Gueguen et al., 2018) thereby leaving an isotopically heavier residual Ni in the fluid. However, the characterization of natural samples shows that the Ni isotope composition of this mineral reflects its Ni seawater composition (Gall et al., 2013). Thus it is not a major source for light Ni isotope removal from the oceans. It is possible that processes like adsorption and coprecipitation of Ni with other minerals, such as calcite, can help explain the removal of light Ni isotopes from the ocean.

3.1.2 Ni adsorption on calcite

Ni adsorbs on calcite by the formation of $NiCO_3$(s) surface complexes (Stipp et al., 1994; Hoffmann and Stipp, 2001). The ions on the calcite surface and the Ni surface complexes remain as partly hydrated and exchangeable until they are incorporated into the calcite structure by recrystallization. (Zachara et al., 1991). The single ion hydration energies of the metal sorbates is also a good approximation for the sorption reversibility of metals given the good correlation found by Zachara (1991).

Ni adsorption takes place by the formation of $NiCO_3(s)$ surface complexes according to the following mechanisms:

1) direct interaction with CO_3 surface sites, which represents about 80% of the Ni interaction:

$$>CO_3H + Ni^{2+} \leftrightarrow >CO_3Ni^{+} + H^{+} \quad (17)$$

2) exchange with Ca at the calcite surface, which is less than 20% of the Ni interaction:

$$>CO_3Ca^{+} + Ni^{2+} \leftrightarrow >CO_3Ni^{+} + Ca^{2+} \quad (18)$$

Most of the studies of Ni adsorption on calcite focus on time of contact with and pH of the fluid. The reason behind it is that Ni adsorption on calcite is considered to be strongly pH dependent (Zachara et al., 1991; Belova et al., 2014). This is similar to other divalent metals where fractional sorption of Me^{2+} increases with increasing pH (Lorens, 1978; McBride, 1980; Davis et al., 1987; Zachara et al., 1988; Zachara et al., 1991). Kinetic experiments show that Ni adsorption is nearly complete within a few hours (Zachara et al., 1991; Lakshtanov and Stipp, 2007; Belova et al., 2014). Nickel, like other Me^{2+}, exhibits an initial fast adsorption followed by slower uptake into the mineral structure by coprecipitation or recrystallization. The first step consists of a fast initial uptake due to ionization of surface hydroxyl groups and is usually complete within a few minutes. During the second step, the equilibrium sorption density is approached asymptotically through structural changes.

3.1.3 Isotope fractionation during adsorption

Analyzing metal isotope ratios in aqueous solution and that sorbed onto mineral surfaces allows for the determination of the fractionation factor associated with sorption (Wiederhold, 2015). Fractionation during sorption is mostly governed by differences in the coordination environment between the dissolved and sorbed element (Wasylenki et al., 2011) or the identity of the solution species sorbing to the surface (Jiskra et al., 2012).

Isotope fractionation between the major aqueous species present in solution has been investigated using ab initio calculations and experimental techniques (Fujii et al., 2011; Fujii et al., 2014). These studies show that isotope fractionation within aqueous species correlates to the bond length of these species. Generally, aqueous species that have lower coordination numbers have shorter bond lengths and preferentially incorporate the heavier isotopes of an element (Schauble, 2004; Zeebe, 2005; Fujii et al., 2013; Bogatko et al., 2013; Colla et al., 2013; Huang et al., 2014).

A number of past studies have measured Ni fractionation as it adsorbs onto mineral surfaces. Wasylenki et al. (2015) determined $\Delta^{60}Ni_{ferrihydrite\text{-}fluid}$ to be -0.35 ± 0.10‰. Similarly (Gueguen et al., 2018) reported a near identical $\Delta^{60}Ni_{ferrihydrite\text{-}fluid} = -0.35 \pm 0.08$‰ value. Spivak-Birndorf et al. (2018) reported that nickel isotope fractionation from aqueous solution onto montmorillonite resulted in a $\Delta^{60}Ni_{montrormillinite\text{-}fluid}$ = -0.11 ± 0.09‰. The adsorption of Ni onto goethite has also been reported to yield the greatest fractionation with $\Delta^{60}Ni_{goethite\text{-}fluid} = -0.77 \pm 0.23$‰ (Gueguen et al., 2018).

3.2 Materials and methods

3.2.1 Materials

All solutions were prepared with high purity (>99%) reagents and high purity deionized MQ water (18 MΩ·cm). All acids used in this study were purified by sub-boiling distillation. Prior to starting the experiments, all plasticware was cleaned using 1N HCl for at least 24 hours. The source of Ni was reagent grade nickel nitrate $Ni(NO_3)_2$ dissolved in MQ water.

Synthetic high purity Merck MESURE® calcite was used for all adsorption experiments. Prior to use, it was aged following a procedure based on that of Reddy and Nancollas (1971) and cleaned with acetone. Calcite aging results in a more uniform crystal diameter size. This process involves storing calcite ($CaCO_3$(s)) in 5 L 0.02 M $NaHCO_3$ (aq) at a ratio of 30 g of $CaCO_3$ per kg of aqueous solution and agitating daily for 30 days. After this time it was filtered using a Merck Millipore 0.22 µm PTFE filter and vacuum filter unit that was initially rinsed with acetone and followed by repeated rinsing with MQ water. Solids were then dried at 60 °C for 24 hours. The acetone rinse removes possible organic contamination originating from growth inhibitors used during calcite synthesis.

The aged CaCOs(s) was 100% calcite, as verified by XRD, and had a BET surface area of about 0.28 m^2/g. SEM analysis (Fig. 16) revealed the rhombohedral morphology of the crystals and demonstrated intergrowths. The average length of the crystals was ~ 6 µm.

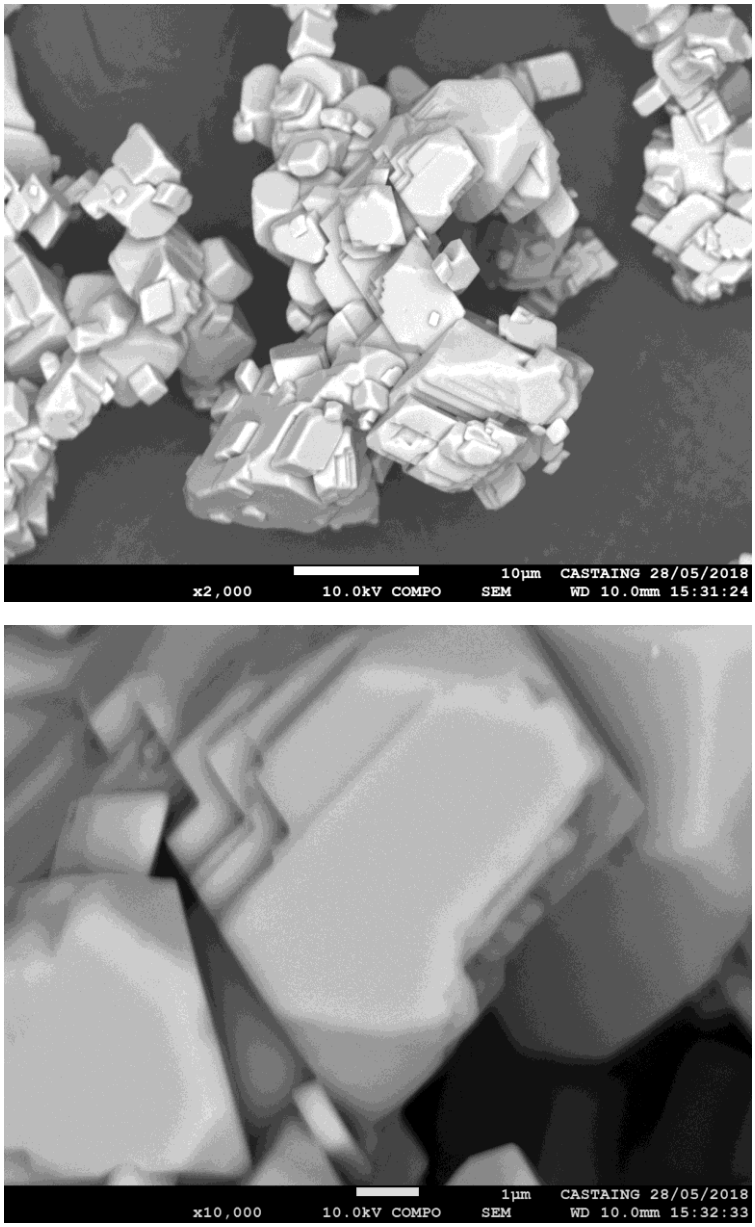

Figure 16. SEM image of aged calcite. They show the rhombohedral morphology of calcite and crystal intergrowth.

3.2.2 Thermodynamic calculations

All aqueous species distribution, fluid saturation states, and chemical activities were calculated using the thermodynamic modeling computer code PHREEQC (Parkhurst and Appelo, 1999). The minteq.v4 database was used after some minor additions of solubility constants (see section 2.2.2).

3.2.3 Adsorption experiments

Three different types of experiments were performed: 1) an experiment with constant pH and varying Ni concentrations to obtain a sorption isotherm, 2) an experiment where the pH and Ni concentration were kept constant and each reactor was sampled at a different time, and 3) an experiment in which pH was varied at a constant Ni concentration. All experimental series consisted of individual experiments where 30 mL fluid/calcite suspensions containing a calcite/fluid ratio of 50 g/kg. The ionic strength of each experiment was kept at 0.01 M NaCl, pCO_2 at 1 atm, and a temperature of 25°C was maintained.

Adsorption experiments were designed to allow sufficient Ni to remain in the aqueous fluid to perform the isotope measurements. This was done by having a high Ni concentration in the fluid phase and avoiding supersaturation with respect to Ni phases which would result in precipitation.

3.2.3.1 Calcite pre-equilibrated solutions

All experiments were run in aqueous solutions that were pre-equilibrated with calcite. These aqueous solutions, which had a total ionic strength of 0.01 M, were prepared using a mixture of NaCl, HCl, and NaOH. They were then allowed to equilibrate with $CaCO_3$(s) in contact with atmospheric CO_2. Their pH was monitored daily and adjusted by using 0.01 M HCl or NaOH if necessary. They were allowed to equilibrate for about 2 weeks, until pH remained stable, showing a variation of no more than 0.05 pH units during 3 consecutive days. After they were kept in contact with $CaCO_3$ until the start of experiments. At this point, they were filtered with a Merck Millipore 0.22 µm teflon syringe filter.

3.2.3.2 Experimental series 1: Adsorption isotherm

Experimental series 5I had the objective of calculating the adsorption isotherm. With this purpose, one gram of calcite and 29.5 g of a prepared aqueous solution were weighed into a

polycarbonate centrifuge tube and allowed to equilibrate for 24 hours. After equilibration, 0.5mL of a Ni solution of the desired concentration were added into the reactor. Different initial concentrations of Ni were used ranging from $6.8x10^{-7}$ to $2.0x10^{-6}$ mol/kg. The reactors were placed in a rotator for 24 hours and at the end of this time, they were centrifuged at 5000 rpm for 15 minutes. The supernatant was filtered using a 0.22 μm teflon syringe filter. An aliquot of this sample was acidified with concentrated HNO_3 to reach a pH of 2 and the stored until it was further analysed. pH was determined immediately after sampling.

3.2.3.3 Experimental series 2: Adsorption as a function of time

Two sets of experiments (3K and 8K) were performed to study time dependence of Ni adsorption on calcite. The first experiment had a duration of 48 hours and focused on the effects of the first few hours of this process. It was performed using a pre-equilibrated aqueous solution having a pH of 9.4 prepared using NH_4Cl 0.1 M as a background electrolyte. The second set had a duration of 7 days and it was run using a pre-equilibrated 0.01 mol/kg NaCl solution at pH 8.3.

1.5 g calcite were weighed into polycarbonate centrifuge tubes along with 29.5 g of a pre-equilibrated aqueous solution at pH 8.3. After they were equilibrated for 24 hours, 0.5 mL of a 6 ppm Ni stock solution was added to reach a final concentration of 100 ppb and a final volume of 30 mL. They were placed on a rotator until sampling. Sampling proceeded in the same fashion as in the adsorption isotherm experiment.

3.2.3.4 Experimental series 3: Adsorption as a function of pH

Adsorption experiments in this series were conducted exactly like those of series 1K. They were performed using a pre-equilibrated 0.01 M NaCl solution with pH ranging from 7.5 to pH 8.6. The concentration of Ni used for all experiments in this series was $1.7x10^{-6}$ mol/kg. Experimental series 6P and 7P were conducted using 33.3 g/L of calcite that was kept in contact with Ni for 24 hours. The experiments run in series 9P were kept in contact with 50 g/L of calcite for 72 hrs.

3.2.4 Determination of Ni concentration in the solutions and solids.

The concentration of Ni in solution was measured by AAS furnace. The amount of Ni adsorbed was determined through mass balance by subtracting amount of Ni measured at the end

of each experiment from that added to the reactor at the beginning of each experiment. This initial Ni concentration was measured by weight and using the concentration of the stock solution measured by AAS.

3.2.5 Determination of the isotopic composition of Ni in aqueous solutions

Sample purification was carried out following protocol described in Quitté and Oberli (2006) with some minor additions resulting in a 5 step Ni purification. Purified samples were then measured on a Neptune ICPMS using standard sample bracketing and Cu doping. Purification and measurement processes are described in detail in Chapter 2. Steps 1, 2, and 5 require the resin AG 1-X8 (from Bio-Rad) to remove Fe and Zn which are main isobaric interferences for Ni. Step 3 is performed using a Triskem Nickel specific resin to remove other matrix elements. Step 4 uses AG50W-X8 (Bio-Rad) to purify the sample.

Nickel isotope measurements were performed at the Observatoire Midi-Pyrénées (OMP) analytical platform in Toulouse France using a Thermo-Finnigan Neptune multi-collector inductively coupled plasma mass spectrometer (MC-ICPMS). Samples were measured in medium resolution mode, using the sample-standard bracketing technique and Cu doping. The concentration of the measured samples varied between 50 and 200 ppb, and the Cu concentration was kept at half that of Ni. Samples were measured in 2 cycles.

A Sigma Aldrich Ni standard was processed through the whole chemical separation procedure with every set of experimental samples to ensure no fractionation occurred during the Ni separation process. No isotope fractionation is observed for the processed standards relative to the corresponding unprocessed standards, thereby confirming the chemical procedure is well suited to study the natural mass dependent isotope fractionation characteristic of our experimental samples. The 2SD (standard deviations) of δ^{60}Ni was calculated based on multiple (typically 3) measurements of each solution and ranged between 0.01 and 0.11‰.

Isotope compositions are presented in delta notation, δ^{60}Ni, corresponding to the ratio of ^{60}Ni relative to ^{58}Ni normalized to the Aldrich ICP standard. The isotopic offset between this metal on the solid and the fluid phase ($\triangle\ ^{60}\mathrm{Ni}_{\ solid-fluid}$) is defined by:

$$\triangle\ ^{60}\mathrm{Ni}_{\ solid-fluid} = \delta^{60}\mathrm{Ni}_{solid} - \delta^{60}\mathrm{Ni}_{fluid} \quad (19)$$

Assuming that loss of Ni from solution was solely caused by Ni sorption on calcite, the average isotopic composition of sorbed Ni during a closed system adsorption experiment can be calculated from the initial and final Ni chemical and isotopic compositions of the fluid and mass balance considerations taking into account (Criss, 1999):

$$\delta^{60}\mathrm{Ni}_{total} m_{\mathrm{Ni},total} = \delta^{60}\mathrm{Ni}_{solid} m_{\mathrm{Ni},solid} + \delta^{60}\mathrm{Ni}_{fluid} m_{\mathrm{Ni},fluid} \quad (20)$$

where $m_{\mathrm{Ni},solid}$ and $m_{\mathrm{Ni},fluid}$ refer to the mass of Ni adsorbed onto calcite and present in the aqueous fluid phase, respectively. It is important to note that $\delta^{60}\mathrm{Ni}_{total}$ and $m_{\mathrm{Ni},total}$ are constant during a closed system reactor experiment.

3.2.6 Determination of the isotopic composition of Ni in the solids

Analyzing the Ni isotopic composition of the solids was difficult due to the fact that at a low adsorption percentage, the amount of Ni in the solid was below the minimum required for measurement. Additional complexity arises from the high desorbability of Ni (Zachara et al., 1991), so it is challenging to process solids at the end of the experiments without avoiding loss of sorbed Ni. On the other hand, by not cleaning them before analysis, contamination from the fluid can be significant due to the small amount of Ni coming from adsorption. Another aspect to consider is Ni contamination incorporated into the bulk during calcite synthesis. Due to these factors, the Ni isotope composition was calculated according to the mass balance equation:

$$\delta_{\mathrm{solid}} = \frac{\delta_{stock\ solution} - \delta_{fluid} * f_{fluid}}{f_{solid}} \quad (21)$$

where δ represents isotopic composition and f represents the fraction of nickel in subscripted phase.

3.3 Results

3.3.1 Ni aqueous speciation

For the pH range of experiments performed, the species present in solution are Ni^{2+}, $NiCO_3$, and $NiHCO_3^+$. Of these species, the main ones are Ni^{2+} and $NiHCO_3$. Ni^{2+} comprises 92 % of Ni at pH 7.6 but only 50 % at pH 8.6. $NiCO_3$ increases in importance from 0 % to about 40 % at pH 8.6 (Fig. 17).

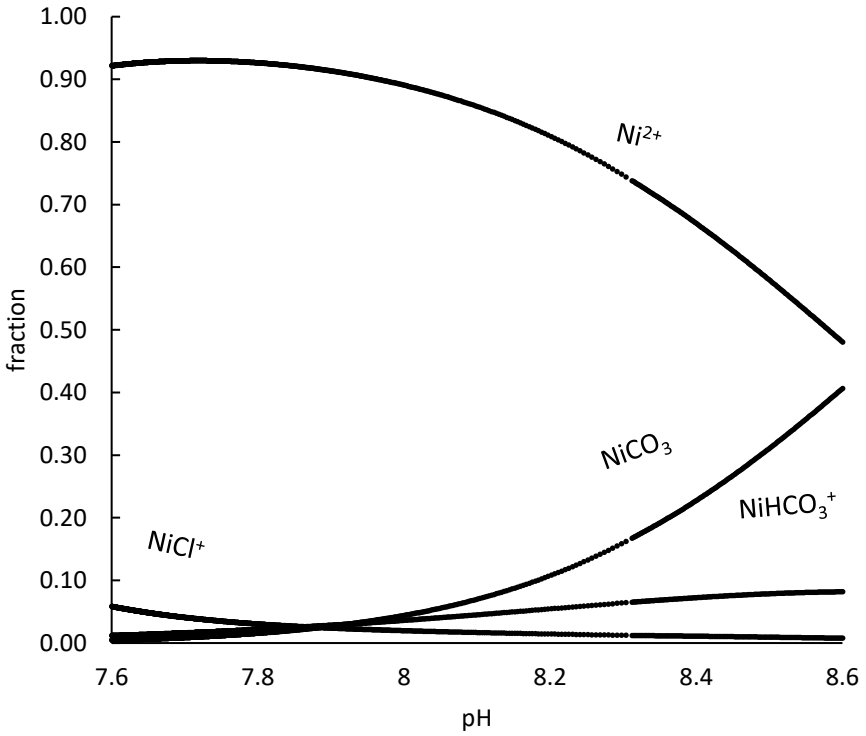

Figure 17. Ni aqueous speciation in a 0.01 M NaCl $CaCO_3$ solution at atmospheric pCO_2. It was calculated using PHREEQC with the minteq.v4 database.

3.3.2 Adsorption isotherm

The results of adsorption isotherm experiments are shown in Table 6 and Fig 18. Table 6 shows concentrations of Ni, a plot of Ni concentration at equilibrium, and concentration adsorbed. The concentration of Ni at equilibrium is plotted against the concentration of Ni adsorbed in Fig. 18. These data can be fitted to a regression line with a slope of nearly 1.

Table 7. Data used to calculate the Ni adsorption isotherm at 25°C and pH 8.3.

Experiment	$[Ni]_{equilibrium}$ *Mol/kg*	$[Ni]_{solid}$ *Mol/kg*
5I-1	1.10E-06	4.09E-07
5I-2	1.14E-06	4.11E-07
5I-3	1.26E-06	5.11E-07
5I-4	1.46E-06	5.21E-07
5I-5	1.58E-06	6.23E-07
5I-6	1.26E-06	5.09E-07
5I-7	1.20E-06	4.84E-07
5I-8	1.20E-06	4.67E-07

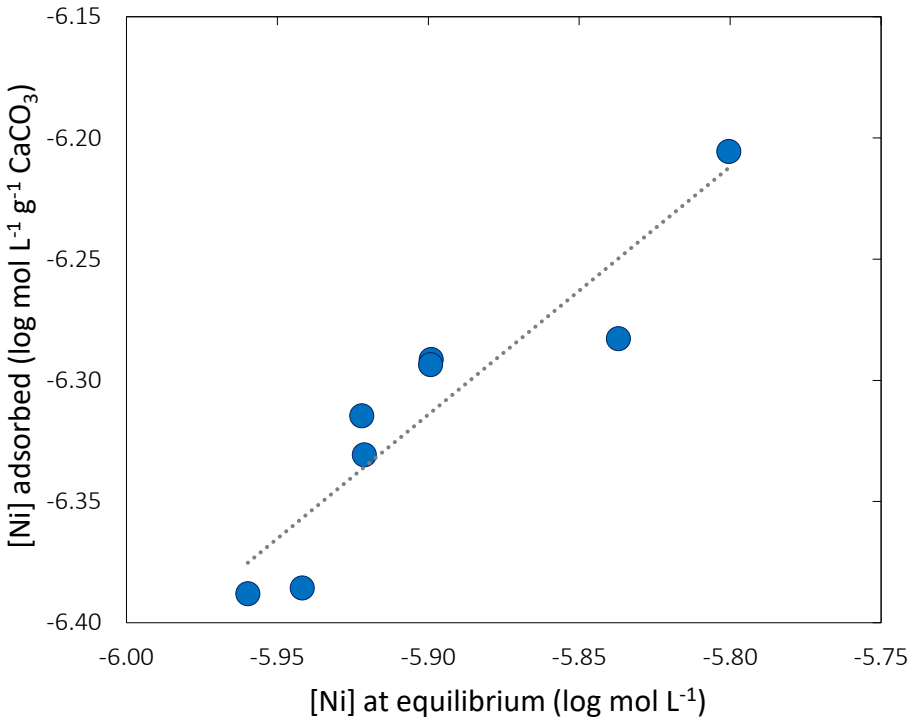

Figure 18. Adsorption isotherm for Ni in 0.01 M NaCl at pH 8.3 and 25°C.

3.3.3 Adsorption as a function of time

Two sets of experiments on adsorption as a function of time were performed using different background electrolytes, pH values, and experimental duration. The results are summarized in Table 7 and Figs. 19-21.

The first experimental series as a function of time (Set 3K, Fig. 19) was performed using 0.1 M NH_4Cl at pH 9.2 as the background electrolyte. A maximum adsorption of 50 % was attained after 24 hours. The maximum duration of this experimental series was 2 days.

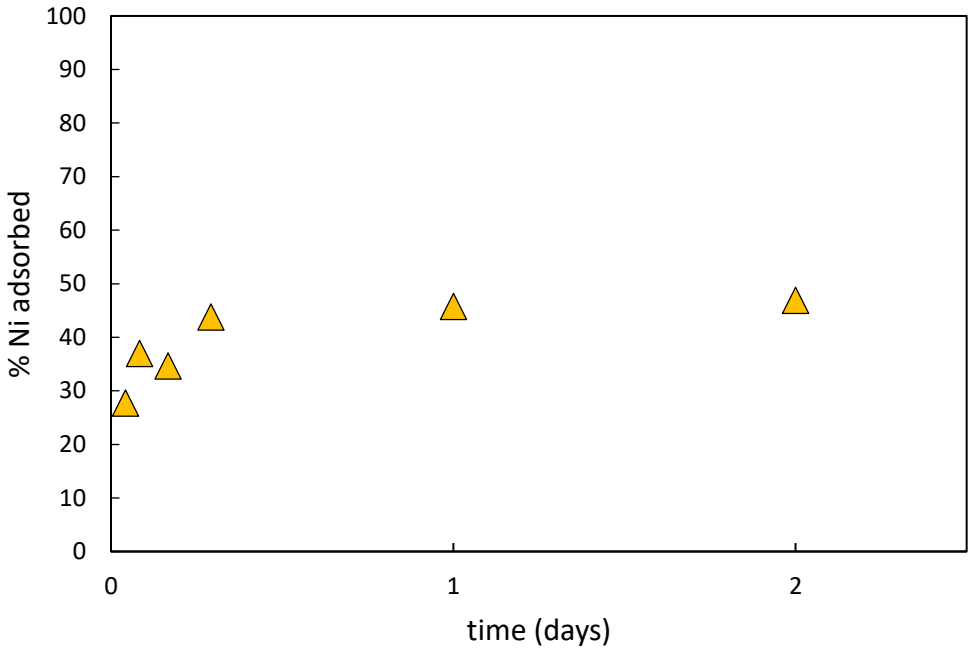

Figure 19. Ni adsorption as a function of time. Series 3K experiments were performed as a function of time using 0.1M NH_4Cl at pH 9.2 as the background electrolyte. The error associated with these measurements is included within the symbol size.

A second experimental series on Ni adsorption as a function of time (Set 8K, Fig. 20) was performed using a solution of 0.01 M NaCl at pH 8.3 pre-equilibrated with calcite as the background electrolyte. In this experiment, the maximum adsorption value reached was 26% after 24 hours. After this time the percentage of Ni adsorbed remained constant between 23.1 and 25.5%.

Some experiments from series set 8K were also analyzed to determine the Ni isotopic composition of the fluids (Fig. 21). The composition of the adsorbed Ni remains constant within analytical uncertainty over time displaying values between -0.93 ± 0.08 and -1.19 ± 0.09 ‰.

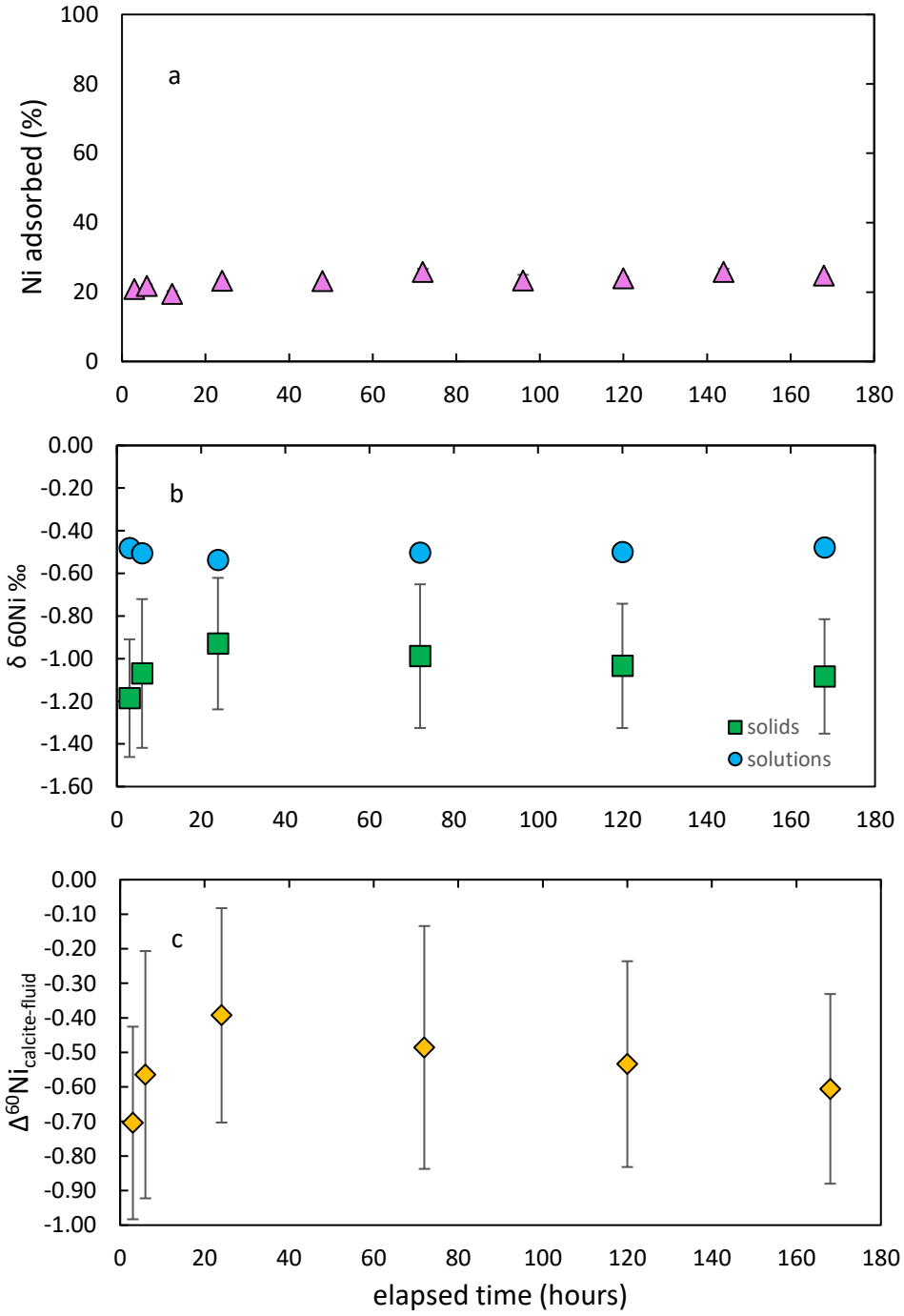

Figure 20. Time dependent adsorption experimental set 8K. The figure shows a) percentage of Ni adsorbed, b) Ni isotopic composition of fluid and adsorbed Ni, and c) fractionation between solid and fluid, as a function of time. The isotopic composition and concentration of adsorbed Ni was calculated via mass balance. Error bars represent 2 standard deviations.

Table 8. Results obtained from experimental series 3K and 8K used to study time dependence of Ni adsorption on calcite

Experiment label	electrolyte	I	pH	time	[Ni] initial	[Ni] final	Ni adsorbed	$\delta\ ^{60}Ni_{fluid}$	2 σ	$\delta\ ^{60}Ni_{solid}$	2 σ	$\Delta_{solid-fluid}$	2 σ
				hours	Ppb	ppb	%	‰		‰		‰	
Series 3K													
3K-01	NH_4Cl	0.1	9.4	4	98.11	90.33	7.8						
3K-02	NH_4Cl	0.1	9.4	8	98.40	86.54	11.9						
3K-03	NH_4Cl	0.1	9.4	12	98.30	83.09	15.2						
3K-04	NH_4Cl	0.1	9.4	24	100.27	85.21	15.1						
3K-05	NH_4Cl	0.1	9.4	48	95.67	79.33	16.3						
Series 8K													
Ni stock solution								-0.63					
8K-01	NaCl	0.01	8.3	3	99.88	79.01	20.9	-0.48	0.04	-1.19	0.28	-0.7	0.28
8K-02	NaCl	0.01	8.2	6	100.11	78.29	21.8	-0.5	0.08	-1.07	0.35	-0.56	0.36
8K-03	NaCl	0.01	8.3	12	100.43	80.79	19.6						
8K-04	NaCl	0.01	8.2	24	100.23	76.91	23.3	-0.54	0.03	-0.93	0.31	-0.39	0.31
8K-05	NaCl	0.01	8.3	48	99.32	76.25	23.2						
8K-06	NaCl	0.01	8.2	72	99.22	73.56	25.9	-0.5	0.1	-0.99	0.34	-0.49	0.35
8K-07	NaCl	0.01	8.2	96	99.17	75.97	23.4						
8K-08	NaCl	0.01	8.2	120	99.00	75.24	24.0	-0.5	0.06	-1.03	0.29	-0.53	0.30
8K-09	NaCl	0.01	8.2	144	98.83	73.27	25.9						
8K-10	NaCl	0.01	8.2	168	99.07	74.47	24.8	-0.48	0.06	-1.08	0.27	-0.61	0.27

3.3.4 Adsorption as a function of pH

To investigate the effect of pH on Ni adsorption on calcite a total of 3 experimental series were performed: 6P, 7P, and 9P (Table 9). The background electrolyte for all these sets was 0.01M NaCl. In sets 5 and 6, 1 g of calcite was used as an adsorbent. In set 9P the amount of adsorbent was increased to 1.5 to obtain a higher percentage of adsorbed Ni. All sets were performed using a distinct Ni stock solution. Another difference between these experimental series is contact time of calcite and the Ni bearing aqueous fluid, which was set to 24 hours for sets 5 and 6 and 72 hours for set 9P.

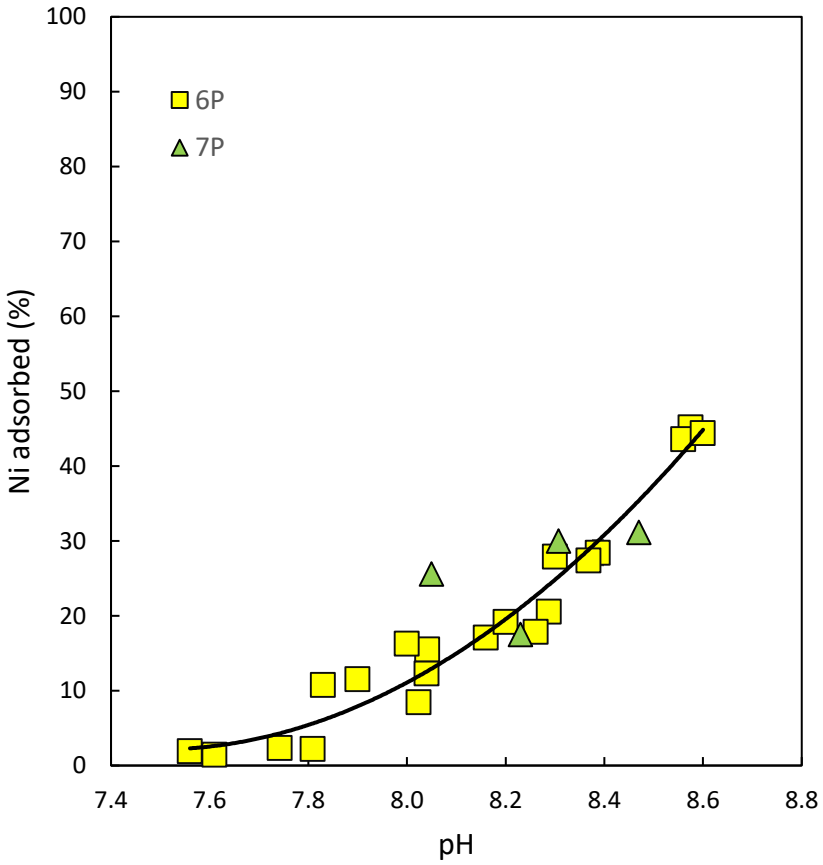

Figure 21. Measured Ni adsorption as a function of pH. squares represent results of series 6P and triangles correspond to results of series 7P. Both experimental series were performed at 25°C and atmospheric pCO_2 using 0.01M NaCl as the background electrolyte.

Experimental series 6P consists of 20 individual experiments whose pH is in the range of 7.7 to 8.6. The percentage of Ni adsorbed increases from nearly 0 to 45.2 percent as the pH increases (Fig. 21). Experimental series 7P consists of 4 experiments with pH values ranging from 8.1 to 8.5 and its corresponding percentage of adsorbed Ni varies from 17.5 to 31.2 (Fig 21). For experimental series 9P, the percentage of adsorbed Ni varied between 9 and 67 % as pH increased from 7.7 to 8.6. The resulting adsorption edge is consistent with all previous work and shows a strong dependence of Ni adsorbed fraction to the pH of the reactive fluid (See Fig 22).

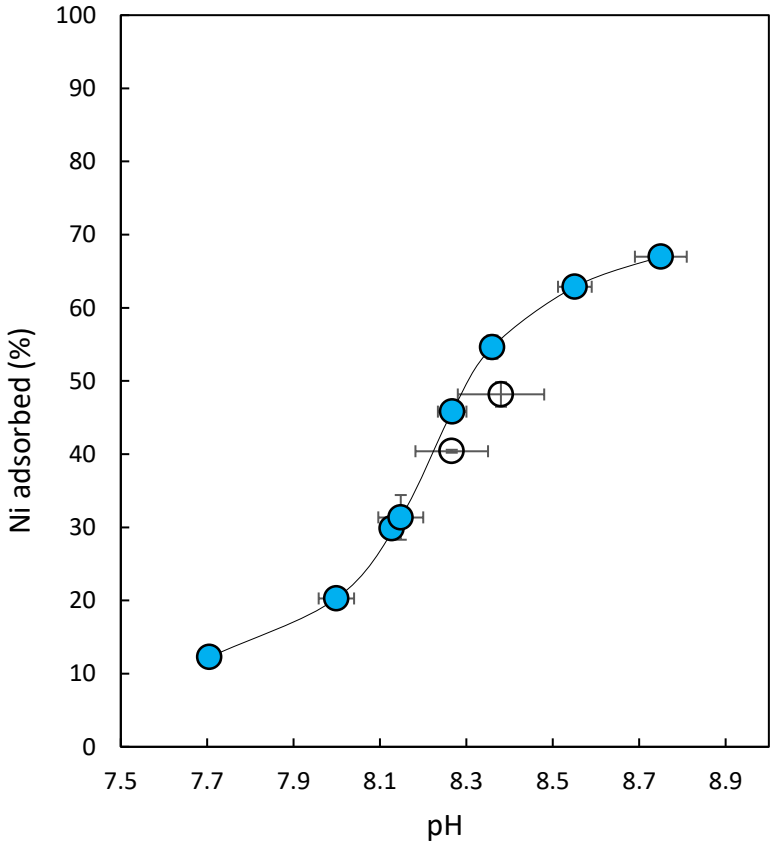

Figure 22. Ni adsorption as a function of pH during series 9P. Colored symbols represent samples on which isotopic analysis was performed. Both experiments were performed at 25°C and atmospheric pCO_2 using 0.01M NaCl as the background electrolyte.

Determining the degree of Ni fractionation as it adsorbed to calcite surfaces posed a challenge. The variation of all measured dissolved Ni isotopic compositions as a function of pH determined in this thesis are plotted together with their corresponding isotopic compositions of solid phases in Fig 23. Note, as described above, the Ni isotopic compositions of solids in this figure were computed from corresponding fluid measurement and mass balance constraints. A large amount of scattering is evident. Considering all of these data are in a single analysis, the fractionation factor would be of $\Delta^{60/58}Ni_{calcite\text{-}fluid}$ = -0.49 ± 0.78‰. The reason behind the scatter and large uncertainties arises from MC-ICPMS measurements. A large variability and uncertainty are associated with measurements made during April 2016 due to machine instability. Such variability can be assessed as a function of pH in Fig. 24 where the values of $\Delta^{60/58}Ni_{calcite\text{-}fluid}$ generated from each data in Fig. 23 are shown as a function of pH. Large uncertainties are evident in those $\Delta^{60/58}Ni_{calcite\text{-}fluid}$ values that are significantly different than -0.5‰. When results of each experimental series are regressed individually, as can be seen in the results summary provided in Table 8, it can be observed that there is consistency of results across the different experimental series despite the scatter.

Table 9. Summary of adsorption experimental data used for calculating the fractionation factor between Ni adsorbed on calcite and Ni in solution

experimental series	average $\Delta^{60}Ni_{calcite\text{-}fluid}$ ‰	2 σ
6P	-0.31	1.24
7P	-0.63	0.13
8K	-0.54	0.45
9P	-0.49	0.16
8K and 9P	-0.5	0.15
all	-0.45	0.78

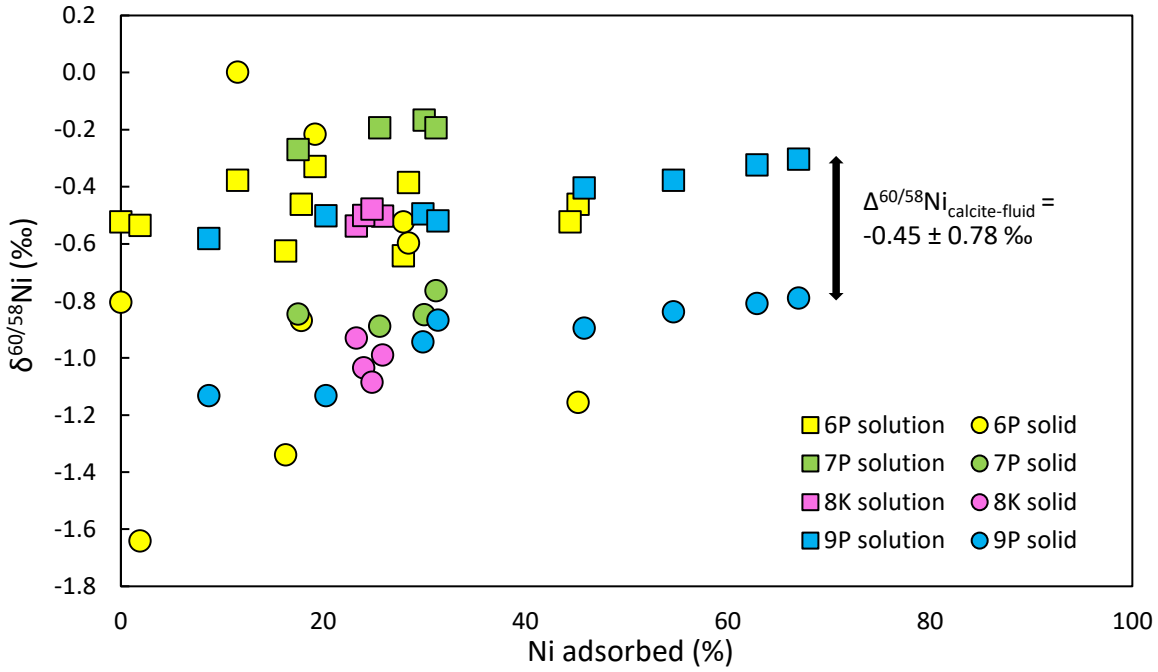

Figure 23. Ni fractionation factor between calcite and containing fluid calculated using all experimental sets. Squares show the composition of fluids and circles composition of adsorbed Ni. The average fractionation factor using all experiments was calculated to be -0.45 ± 0.78 ‰

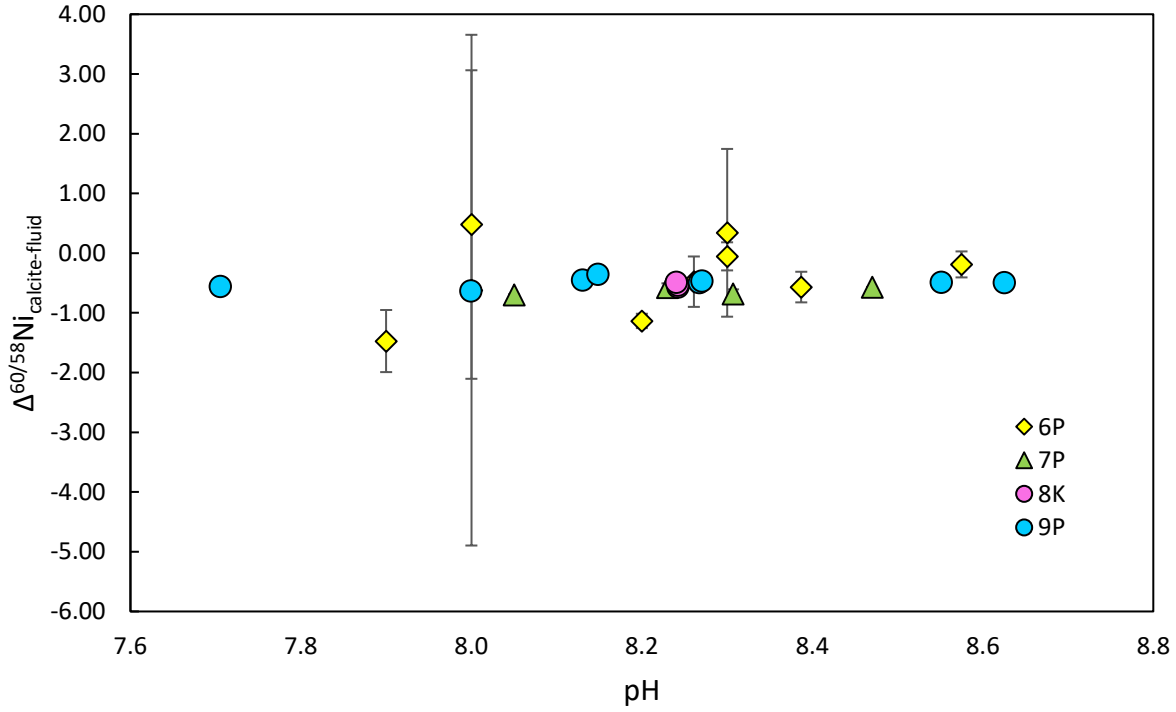

Figure 24. Ni isotope fractionation between calcite and fluid as a function of pH (using all experimental data).

Table 10. Summary of results of experimental series 6P, 7P, and 9P designed to determine the fractionation factor of Ni during its adsorption on calcite as a function of pH.

Experiment number	electrolyte	I	pH	time	[Ni] start	[Ni] end	Ni adsorbed	$\delta\ ^{60}Ni_{fluid}$	2 σ	$\delta\ ^{60}Ni_{solid}$	2 σ	$\Delta_{solid-fluid}$	2 σ
				hours	ppb	ppb	%	‰		‰		‰	
Series 6: adsorption as a function of pH, at 25°C, 0.01M NaCl and using 1g of calcite as a sorbent.													
Ni stock solution 1							0	-0.52	0.17				
6P-01	NaCl	0.01	7.7	24	98.03	95.67	2.36						
6P-02	NaCl	0.01	7.6	24	98.38	96.94	1.45						
6P-03	NaCl	0.01	7.8	24	98.24	96.02	2.21						
6P-04	NaCl	0.01	7.8	24	98.28	97.53	10.75						
6P-05	NaCl	0.01	8.0	24	98.32	86.02	12.31						
6P-06	NaCl	0.01	8.0	24	98.46	90.03	8.43						
6P-07	NaCl	0.01	8.2	24	98.48	81.4	17.09						
6P-08	NaCl	0.01	8.0	24	98.81	83.32	15.49						
6P-09	NaCl	0.01	8.3	24	98.5	77.95	20.55						
6P-10	NaCl	0.01	8.3	24	98.3	80.47	17.84	-0.46	0.3	-0.8	0.79	-0.34	0.42
6P-11	NaCl	0.01	8.4	24	98.67	70.24	28.43	-0.38	0.3	-0.87	0.41	-0.48	0.26
6P-12	NaCl	0.01	8.4	24	97.77	70.37	27.4						
6P-13	NaCl	0.01	8.6	24	99.14	53.95	45.19	-0.46	0.3	-0.6	0.31	-0.14	0.22
6P-14	NaCl	0.01	8.6	24	98.73	55.12	43.61						
6P-15	NaCl	0.01	7.6	24	102.06	98.13	1.9	-0.53	0.3	-1.15	8.55	-0.62	4.28

6P-16	NaCl	0.01	7.9	24	102.13	88.71	11.53	-0.38	0.3	-1.64	0.99	-1.26	0.52
6P-17	NaCl	0.01	8	24	101.99	84.03	16.29	-0.62	1.3	0	5	0.63	2.58
6P-18	NaCl	0.01	8.2	24	102.18	81.22	19.19	-0.33	0.12	-1.34	0.21	-1.01	0.12
6P-19	NaCl	0.01	8.3	24	102.26	72.7	27.92	-0.64	1.12	-0.21	2.58	0.43	1.4
6P-20	NaCl	0.01	8.6	24	102.03	56.49	44.4	-0.52	0.3	-0.52	0.36	0	0.24
Series 7: adsorption as a function of pH, at 25°C, 0.01M NaCl and using 1g of calcite as a sorbent.													
Ni stock solution 2								-0.37					
7P-01	NaCl	0.01	8.1	24	103.26	81.22	25.6	-0.19	0	-0.89	0	-0.69	
7P-02	NaCl	0.01	8.2	24	102.12	81.22	17.53	-0.27	0.08	-0.84	0.12	-0.58	0.07
7P-03	NaCl	0.01	8.3	24	103.33	81.22	29.99	-0.17	0.13	-0.85	0.07	-0.68	0.07
7P-04	NaCl	0.01	8.5	24	102.74	81.22	31.15	-0.19	0	-0.76	0	-0.57	0
Series 9: adsorption as a function of pH, at 25°C, 0.01M NaCl and using 1.5g of calcite as a sorbent.													
Ni stock solution 3								-0.63					
9P-01	NaCl	0.01	7.7	72	102.89	94.16	8.7	-0.58	0.02	-1.13	0.69	-0.55	0.69
9P-02	NaCl	0.01	8	72	103.69	83.41	20.28	-0.5	0.01	-1.13	0. 28	-0.63	0.28
9P-03	NaCl	0.01	8.1	72	103.88	74.02	29.86	-0.49	0.05	-0.94	0.24	-0.45	0.24
9P-04	NaCl	0.01	8.2	72	103.95	72.59	30.17						
9P-05	NaCl	0.01	8.1	72	103.61	57.8	31.36	-0.52	0.05	-0.87	0.25	-0.35	0.25
9P-06	NaCl	0.01	8.3	72	103.73	49.1	45.81	-0.4	0.03	-0.89	0.13	-0.49	0.13
9P-07	NaCl	0.01	8.4	72	103.39	62.99	39.07						
9P-08	NaCl	0.01	8.3	72	103.8	55.64	54.63	-0.38	0.04	-0.84	0.10	-0.46	0.11
9P-09	NaCl	0.01	8.6	72	103.92	41.04	62.88	-0.32	0.02	-0.81	0.10	-0.49	0.10
9P-10	NaCl	0.01	8.6	72	103.5	36.51	66.99	-0.3	0.01	-0.79	0.11	-0.49	0.11

If only the data originating from analyses when the ICP-MS was providing stable and more accurate results is used one obtains Fig. 25. In these studies, the composition of aqueous solutions varied from -0.58 to -0.30 ‰ while solids were calculated to be between -1.13 to -0.79 ‰. Lighter isotopes of Ni are adsorbed onto calcite leaving the heavier isotopes in solution. The fractionation factor is pH independent (Fig. 26) having an average of $\Delta_{calcite\text{-}fluid} = -0.49 \pm .16$.

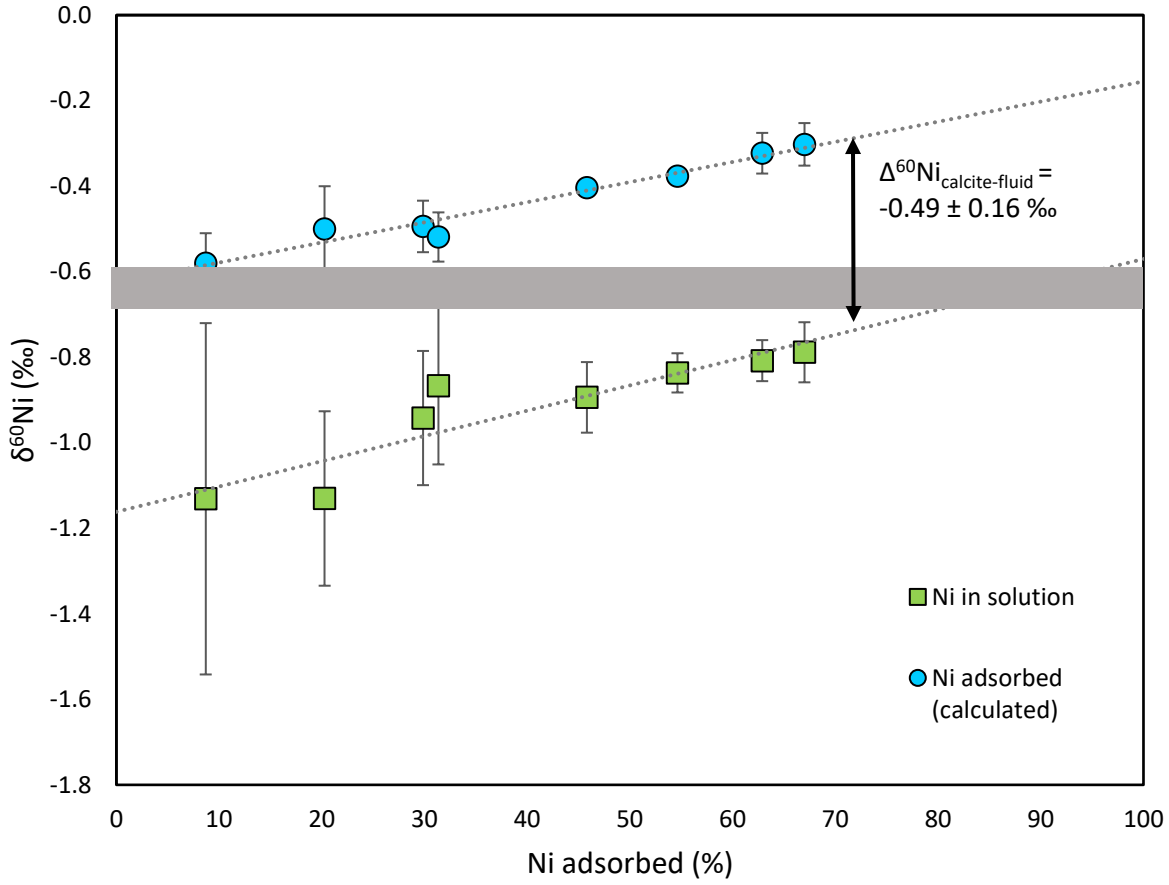

Figure 25. Isotope fractionation factor between Ni in solid (blue squares) and Ni remaining in solution (green circles). The arrow shows an average of $\Delta^{60/58}Ni_{calcite\text{-}fluid} = -0.49 \pm 0.16$ ‰ and shaded area represents the isotopic composition of Ni stock solution.

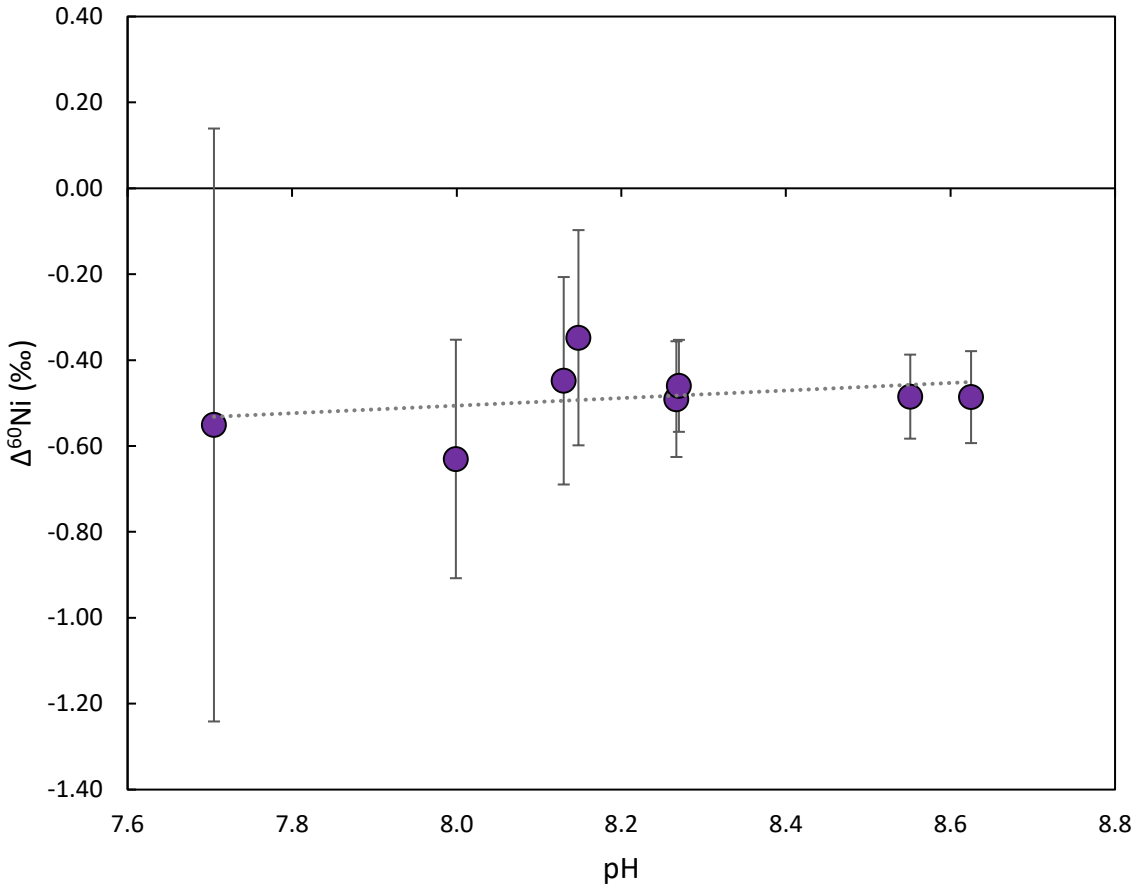

Figure 26. shows the pH dependence of the fractionation factor between Ni adsorbed and Ni in solution

3.4 Discussion

3.4.1 Comparison with previous results

The plot of the Ni concentration at equilibrium and the concentration adsorbed can be fitted to a regression line with a slope of nearly 1. This slope means that the partitioning solid-liquid is independent of Ni concentration while the linear fit to the data is consistent with a Freundlich isotherm. The fit of measured Ni to this isotherm and values found for the linear regression are consistent with the observed behavior of Ni^{+} reported in previous works (see table 5) and other

Me^2 (Zachara et al., 1991; Lakshtanov and Stipp, 2007; Lamana, 2010; Belova et al., 2014). The data are plotted as a log-log plot (Fig. 18).

Table 11. reported Ni sorption isotherms

Author	Isotherm
Zachara (1991)	y= 1.00X – 0.28
Lakshtanov and Stipp (2007)	y = 0.99x - 1.11
Lamana (2010)	y = 1.01x + 0.89
Belova et al. (2014)	y = 1.1 x – 0.19 *
	*calculated from reported data
This study	y= 1.02x – 0.28

These two experimental series show that uptake of Ni by calcite reaches maximum sorption levels after 24 hours and subsequently remains unchanged. This behavior is consistent with previous Ni adsorption investigations and with the behavior of other divalent cations (McBride, 1980; Zachara et al., 1988). Usually, metals exhibit an initial fast adsorption followed by a much slower uptake that can be attributed to recrystallization and incorporation into calcite (Zachara et al., 1988).

Nickel adsorption onto calcite surfaces increases with pH to pH ~ 9 which is in accord with the previous studies (Zachara et al., 1991; Belova et al., 2014; Tahervand and Jalali, 2017).This is associated with the buildup of a negative charge on the calcite surface. Within the framework of calcite surface complexation models (Van Cappellen et al., 1993; Pokrovsky et al., 1999; Pokrovsky et al., 2000), Ni could be adsorbed according to the following reaction (Pokrovsky et al., 2002b):

$$>CO_3^- + Ni^{2+} = >CO_3Ni^+ \quad (22)$$

where $>CO_3^-$ and $>CO_3Ni^+$stand for the deprotonated carbonate site and the Ni surface complex formed on the carbonate site, respectively. The increase of $>CO_3^-$ concentration with increasing pH to pH ~ 9 accounts for the corresponding increase of the extent of Ni sorption.

3.4.2 Isotopes

The Ni isotope fractionation during adsorption on the calcite surface exhibits parallel linear trends with a nearly constant offset. Such behavior was interpreted to stem from an equilibrium exchange between aqueous and sorbed Ni with reversible adsorption and desorption reactions (Dong and Wasylenki, 2016). The relatively small fractionation factors found in this work are consistent with those determined in previous studies of Ni adsorption on ferrihydrite, montmorillonite , and goethite (Wasylenki et al., 2015; Spivak-Birndorf et al., 2018; Gueguen et al., 2018) where fractionation between Ni adsorbed and Ni in solution ranges between = -0.11 ± 0.09‰ and = −0.77 ± 0.23‰, with a preferential incorporation of the light Ni isotopes into the solid phases.

Experimentally determined isotopic compositions of Ni sorbed onto ferrihydrites determined that light Ni goes onto the solid phase at a $\Delta_{dissolved\text{-}sorbed}$= 0.35 +- 0.1 (Gueguen et al., 2018) and the observed fractionations for adsorption and coprecipitation experiments were indistinguishable (Wasylenki et al., 2015). As for experiments in which ferrihydrite had been aged for up to 30 days and partially transformed to goethite and hematite, the measured $\Delta^{60}Ni_{dissolved\text{–}sorbed}$ was +0.23 ± 0.07‰ [within 1 standard deviation] (Wasylenki et al., 2015). Ni coprecipitation with ferrihydrite and then transformation of ferrihydrite to hematite yields a $\Delta^{60/58}Ni_{solution\text{-}solid}$ value of -0.04 to +0.77‰, which shows no fractionation considering the current analytical uncertainties of ±0.09‰ (Wang 2017).

Adsorption to goethite generates the greatest fractionation with $\Delta^{60/58}Ni_{Min\text{-}aq}$=−0.77 ± 0.23‰ (n=14, 2sd) whereas adsorption to 2-line ferrihydrite samples yield $\Delta^{60/58}Ni_{Min\text{-}aq}$=−0.35 ± 0.08‰ (n=16, 2sd) (Gueguen et al., 2018). In talc and goethite, a preferential sorption of light Ni isotopes was observed. In talc, $\Delta^{60/58}Ni_{sorbed\text{-}dissolved}$ was between -0.29 and -0.86‰ (Gueguen, 2013). In goethite, Δ 60/58Nisorbed-dissolved was between -0.43 and -0.94‰ (Gueguen, 2013). For goethite, increasing the amount of Ni sorbed from 3% to 82% results in Δ60 $\Delta^{60/58}Ni_{sorbed\text{-}dissolved}$ that varied between -0.23‰ and +0.17‰, respectively. The spectroscopic data of Ni-$CaCO_3$, which suggests the formation of $Ni(CO_3)_2$ in solution and successive precipitation, could contribute to the association of heavy isotopes with the solid phase.

3.4.3 Interpretation of fractionation factors

A number of past studies have measured Ni fractionation as it adsorbs onto mineral surfaces. Wasylenki et al. (2015) determined $\Delta^{60}Ni_{ferrihydrite\text{-}fluid}$ during 25°C adsorption experiments to be -0.35 ± 0.10‰. Similarly, Gueguen et al. (2018) reported an identical $\Delta^{60}Ni_{ferrihydrite\text{-}fluid}$ = -0.35 ± 0.08‰ from corresponding experiments. Spivak-Birndorf et al. (2018) reported that nickel isotope fractionation from aqueous solution onto montmorillonite resulted in a $\Delta^{60}Ni_{montrormillinite\text{-}fluid}$ = -0.11 ± 0.09‰. The adsorption of Ni from aqueous solution onto goethite was reported to yield the greatest fractionation with $\Delta^{60}Ni_{goethite\text{-}fluid}$ = -0.77 ± 0.23‰ (Gueguen et al., 2018). These relatively small fractionation factors are consistent with that generated for the adsorption of Ni onto calcite in the present study, $\Delta^{60}Ni_{calcite\text{-}fluid}$ = -0.49 ± 0.16‰.

This study shows that calcite preferably adsorbs light Ni isotopes. In contrast, calcite preferentially absorbs heavy Zn, with $\Delta^{66}Zn_{adsorbed\text{-}solution}$ averaging 0.41 ± 0.18‰ and 0.73 ± 0.08‰ in 0.1 and 0.7 M aqueous NaCl solutions, respectively (Dong and Wasylenki, 2016). This preferential uptake of heavy Zn was interpreted to stem from a change in coordination between the aqueous six-fold $Zn(H_2O)_6^{2+}$ complex and Zn adsorbed on the calcite surface, which has a four-fold coordination (Dong and Wasylenki, 2016). This tetrahedral coordination of Zn on the calcite surface was confirmed through EXAFS analysis (Elzinga and Reeder, 2002). Similarly, changes in the coordination geometry of metal cations as they adsorb onto mineral surfaces has been shown to cause isotopic fractionation (e.g. for Ga isotopes on calcite and goethite surfaces, Yuan et al., 2018)). This behavior of Zn contrasts with that of Ni, which likely does not change coordination number as it adsorbs to calcite surfaces from aqueous solution. In cases where coordination number does not change upon adsorption, small distortions of bond angles and lengths can also drive isotopic fractionation (Juillot et al., 2008; Brennecka et al., 2011; Wasylenki et al., 2014; Wasylenki et al., 2015; Gueguen et al., 2018).

Several experimental and theoretical studies have been carried out to determine the Ni-O bond length in aqueous $Ni(H_2O)_6^{2+}$. Experimentally measured bond lengths range between 2.05-2.07 Å (XRD, (Caminiti et al., 1977; Magini et al., 1982)and 2.07 Å (EXAFS, Sandstrom, 1979). These values are in good agreement with DFT (Density Functional Theory) calculations for the cluster $Ni(H_2O)_{18}^{2+}$ (2.073 Å, Fujii et al., 2011). They are slightly shorter than Ni-O bond length in

gaspeite ($NiCO_3$) as determined by XRD (2.076 Å, Pertlik, 1986). This suggests that the replacement in nickel environment, during its adsorption at calcite surface, of an H_2O by a carbonate group should result in a slight increase of the Ni-O bond length and induce an enrichment in light isotopes of the Ni surface complex formed.

Previous studies have reported that the isotopic fractionation of metals between a fluid and a mineral phase also depends on the aqueous speciation of this metal (Balan et al., 2018; Fujii et al., 2011, 2014; Mavromatis et al., 2018; Schott et al., 2016). As our experiments were performed at pHs ranging from 7.7 to 8.6, Ni aqueous speciation was impacted by the formation with increasing pH of $NiHCO_3^+$ and $NiCO_3°$ at the expense of the Ni^{2+} aquo ion. Based on the thermodynamic constants for Ni aqueous species from the minteq.v4 database, Ni^{2+} accounts for 92% of total dissolved Ni at pH 7.7 but for only 48% at pH 8.6. At the same time, if $NiHCO_3^+$ and $NiCO_3°$ concentrations are negligible at pH 7.7, they represent at pH 8.6 respectively 8 and 41% of dissolved nickel. Based on Fujii et al. (2011, 2014), DFT calculations of reduced partition function ratios among Ni aqueous species, the equilibrium fractionation factor at 25°C between aqueous Ni^{2+} and $NiCO_3°$ ($\Delta^{60}Ni_{Ni+2\text{-}NiCO3°}$) is equal to -0.557‰ and that between Ni^{2+} and $NiHCO_3^+$ ($\Delta^{60}Ni_{Ni+2\text{-}NiHCO3+}$) is -0.355‰. As such the nickel carbonate and bicarbonate complexes present in solution at pH 8.6 should make $Ni^{2+}_{(aq)}$ and adsorbed Ni ~0.26‰ lighter than at pH 7.7. The data of the present study do not show this slight enrichment of adsorbed Ni in light isotopes (^{58}Ni) when solution pH increases from 7.7 to 8.6. However, it should be noted that according to the stability constants values of $NiCO_3°$ and $NiHCO_3^+$ recently published by Baeyens et al. (2003), Ni^{2+} would account at pH 8.6 for 69% of total dissolved Ni, and $NiCO_3°$ and $NiHCO_3^+$ for only 25 and 2%, respectively. The subsequent enrichment of Ni^{2+}(aq) and adsorbed Ni in light isotope would be of ~0.13‰ which is within the uncertainty attached to our isotopic measurements.

4.3 Implications for natural systems.

A number of previous works have concluded that our current understanding of the Ni isotopic balance in the oceans requires the identification of either another source of isotopically heavy Ni or another sink of isotopically light Ni. Various processes have been suggested as the possible light Ni sink including adsorption of Ni on ferrihydrites and incorporation into sedimentary sulfides (Gueguen et al., 2013; Wasylenki et al., 2015; Vance et al., 2016). The present study considered the possibility that Ni adsorption onto calcite surfaces may also contribute to

resolving this imbalance in the global marine Ni budget. This study shows that light Ni is preferentially adsorbed onto calcite at $\Delta^{60}Ni_{calcite\text{-}solution}$= -0.49 ± 0.16‰. Although the mass of Ni removed from the ocean by adsorption onto calcite may be too small to completely resolve the currently perceived Ni isotope imbalance, considering the large mass of calcite formed annually, it may be a significant contributor to resolving this imbalance.

3.5 Conclusion

Experiments in the present study were performed to determine the degree of Ni isotope fractionation imparted by adsorption of Ni from an aqueous solution onto calcite surfaces. Major findings of this study include:

1) There was no variation in the isotopic composition of Ni adsorbed onto calcite over time.
2) Calcite surfaces preferentially adsorb isotopically light Ni with an average fractionation factor: $\Delta^{60}Ni_{calcite\text{-}fluid}$ = -0.5 ± 0.15‰. This fractionation factor is independent of the amount of adsorbed Ni indicating an equilibrium isotope exchange process.
3) Ni does not change coordination number as it adsorbs to calcite surfaces from aqueous solution; however, the Ni-O interatomic distance is slightly longer for Ni incorporated in calcite as it is for $Ni(H_2O)_6^{2+}$. This change in coordination geometry is likely the mechanism driving fractionation of Ni isotopes during their incorporation on calcite.
4) A preferred adsorption of light Ni isotopes onto calcite from seawater could help resolve, at least in part, the current perceived Ni isotope budget imbalance in oceans.

Chapter 4. Ni isotope fractionation during its coprecipitation with calcite

4.1 Introduction

4.1.1 Divalent metals as proxies of past seawater composition

Elemental exchange reactions in the crystal lattice of carbonate minerals commonly occur in environmental settings. Probably the most well studied replacement is that of Ca^{2+} with other divalent cations in calcite and aragonite (Lorens, 1981; Mucci and Morse, 1983; Tesoriero and Pankow, 1996; Lakshtanov and Stipp, 2007; von Allmen et al., 2010) since the isotopic compositions of divalent metals in calcium carbonates have the potential to be used as proxies of past environments. The reason behind it being that when these cations substitute for Ca, they record the composition of the reactive fluid from which they precipitated (Sanyal et al., 1996; Alibert and McCulloch, 1997; Mix et al., 1999; Hall and Chan, 2004; Mavromatis et al., 2013; Rodler et al., 2015; Mavromatis et al., 2019).

The influence of calcite precipitation rates on the isotope fractionation of divalent metals has been recently investigated for its potential application in paleoceanography studies. Indeed, as the rate of attachment of lighter isotopes to growing crystals is faster than that of the heavier isotopes, the isotopic signatures of divalent trace elements in marine calcites can provide insight into calcite precipitation rate, the saturation state of seawater relative to this mineral and, hopefully, the associated pCO_2. Interestingly, whereas the extent of isotope fractionation of Sr and Ba (Böhm et al., 2012; Mavromatis, personal communication) increases with calcite growth rate, that of Mg isotope fractionation decreases (Mavromatis et al., 2013; Saenger and Wang, 2014). This behavior has been attributed to the differences in the desolvation rates of these metals relative to Ca^{2+} (Mavromatis et al., 2013) . For instance, Sr^{2+} and Ba^{2+} desolvation rates are similar to that of Ca^{2+}, whereas Mg^{2+} desolvation rate is near 4 orders of magnitude slower. This results, at fast calcite growth rates, in the partial hydration of Mg incorporated in calcite and a smaller isotope fractionation between aqueous Mg and calcite Mg (Mavromatis et al., 2013). The isotopic signatures in calcite of divalent metal traces exhibiting opposite behaviors thus should help to better characterize the chemical environments in which marine calcites were formed. The nickel isotope signatures of marine calcites should be very useful in this regard because nickel forms in solution very strong aquo ions with, among all divalent metals, the slowest rate of exchange of water molecules in its hydration sphere (~ 5 orders of magnitude lower than that of Ca^{2+}). Evaluation and calibration of this proxy requires quantifying nickel isotope fractionation during its co-precipitation

with calcite and the dependence of this fractionation on calcite growth rate. The present chapter presents the first experimental modeling of Ni isotope fractionation between aqueous solution and calcite precipitated abiotically at Earth's surface conditions. Overall, the results of this study suggest that the Ni isotopic composition of natural calcite has the potential to shed light on the ocean saturation state with respect to calcite and P_{CO_2} at the time of this mineral formation.

4.1.2 Theoretical background

Ion incorporation into calcite takes place primarily at kink sites at the mineral aqueous interface (De Yoreo et al., 2009; Nielsen et al., 2012). Ni can get incorporated into the calcite structure through a rearrangement of the solid (Lakshtanov and Stipp, 2007). This process requires the formation of surface complexes that remain hydrated until Ni gets incorporated by recrystallization (Hoffmann and Stipp, 2001).

The affinity of calcite for Ni can be measured using the partition coefficient, D_{Ni}. The partitioning of an element between calcite and its coexisting reactive fluid is commonly described using thermodynamics by the Henderson and Kracek (1927) partition coefficient. This method of calculating the partition coefficient can be used if Ca and Ni complexation is negligible (Lakshtanov and Stipp, 2007). Partitioning between calcite and fluid can be defined as

$$D_{Ni}=\frac{X_{Ni}}{X_{Ca}}\frac{[Ca]}{[Ni]} \quad (23)$$

where *[Ni]* and *[Ca]* stand for the concentrations of Ni and Ca in solution, X_{Ni} and X_{Ca} refers to the molar fraction of Ni and Ca in the solid, respectively and [Ni] and [Ca] stand for the concentrations of Ni and Ca in solution, X_{Ni} refers to the fraction of Ni in the solid, and X_{Ca} designates the molar fraction of Ca in the solid.

The molar fraction of Ni in the solid, X_{Ni} can be calculated in experiments where Ni is added into a mixed flow reactor using

$$X_{Ni} = \frac{n_{Ni(added)} - n_{Ni(removed)}}{n_{Ca(added)} + n_{Ni(added)} - n_{Ca(removed)} - n_{Ni(removed)}} \quad (24)$$

where $n_{Ca(added)}$ and $n_{Ni(added)}$ represent the number of moles of Ca and Ni, respectively, added to the reactor in one day, and $n_{Ca(removed)}$ and $n_{Ni(removed)}$ stand for the number of moles of Ca and Ni respectively removed by sampling during that day.

For dilute solid solutions ($X_{Ni} < 0.001$), the Ni partition coefficient D_{Ni}, has been estimated to be about 3.5 by Wang and Xu (2001) and between 0.1 and 6 by Curti (1999). Carlsson and Aalto (1998) reported this partition coefficient to be about 2 using liquid scintillation counting. In contrast, Lakshtanov and Stipp (2007) measured the partition coefficient of Ni between the aqueous fluid and calcite to be about 1 and weakly dependent on the calcite precipitation rate (Lakshtanov and Stipp, 2007). The partition coefficient of Ni has also been experimentally determined during its incorporation into foraminiferal calcite, where D_{Ni} values ranged from 0.4 to 2 (Munsel et al., 2010).

The greater the partition coefficient, the more affinity an element has for the solid. The partition coefficient values calculated for Ni indicate that its incorporation into calcite is moderate. Out of the divalent metals, Be, Mg and Ba have values lower partition coefficients than and Ni and are expected to have a lower affinity for calcite (Pingitore and Eastman, 1984; Tesoriero and Pankow, 1996; Rimstidt et al., 1998; Saulnier et al., 2012) than Ni. On the other hand, Mn, Fe, Cu and Zn have partition coefficient values higher than Ni, showing a higher affinity for calcite (Kitano et al., 1980; Lorens, 1981; Dromgoole and Walter, 1990; Marchitto, 2011). In contrast, rare earth elements incorporate more strongly into calcite, with partition coefficient values of up to 4000 (Zhong and Mucci, 1995; Webb and Kamber, 2000; Voigt et al., 2017).

4.2 Methodology

4.2.1 Experimental setup

Experiments of Ni coprecipitation with calcite were designed to measure Ni partition coefficient (D_{Ni}) and isotopic fractionation factor ($\Delta^{60}Ni_{calcite\text{-}fluid}$) between calcite and the fluid. This was achieved by growing Ni-bearing calcite from a Ni containing solution onto calcite seeds. Experiments were performed in mixed flow reactors using the constant addition method described in Tesoriero and Pankow (1996) with a few adaptations (see Fig. 27). Precipitation of Ni bearing calcite was performed by addition to the mixed flow reactors of 2 separate solutions, one containing aqueous Ni and Ca ions and the other containing carbonate ions. When these two solutions were

pumped into the reactor, their mixing led to calcite supersaturation in the fluid contained in the reactor, which results in the growth of calcite on the calcite seed material. The precipitation rates were modified by varying the flow rate and molarities of the inlet solutions and the amount of calcite seed material.

To avoid the dissolution of the calcite seed material in the reactors, and to better account for the mass of calcite precipitated in the reactors, the initial reactive aqueous solutions were pre-equilibrated with calcite. These solutions were pre-equilibrated by placing a 0.2 M NaCl solution in contact with calcite and 1 atm CO_2 for 12 hours. The fluid was then separated from the calcite using a Merck Millipore 0.2 μm syringe filter. Afterwards, 300 g of this solution was added to the reactors along with 0.75 to 3.0 g of calcite seeds. This initial aqueous solution and the calcite seed were then allowed to reequilibrate overnight while bubbling pure CO_2 in the reactor fluid. In some co-precipitation experiments, a small aliquot of 10,000 ppm Ni was added to the initial reactive fluid to accelerate the attainment of steady state aqueous Ni concentrations (see 2.2.4.2).

The two inlet solutions consisted of 1) a NaCl and $CaCl_2$ bearing aqueous solution and 2) a $NaCO_3$ bearing aqueous solution. The molalities of $CaCl_2$ and $NaCO_3$ ranged between 0.06 and 0.2 mol/kg, and NaCl was added to these solutions to fix their ionic strength to 0.2 mol/kg. The ionic strengths of these inlet solutions were selected to be consistent with that of the initial reactive fluid in the reactor. The two inlet solutions were pumped into the reactor at equal flow rates using a peristaltic pump. The flow rates ranged from approximately 10 to 40 g/day depending on the experiment; these fluid flow rates were constantly verified throughout each experiment by weighing of the inlet fluid reservoirs.

The mass of aqueous solution in the reactor was kept constant by removing a volume equal to that was added every 24 hrs (or 48 hrs in the case of slower precipitation rate experiments, where the volume added, V_{in}, per day was less than 10 % of that of the reactor volume). Pumping of the input solutions was continued until a steady-state fluid composition was attained in the reactor. At steady-state, the addition of Ca and carbonate by the addition of fluid is the same as that precipitated in the calcite, so the composition of the aqueous solution in the reactor remains constant. The attainment of steady-state was confirmed by regularly measuring the pH, aqueous Ca and Ni concentrations, and the alkalinity of these solutions.

The reactor temperature was kept at 25 +/- 2 ºC using a Fisher thermostatic bath. The calcite powder was held in suspension using a Teflon floating stirrer, which prevents grinding of the calcite

against the bottom of the vessel. To minimize evaporation in long-term experiments, the CO_2 gas was passed through a 0.2 M NaCl solution before incorporating it in the reactor.

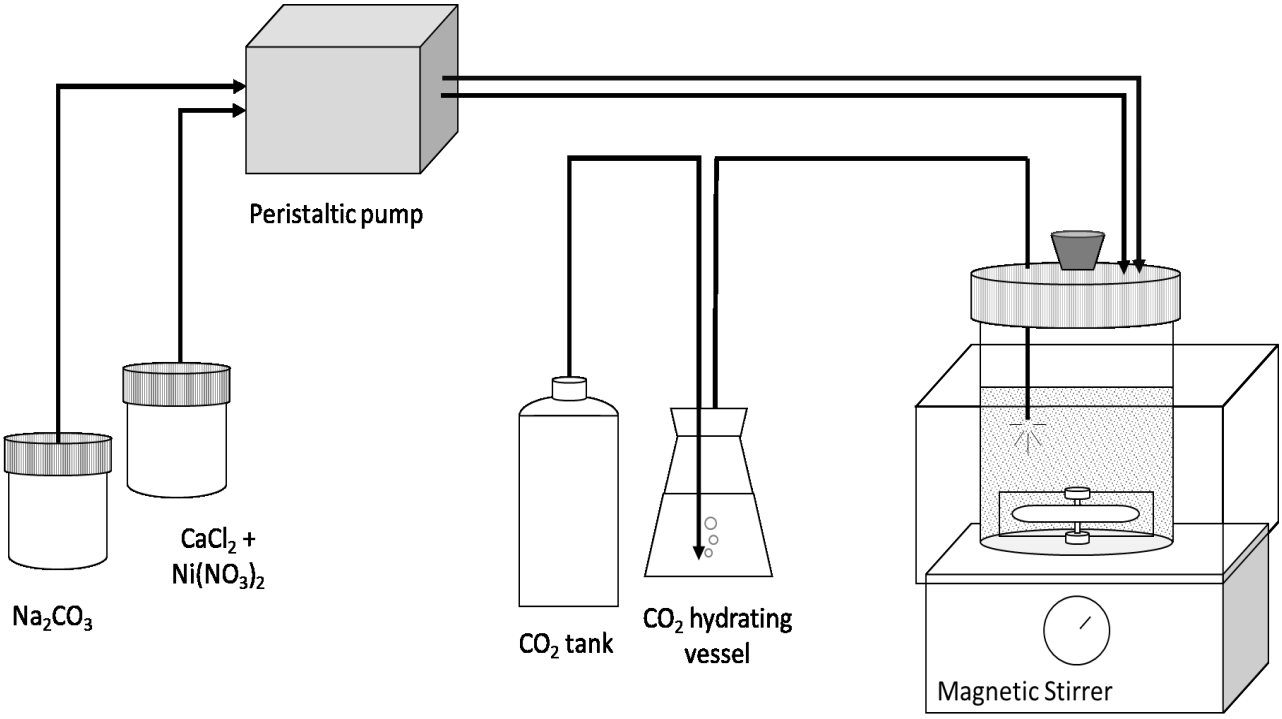

Figure 27. Schematic illustration of the experimental design used for coprecipitation experiments: the reactor was placed in a thermostatically controlled vessel, the aqueous solution was agitated using a suspended stirring bar. Equilibrium with a constant CO_2 partial pressure was achieved by bubbling presaturated air into the reactor with a peristaltic pump.

4.2.2 Sampling

To minimize the removal of calcite from the system, stirring was stopped a few minutes prior to aqueous fluid sampling to allow the solid material to settle. The fluid was sampled through a 0.22 μm Merck Millipore Teflon syringe filter. Three sub-samples were taken; one for alkalinity, one for dissolved element concentration measurement, and one for isotopic composition analysis. The fluid samples collected for elemental and for isotopic analysis were acidified shortly after sampling using double distilled HNO_3 (for AAS measurements) or HCl (for samples to be prepared for isotope analysis).

4.2.3 Thermodynamic calculations

Aqueous species distribution, fluid saturation states and chemical activities were calculated using the thermodynamic modeling computer code PHREEQC (Parkhurst and Appelo, 1999). The minteq.v4 database was used after some minor additions to the solubility constants (see section 2.2.2).

4.2.4 Chemical analysis

The alkalinity of the collected fluid samples was measured shortly after sampling via a 0.05 M HCl acidimetric titration using a Schott TA 10 plus volumetric automatic titrator. The measurements were performed following the Gran method (Stumm, 1996) and had an uncertainty of ±1% with a detection limit of 5×10^{-5} eq/l.

The pH of the fluids was measured in situ, using a Mettler Toledo glass pH electrode calibrated before each measurement using Thermo Fisher buffers (pH=4.006, 6.865 and 9.183 at 25°C). The buffers used for electrode calibration were kept in the same thermostat bath.

Calcium and nickel concentrations of fluids were measured by flame Atomic Absorption Spectroscopy (AAS) using a Perking Elmer AAnalyst 400. The uncertainty of these measurements is ±2% and of ±1% for Ca and Ni respectively, and the spectrometer has a detection limit of $7\text{x}10^{-7}$ mol/kg.

4.2.5 Calcite growth rates and Ni partition coefficients

At steady state conditions, calcite growth rate (mol m^{-2} s^{-1}) can be estimated based on mass balance calculations using the number of moles of Ca introduced in the reactor per unit time corrected for the number of moles of Ca removed at the same period of time via sampling as:

$$R_p = \frac{\frac{n_{Ca(add)} - n_{Ca(rem)}}{86400}}{S} \quad (25)$$

where *S* denotes the total surface area of calcite in the reactor and is expressed in m^2 and 86,400 is the number of seconds within 24 h. The specific surface area of precipitated calcite at the end of

the experimental runs was the same within the precision of measurements than that of calcite seeds. Thus the surface area of calcite precipitated at steady-state conditions was estimated based on the amount of calcium removed by calcite precipitation and the specific surface area of calcite seeds. Note that rate estimations using Eq. 24 are not taking into account the amount of Ni incorporated in the precipitated calcite as this is negligible compared to that of Ca.

Ni partitioning coefficient between calcite and the reactive fluid at chemical steady state conditions can be estimated based on mass balance calculations as:

$$D_{Ni} = \frac{\frac{n_{Ni(add)} - n_{Ni(rem)}}{n_{Ca(add)} + n_{Ni(add)} - n_{Ca(rem)} - n_{Ni(rem)}}}{\left(\frac{[Ni^{2+}]}{[Ca^{2+}]}\right)_{fluid}} = \frac{[X_{Ni}]_{cc}/[X_{Ca}]_{cc}}{[Ni^{2+}]_{fluid}/[Ca^{2+}]_{fluid}} \quad (26)$$

where $n_{i(add)}$ and $n_{i(rem)}$ stand for the number of moles of the i*th* species added in the reactor and removed from the reactor via sampling, respectively, within 24 h, and $[i]_{fluid}$ and $[i]_{cc}$ represent the concentration of the i*th* species in the fluid and calcite, respectively. Note here that Eq. 25 is based on the assumption that at steady state conditions the Ni/Ca ratio of the forming crystal is identical to that of the inlet solution

4.2.6 Isotope Analysis

Liquid samples were prepared for Ni isotopic analyses by ion exchange chromatography. The samples were first evaporated to dryness in perfluoroalkoxy alkanes (PFA) vials on hotplates. Then the dry residues were dissolved in 2 M aqueous HCl. For the solid samples, 2 subsamples were first taken for XRD and SEM analysis, the remaining solids were dissolved into 4 M HCl.

A calcium fluoride precipitation step was performed for the originally solid samples. This step was necessary to reduce the amount of dissolved calcium loaded onto the columns and avoid surpassing the resin capacity. For this purpose calcium was precipitated as CaF_2 by adding HF to the fluids containing the dissolved solid samples. To do so, the chlorides in the fluids were replaced by fluorides by taking up the sample in 5 mL 1 M HF and heating it up for about 2 hours, then evaporating it. Then the sample was taken up in 5 mL 1 M HF and heated on a hot plate once

more. Afterwards, the samples were centrifuged for 10 minutes at 4500 rpm and the supernatant was placed in a Teflon beaker to separate the solids from the fluid. Two mL of MQ water were then added to the centrifuge tubes, and the supernatant after centrifugation was added to the previously recovered sample in the Teflon beaker. Then samples were evaporated and taken up in 2 M HCl.

Nickel was separated from other matrix elements prior to isotope analysis. This was done using a 5 step separation procedure modified from that of Quitté and Oberli (2006) and described in detail in section 2.1.4. The first two steps require the anion exchange resin AG 1-X8 (from Bio-Rad). During these steps, Fe and Zn, the main isobaric interferences for Ni, are removed. The removal of Fe and Zn can be performed in a single step, it is necessary however, to perform the separation in 2 steps to optimize their separation (Quitté and Oberli, 2006). The third step is performed using a Triskem Nickel specific resin, which is based on the complexation of Ni with Dimethylglyoxime (DMG) to form Ni-DMG. The fourth step uses the AG50W-X8 (Bio-Rad) cation exchange resin to purify the sample. The last step uses the AG1-X8 anion exchange resin to remove the Fe introduced during the nickel specific resin step (see chapter 2 for more details).

4.3 Results

A total of 14 experiments were performed in this study. A summary of the experimental conditions and the steady-state reactive fluids compositions is provided in Table 11. Figures 28-33 show the results associated with these experiments. Table 11 also presents the values of Ni mole fraction in calcite and partition coefficients calculated using Eq. 24. The results on this table are based on the assumption that all of the aqueous Ca and Ni are present as Ca^{2+} and Ni^{2+} as the speciation of the fluids, calculated using phreeqc, indicates that the Ca^{2+} and Ni^{2+} aquo-ions account for more than 99% of total aqueous Ca and Ni.

Table 12. Summary of the results of the coprecipitation experiments.

label	Log R_p Mol m^{-2} s^{-1}	[Ca] inlet M/kg	[Ni] inlet M/kg (x 10^{-4})	m seed g	[Ni]ss M/kg (x 10^{-5})	[Ca]ss M/kg	X_{Ni} (mol %) (x 10^{-3})	D_{Ni}
C15	-7.23	0.21	1.75E	1.5	0.94	0.014	0.84	1.23
C16	-7.23	0.21	1.75	1.5	1.24	0.014	0.83	0.93
C17	-6.92	0.21	1.75	0.75	7.16	0.011	0.84	1.24
C18	-7.53	0.21	1.75	3.0	8.26	0.013	0.84	1.29
C19	-8.01	0.06	0.82	1.5	2.20	0.015	1.33	0.89
C20	-8.57	0.06	0.82	3.0	2.28	0.013	1.27	0.73
C21	-6.49	0.20	4.77	0.75	4.38	0.016	2.35	0.84
C23	-7.10	0.21	4.77	3.0	6.15	0.022	2.21	0.81
C26	-7.38	0.20	1.70	2.0	0.84	0.012	0.88	1.25
C27	-7.91	0.10	1.21	2.0	2.57	0.024	1.27	1.20
C29	-8.20	0.06	0.82	2.6	1.47	0.013	1.43	1.26
C31	-8.29	0.06	0.81	2.0	2.96	0.019	1.29	0.84
C36	-7.68	0.07	0.68	2.2	0.98	0.011	1.00	1.16
C37	-7.37	0.20	1.70	4.0	1.03	0.011	0.85	0.92

4.3.1 Mineralogy and composition of the precipitated phases

The X-ray diffraction (XRD) patterns of the solids recovered from the reactions after all experiments appear identical to the original calcite seeds. This indicates that the precipitated material is composed of calcite. Scanning Electron Microscope (SEM) images corroborate this conclusion, showing that the precipitated solids maintained their typical calcite rhombic morphology. No aragonite needles were detected via these observations. Figure 28 shows a

comparison of the original synthetic calcite used as seed material and the calcite recovered at the end of experiment C17.

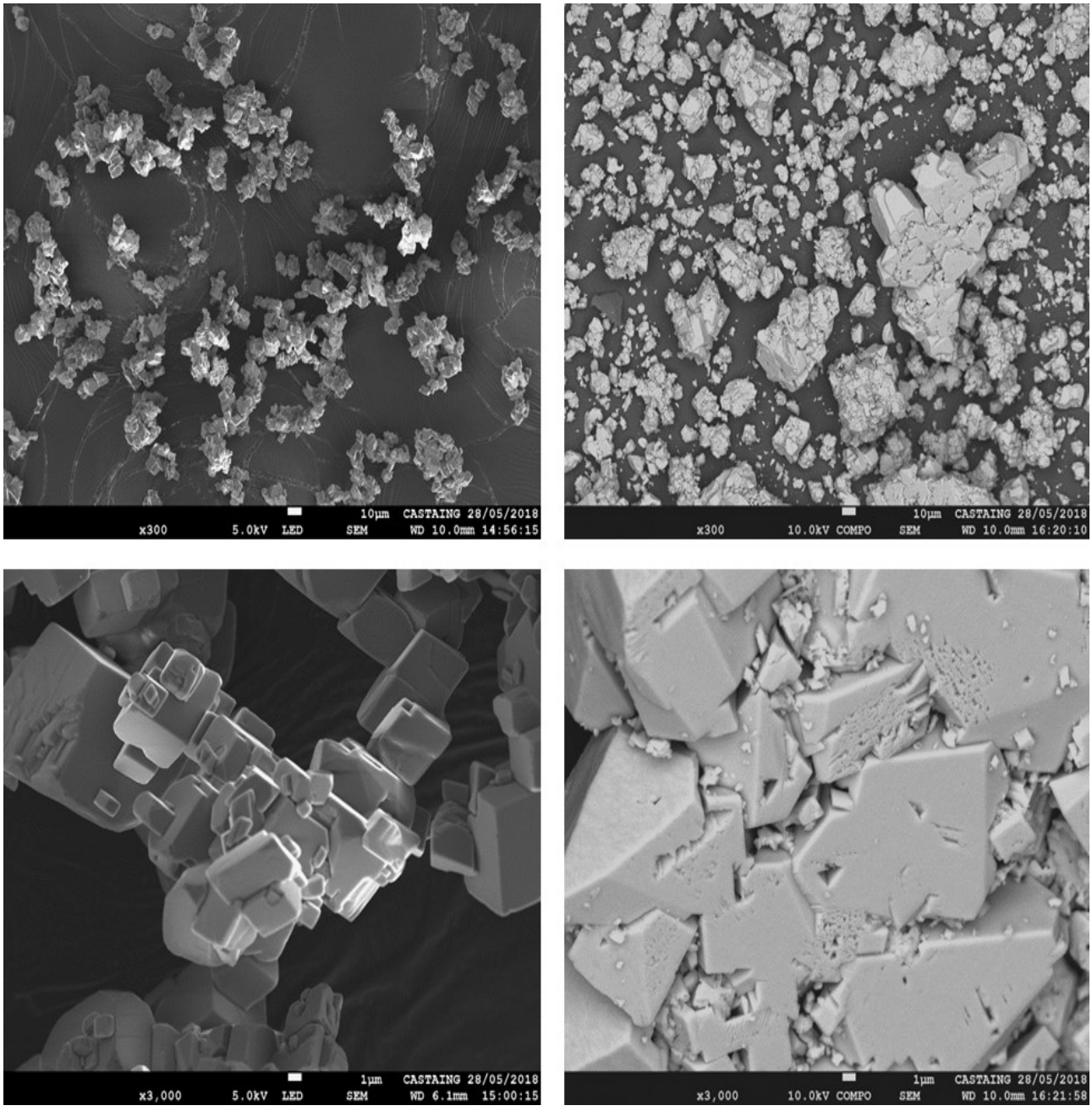

Figure 28. SEM image of the calcite seed material (left) and of the calcite recovered after experiment C17 (right). The scale of the images is provided in the figure.

The mole fraction of nickel, X_{Ni}, in the precipitated calcite was calculated from the composition of the reactive fluid at steady-state using Eq 24. The fraction of Ni in calcite is plotted as a function of aqueous Ni to Ca concentration ratios in Fig. 32.

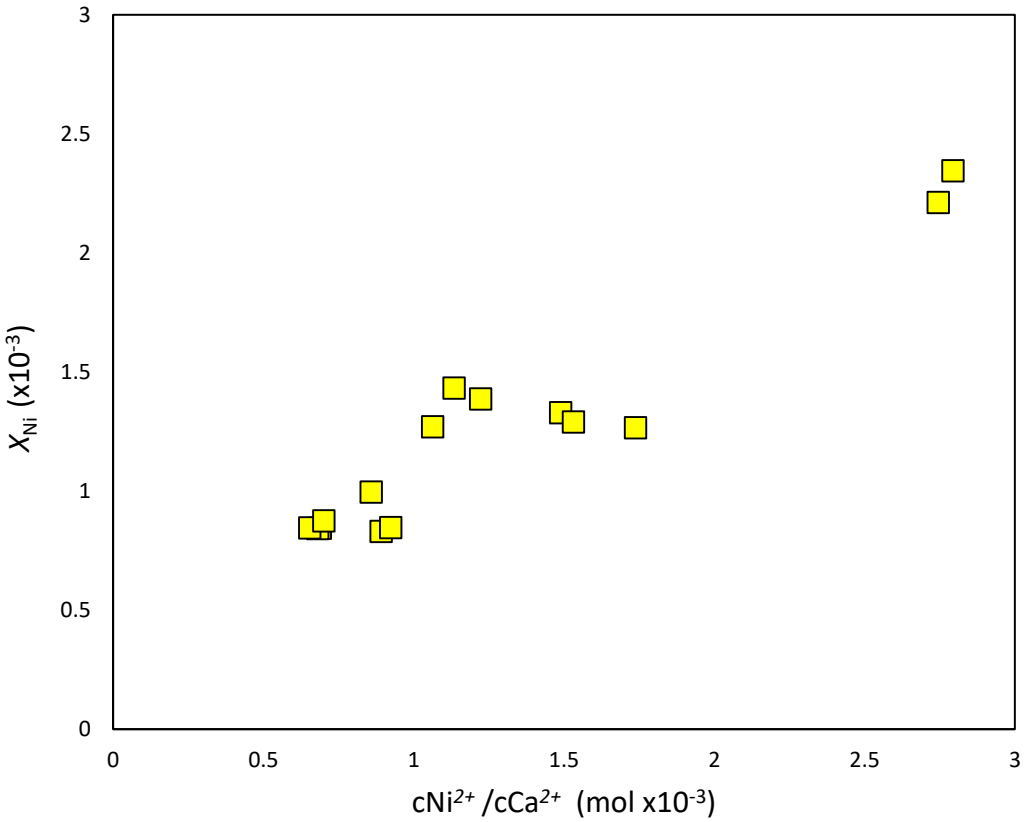

Figure 29. Ni molar fraction in calcite, X_{Ni}, as a function of the steady state Ni^{2+} to Ca^{2+} concentration ratio in the aqueous solution. The error associated with these measurements is included within the symbol size.

4.3.2 Chemical composition of the reactive fluids

Steady-state aqueous Ca concentrations and alkalinities were usually achieved within 3 days during the experiments. A significantly longer time (up to 21 days), however, was required for the attainment of steady-state aqueous Ni concentrations. The time to reach steady-state depended on the Ca and Ni concentrations in the inlet solutions and the pumping rate. Figure 30 shows a representative plot of the temporal evolution of aqueous fluid compositions during a flow experiment performed in this study. In this experiment, no Ni was initially present in the rector.

The reactive fluid reaches a steady-state Ni composition of about 9.37×10^{-6} mol/kg after 6 days. The calcium concentration is relatively stable throughout the experiment and has a steady state concentration of 0.014 mol/kg. The alkalinity concentration also remains almost unchanged and has a steady state concentration of 545.6 ppb. Note the initial fluids in the reactor were pre-equilibrated with calcite (see above).

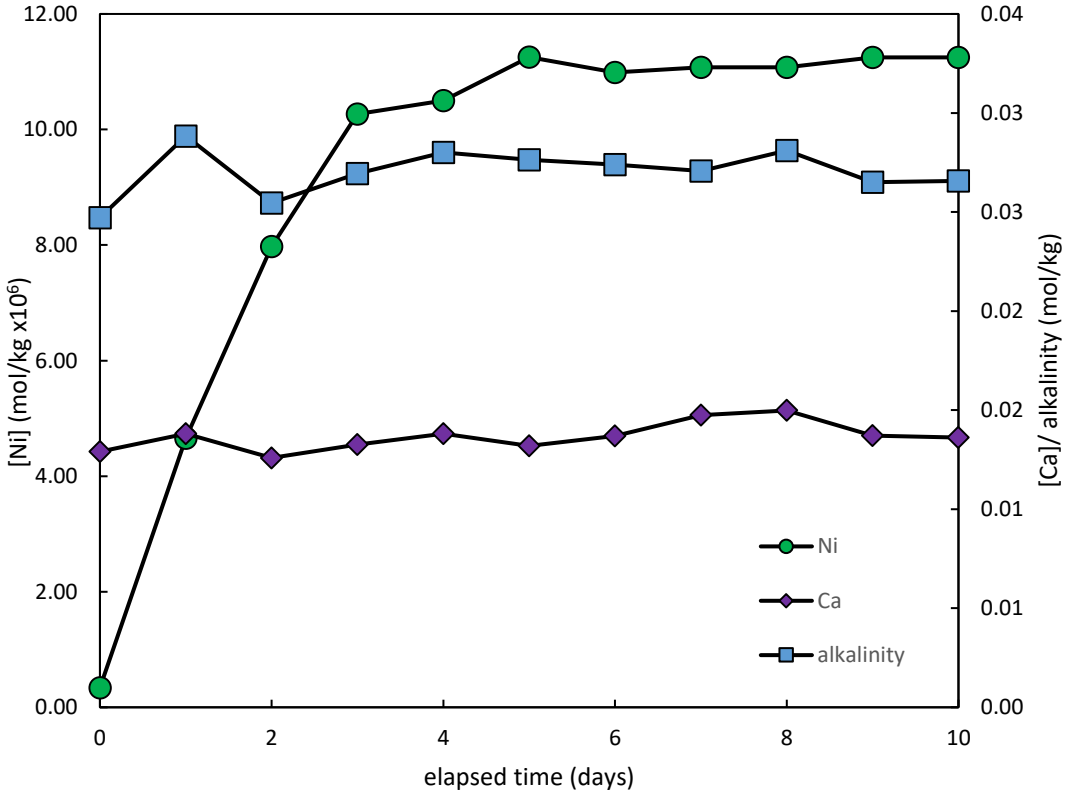

Figure 30. Reactive fluid Ni, and Ca concentrations and alkalinity during experiment C15. These results illustrate a typical fluid evolution of the flow experiments performed in this study with the eventual attainment of fluid steady state. The purple diamonds show the temporal evolution of calcium, while alkalinity is shown by the blue squares. Both are shown on the right scale. Nickel concentrations are represented by the green circles and its scale is shown on the left. Analytical uncertainty is included in symbol size.

4.3.3 Ni partition between calcite and fluid D_{Ni}

The nickel partition coefficient, D_{Ni}, was determined once the outlet fluids attained steady-state concentrations, from the number of moles of Ca and Ni precipitated and the concentration of Ca and Ni in the reactive fluid (using Eq. 26). For the fluid composition range studied, precipitation rates (determined using eq.24), varied between 1.22×10^{7} and 2.72×10^{9} mol m^2 s^{-1}, and the measured Ni partition values fall between 0.73 and 1.29. No effect of precipitation rate on the partition coefficient can be observed (see Fig. 31).

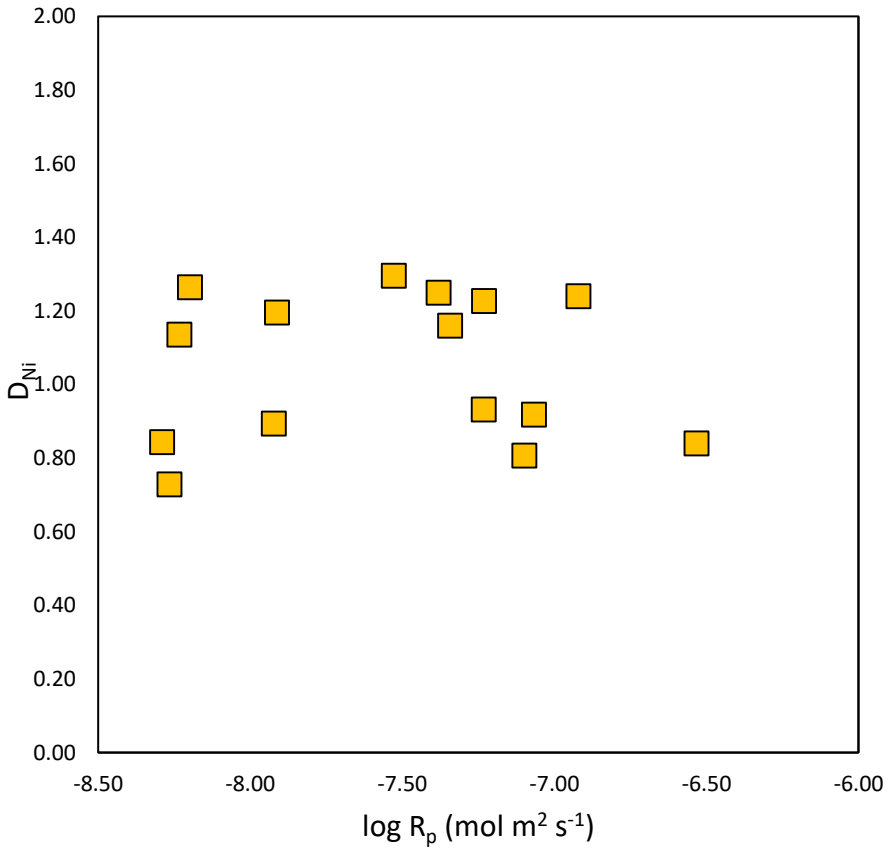

Figure 31. Measured nickel partition coefficients as a function of the logarithm of the calcite precipitation rate. The error associated with these measurements is included within the symbol size.

4.3.4 Ni isotope fractionation during calcite precipitation

The isotopic compositions of reactive fluids and precipitated solids are compiled in Table 12. This table also shows the Ni isotope fractionation factor between solid and solution, which was calculated from the measured isotopic composition of calcite and using a second approach that consists in calculating the isotope composition of the solid phase. Both methods of calculating $\Delta^{60}Ni_{calcite\text{-}fluid}$ are depicted in Fig. 32.

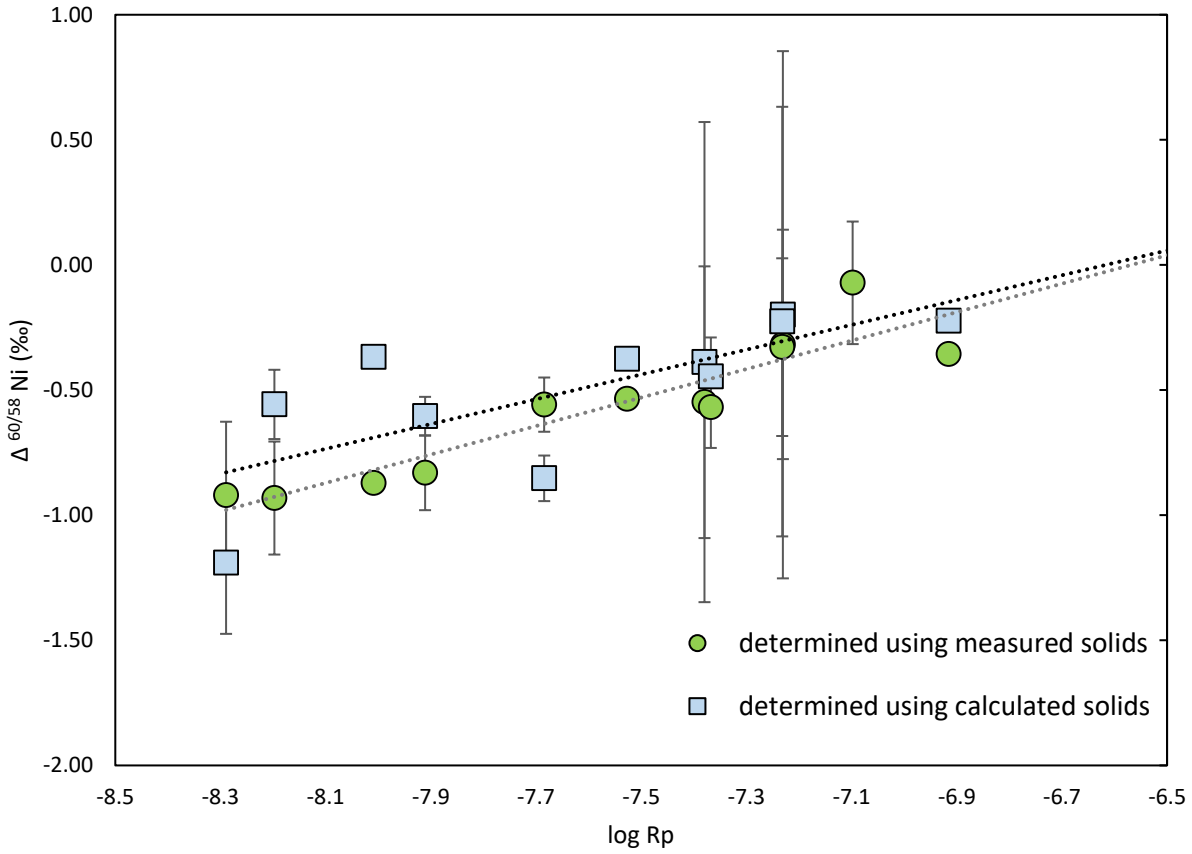

Figure 32. Ni isotope fractionation factors between calcite and the reactive fluid as a function of the calcite precipitation rate. Both fractionation factors determined directly from measured solid compositions, and those generated by first calculating the isotopic compositions of the solids through mass balance constraints are shown.

Table 13. Results of isotopic analysis of fluids and solids recovered from the coprecipitation experiments.

						Measured fraction factor		Calculated fraction factor	
Label	Log R_p	$\delta^{60}Ni_{fluid}$	2σ	$\delta^{60}Ni_{calcite}$	2σ	$\Delta^{60}Ni_{calcite-fluid}$	2σ	$\Delta^{60}Ni_{calcite-fluid}$	2σ
	Mol m^{-2} s^{-1}			‰		‰		‰	
Inlet		-0.52							
C15	-7.23	-0.35	0.37	-0.66	0.27	-0.32	0.46	-0.2	1.05
C16	-7.23	-0.32	0.32	-0.65	0.14	-0.33	0.36	-0.23	0.86
C17	-6.92	-0.32	0.01	-0.68	0.01	-0.36	0.01	-0.22	0.01
C18	-7.53	-0.19	0.02	-0.72	0.01	-0.53	0.02	-0.38	0.01
C19	-8.01	-0.33	0.03	-1.21	0.01	-0.87	0.03	-0.37	0.03
C20	-8.57	-0.58	0.02	-1.37	0.04	-0.79	0.04	0.11	0.19
C23	-7.1	0.11	0.13	0.04	0.21	-0.07	0.24	-0.8	0.96
C26	-7.38	-0.18	0.54	-0.73	0.05	-0.55	0.54	-0.39	0.08
C27	-7.91	-0.21	0.07	-1.04	0.13	-0.83	0.15	-0.6	0.06
C29	-8.2	-0.2	0.13	-1.13	0.19	-0.93	0.23	-0.56	0.14
C31	-8.29	-0.1	0.28	-1.02	0.08	-0.92	0.29	-1.19	0.28
C36	-7.68	0.05	0.09	-0.5	0.06	-0.56	0.11	-0.85	0.09
C37	-7.37	-0.12	0.1	-0.69	0.13	-0.57	0.16	-0.45	0.16

For the case of measured calcite, $\Delta^{60}Ni_{calcite-fluid}$ was calculated using:

$$\Delta^{60}Ni_{calcite-fluid} = \delta^{60}Ni_{calcite} - \delta^{60}Ni_{fluid} \quad (27)$$

The values of $\delta^{60}Ni_{fluid}$ used for this calculation were those of the outlet steady-state fluids sampled at the end of each experiment. The isotopic compositions of the solids were obtained from those recovered at the end of the experiments.

In addition, an alternative determination of this fractionation factor was obtained by calculating the isotopic composition of the solid from the inlet fluid and corresponding fluid compositions using mass balance calculations:

$$\delta_{Ni\ in\ calcite} = \frac{\delta_{stock\ solution} - \delta_{Ni\ in\ fluid} * f_{Ni\ in\ fluid}}{f_{Ni\ in\ calcite}} \quad (28)$$

where δ_i represents the isotopic composition of the denoted phase and f_i is the molar fraction of the i*th* phase.

It can be seen that there is generally a good agreement between the Ni isotope fractionation factor determined using the measured and calculated isotope composition of solids. In both cases, the negative values of $\Delta^{60}Ni_{calcite\text{-}fluid}$ reflect the preferential incorporation of light Ni isotopes in precipitated calcite. The values of Ni fractionation factor range between about -0.3 and -1 ‰ when calculated from measured solids and from -0.2 to -1.19 ‰ when solids are calculated via mass balance. In both cases, the data exhibit a dependence on calcite growth rate where the extent of fractionation decreasing with increasing calcite growth rate.

4.4 Discussion

4.4.1 Ni distribution coefficient between calcite and solution

The Ni mole fraction (X_{Ni}, Fig. 29) in the precipitated calcite at the end of all experiments displays a positive correlation with the ratio of the concentrations of Ni^{2+} to Ca^{2+}. This behavior is similar to that reported by Lakshtanov and Stipp (2007). The Ni partition coefficient values, D_{Ni} (Fig. 31), found in this study ranged from 0.73 to 1.25. These values are consistent with those proposed by Lakshtanov and Stipp (2007) who reported that D_{Ni} ranged from 0.93 to 1.15. In contrast to this previous study, our data exhibits no systematic variation with the calcite precipitation rate. This lack of correlation between the precipitation rate and D_{Ni} could be explained by the equal affinity of Ni^{2+} for the fluid and calcite lattice as revealed by $D_{Ni} = 1$ which induces the same Ni concentration in calcite bulk crystal and in the distorted/hydrated thin layer present at the crystal surface, in accord with Watson (2004) growth entrapment model.

The Ni composition of carboniferous limestones from the lower Yangtze sediments has been reported to be between 1.52 and 12.92 ppb (Zhao and Zheng, 2014). If an average concentration is

calculated to be 2.69 ppb and combined with the average concentrations in seawater of Ni of 0.8 nmol/kg (Sohrin and Bruland, 2011) and Ca corresponding to 0.01 mol/kg (Dickson and Goyet, 1994), the resulting D_{Ni} value would be 5.9, which is relatively close to the value proposed in this study. This value is especially reasonable given the variability found in the literature values for both, the Ni concentration in sediments and Ni concentration is seawater.

4.4.2 Control of Ni isotope composition in calcite

As the nickel adsorbed at the calcite-solution interface, Ni incorporated into calcite lattice is enriched in light isotopes. This enrichment in light isotopes can be explained, as for Ni sorption on calcite surface, by small changes in Ni structural environment, especially in the Ni-O bond length between Ni-bearing calcite and the Ni aquo ion. Ni keeps the same octahedral coordination in its aquo ion, its pure carbonate phase (gaspeite) and when incorporated as a trace in calcite. Because the Ca-O bond length in calcite (2.36 Å; Reeder 1990) is significantly longer than the Ni-O bond length in gaspeite (2.07 Å; Pertlik 1986), Ni-O bond length should be slightly longer in Ni-bearing calcite than in gaspeite. There is no data on the Ni-O bond length in Ni^{2+}-doped calcite but, based on available data on Zn-O and Co-O bond length in the pure Zn carbonates, smithsonite and spherocobaltite (Zn-O = Co-O = 2.11 Å ; Reeder et al. 1999) and the Zn- and Co-doped calcites (Zn-O =2. 15 Å, Co-O =2. 16 Å; Reeder et al., 1999), a Ni-O bond length equal to 2.11/2.12 Å can be assumed for the Ni-bearing calcite precipitated in the present study. This bond length is significantly longer than that reported for Ni-O in the Ni aquo ion (2.05/2.07 Å; Caminiti et al., 1977; Sandstrom, 1979; Magini et al., 1982; Fujii et al., 2011) which explains the enrichment in light isotopes of nickel co-precipitated with calcite.

4.4.3 Ni isotope fractionation factor as a function of calcite growth rate and implications for natural systems.

4.4.3.1 Can Ni be used as a proxy of past seawater composition?

When minerals precipitate from solution at high precipitation rates the system is not at isotopic equilibrium. The preferential incorporation of light isotopes along with the precipitation

rate dependence that has been shown in several studies (Böhm et al., 2012; Mavromatis et al., 2013) and suggests that the fractionations are mostly kinetic in origin.

The influence of calcite precipitation rates on isotope fractionation has been previously investigated. For instance, investigations of calcium isotopes in experimentally precipitated and diagenetically altered calcite have provided evidence for very strong precipitation rate effects on isotope fractionation (Fantle and DePaolo, 2007; Tang et al., 2008; AlKhatib and Eisenhauer, 2017).

The effect of precipitation rate on the extent of isotope fractionation of a metal into the calcite structure has been attributed to the differences in the desolvation rates of this metal isotopes, with the lighter isotopes having a higher desolvation rate (i.e. exchange rate of water molecules in their hydration sphere;Hofmann et al., 2012). Ions in aqueous solution have to be dehydrated before they can be incorporated into the calcite crystal lattice (e.g. Marriott et al., 2004; Raiteri and Gale, 2010) and water molecules have smaller residence times in the solvation shells around lighter isotopes. For metals like Ca, and Sr, which at equilibrium are preferentially enriched in light isotopes, this factor, along with the faster aqueous diffusion coefficients of lighter isotopes, has been suggested as the primary mechanism responsible for the increase with calcite growth rate of the enrichment of light isotopes in calcite crystals (Hofmann et al., 2012). Note, however, that in the case of preferential equilibrium incorporation of heavier isotopes, an increase of growth rate would reduce the extent of isotope fractionation.

During this study, the extent of Ni isotope fractionation between the aqueous fluid and calcite decreases with increasing calcite growth rate. This behavior is similar to that observed for Mg, but contrasts to that observed for Ca and Sr in calcite (Böhm et al., 2012; Mavromatis et al., 2013; AlKhatib and Eisenhauer, 2017). These observations are consistent with the relative rate of exchange of H_2O in the aqueous metal coordination sphere compared to that of Ca. In the comparison of the fractionation factors between calcite and aqueous fluid for Ni, Mg, Sr, and Ca plotted as a function of the calcite precipitation rate (Fig. 33) it is clear that Sr, with a water exchange rate similar to Ca ($10^{-8.9}$ and $10^{-8.8}$ s^{-1}, respectively) shows a similar trend to that of Ca, while Ni and Mg, having a slower water exchange rate ($10^{-4.3}$ and $10^{-5.4}$ s^{-1} respectively), show a variation of the extent of fractionation relative to the precipitation rate that is opposite to that of Ca. As the desolvation rate of Ca^{2+} is the rate limiting step for calcite growth, it would be difficult for Ni that desolvates at rates 5 orders of magnitude slower to become completely desolvated in

bulk calcite except at very slow calcite precipitation rates (Watkins and Watson, 2017). As a result, there is, at fast calcite growth rate, less isotope fractionation between calcite partially hydrated Ni and the Ni aquo ion than between calcite dehydrated Ni and the Ni aquo ion at very slow growth rates. The data reported in Fig. 32 suggest an equilibrium value (i.e. for equal calcite dissolution and precipitation rates) of $\Delta^{60}Ni_{calcite\text{-}solution}$ ~ -1.0 ‰. This value, significantly more negative than the corresponding value for Ni sorption at calcite surface ($\Delta^{60}Ni_{calcite\text{-}solution}$ = - 0.49 ‰), likely reflect longer Ni-O bond length in Ni incorporated in the crystal lattice than in Ni surface complexes.

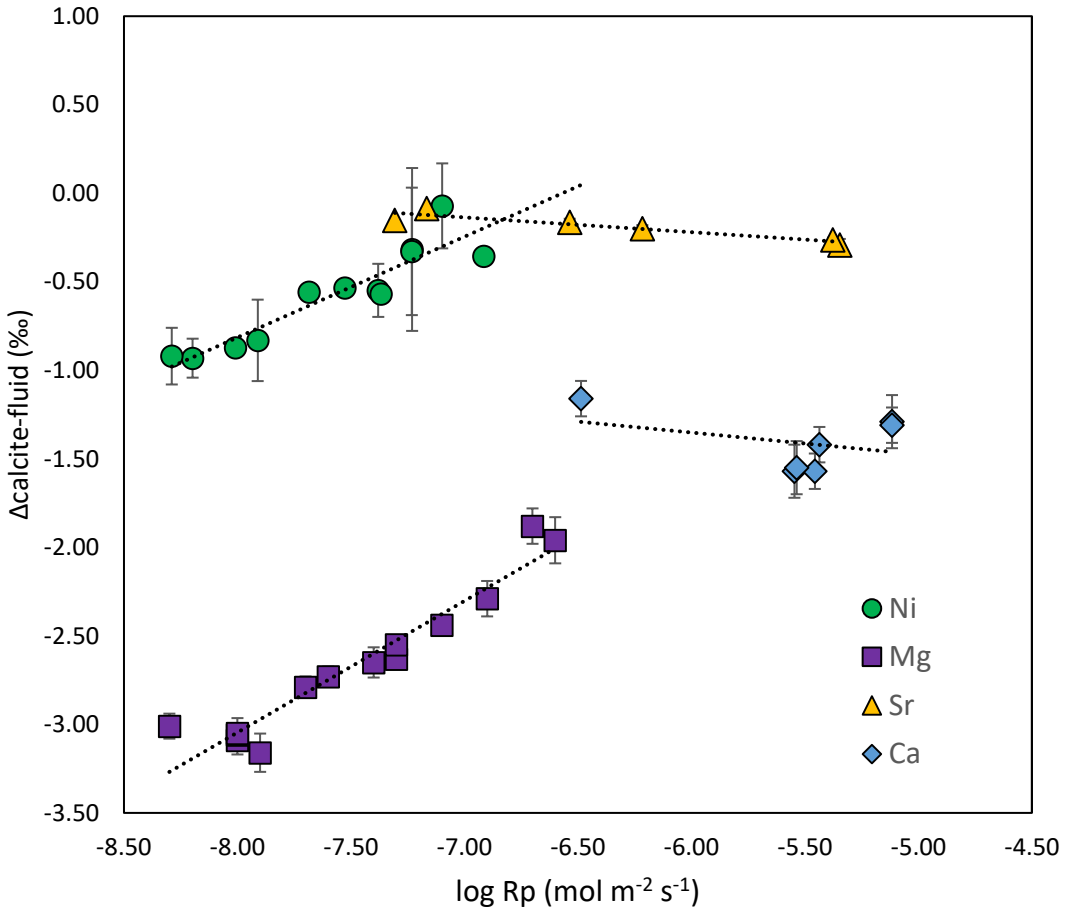

Figure 33. fractionation factor between calcite and fluid for Ni, Mg, Sr, and Ca plotted as a function of the calcite precipitation rate. The data plotted was obtained from Mavromatis et al. (2013), AlKhatib and Eisenhauer (2016), and Bohm et al. (2012.)

Indeed, it has been shown that the high hydration energy of aqueous Ni slows its dehydration on the calcite surface and within its surface layer. Nickel surface complexes remain partly hydrated, exchangeable ions until they are eventually incorporated into the calcite structure by recrystallization (Stipp et al., 1994). This relatively slow desolvation rate relative to Ca^{2+} results in a kinetic isotope fractionation involving dehydration of ions and these deviations from equilibrium fractionation can be used to gather information on geochemical processes and paleoenvironments. Given the clear correlation that exists between the fractionation factor of Ni incorporated in calcite and that remaining in solution, Ni isotope compositions of calcite have the potential to be used as a proxy of seawater composition at the time of its incorporation into calcite.

4.4.3.2 Ni isotope imbalance in the ocean

A number of previous studies have concluded that our current understanding of the Ni isotopic balance in the oceans requires the identification of either another source of isotopically heavy Ni or another sink of isotopically light Ni. Various processes have been suggested as the possible light Ni sink including adsorption of Ni on ferrihydrites (Wasylenki et al., 2015) however, despite $5.1x10^8$ mol of Ni being removed from the ocean via incorporation into ferromanganese crusts, this reservoir shows no difference in its isotope composition compared to seawater (Gall et al., 2017). Another suggested sink of light Ni is the incorporation of nickel into sedimentary sulfides (Gueguen et al., 2013; Wasylenki et al., 2015; Vance et al., 2016). It was shown in Black Sea samples that lighter Ni is incorporated into sediments, leaving residual water up to 1.2‰ heavier than the input water (Vance et al., 2016). The processing of water through such basins, however, is too slow to explain the heavy Ni isotope compositions of seawater (Vance et al., 2017). This thesis shows that light Ni is preferentially adsorbed onto calcite with $\Delta^{60}Ni_{calcite\text{-}solution}$= -0.49 ± 0.16‰ and also preferentially co-precipitated with calcite ($\Delta^{60}Ni_{calcite\text{-}solution}$ ~ -1.0 ‰). These results suggest that Ni adsorption onto calcite surfaces may contribute to resolving this imbalance in the global marine Ni budget given the large mass of calcite precipitated in the oceans. An amount of about $5.7x10^{13}$ mol of $CaCO_3$ (Milliman and Droxler, 1996) containing ~ 2.69 ppm of Ni (Zhao and Zheng, 2014) is precipitated annually. This mass of calcite would result in the removal of 2.61 $x10^8$ moles of Ni per year. The amount of Ni removed this way is of the same order of magnitude as the main sink of Ni in the ocean, the co-precipitation of Ni in the ferromanganese crust (Gall et al., 2013), making it a significant contribution to the Ni isotope budget in the ocean.

4.5 Conclusions

Experiments to determine the effect of precipitation rate on the isotope fractionation of Ni between the Ni incorporated into calcite and the Ni in solution were performed as a function of calcite precipitation rate from 1.22×10^{-7} and 2.72×10^{-9} mol m^2 s^{-1}. The major results include:

1) Ni does not change its coordination number as it gets incorporated into calcite from aqueous solution, however, the Ni-O interatomic distance is significantly longer for Ni incorporated in calcite as it is for $Ni(H_2O)_6^{2+}$. This change in coordination geometry is likely the mechanism driving the preferential incorporation of light Ni isotopes in the calcite structure The value of Ni equilibrium fractionation factor, $\Delta^{60}Ni_{calcite\text{-}solution}$, derived in this study is close to -1.0 ‰ and thus is more negative than the corresponding value for Ni sorption on calcite surface (-0.49 ‰). This difference likely reflects longer Ni-O bond lengths for the Ni trace in calcite than for the Ni species adsorbed at the calcite surface.
2) Nickel isotope fractionation into calcite depends on the calcite precipitation rate. The measured nickel isotope fractionation factor decreases from -1.0 to -0.36 ‰ as the base 10 logarithm of the calcite precipitation rate increases from -8.29 to -6.92 mol m^{-2} s^{-1}. The decrease in the extent of Ni isotope fractionation as the precipitation rate increases is attributed to the slow dehydration rate of aqueous Ni^{2+}. This slow dehydration rate hinders the incorporation of dehydrated Ni^{2+} into calcite. This behavior is similar to that previously observed for Mg, but contrasts to the previously observed behavior of Ca and Sr. These observations likely stem from the rate of exchange of H_2O of the aqueous metals in their coordination sphere compared to that of aqueous Ca^{2+}. The precipitation rate of marine carbonates is determined by the saturation state of the ocean with respect to these minerals. At the same time, the saturation state of carbonates is influenced by pH, pCO_2 and temperature. As Ni isotope fractionation in calcite depends on its precipitation rate, measured Ni isotope compositions have the potential to reveal past environmental conditions.
3) The preferred enrichment in light Ni isotopes on/in calcite from seawater during adsorption and precipitation represents a significant contribution to solving the Ni isotope budget imbalance in the ocean given the big amount of Ni that gets incorporated into carbonates (about 1.53×10^8 moles of Ni per year).

Chapter 5. General conclusions

5.1 Conclusions

The objective of this thesis was to characterize the stable isotope fractionation of Ni linked to its interactions with calcite. To do so, experiments were performed to study 1) Ni adsorption on the calcite surface as a function of time and pH, and 2) Ni coprecipitation with calcite as a function of precipitation rate. The main findings are discussed in this chapter along with suggestions for future research.

In order to assess how the speciation of the solution affects the fractionation of Ni during adsorption on calcite, the Ni isotope fractionation was studied as a function of pH of the Ni containing solution. The main results show that calcite surfaces preferentially adsorb Ni light isotopes with an average fractionation factor, $\Delta^{60}Ni_{calcite\text{-}fluid} = -0.49 \pm 0.16‰$. This fractionation factor is independent of the pH of the solution.

The impact of solution pH increase and the subsequent formation of aqueous $NiCO_3°$ and $NiHCO_3^+$ on $Ni^{2+}(aq)$ isotopic was estimated using DFT calculations of reduced partition function ratios of this species from Fujii et al. (2014). Based on the most recently published stability constants of these species (Baeyens et al., 2003), an enrichment of $Ni^{2+}(aq)$ and adsorbed Ni in light isotopes of ~0.13‰ at pH = 8.6 was calculated, which is within the uncertainty of our isotopic measurements. In order to answer this question more precisely, this study could be extended to include higher pH values - where a higher percentage of aqueous Ni is found as $NiCO_3°$ - and in the presence of other organic and inorganic ligands that would affect the speciation of Ni in solution.

The second part of this study was devoted to finding the isotope fractionation occurring during the coprecipitation of Ni with calcite as a function of precipitation rate from $1.22x10^{-7}$ to $2.72 x10^{-9}$ mol m^2 s^{-1}. The isotope data indicate that calcite the light isotopes of Ni are preferentially incorporated in calcite with an equilibrium fractionation factor ~ -1.0‰ and the extent of isotope fractionation between the fluid and calcite decreases with increasing growth rate.

Several remarks regarding crystal growth can be inferred from the work performed during this thesis. First, the fractionation observed during adsorption and coprecipitation experiments was attributed to the change in coordination geometry occurring during adsorption. The Ni-O interatomic distance is slightly longer for Ni incorporated in calcite as it is for Ni species adsorbed

on calcite surface and $Ni(H_2O)_6^{2+}$; this accounts for the enrichment in light isotopes of adsorbed and coprecipitated Ni and the greater extent of isotope fractionation during Ni coprecipitation than adsorption. A second observation regarding mineral growth is, unlike what is observed for isotopes, the lack of correlation between the precipitation rate and Ni partition coefficient between calcite and the fluid (D_{Ni}). This stems from the equal affinity of Ni^{2+} for the fluid and calcite lattice, as revealed by $D_{Ni} = 1$, which induced the same Ni concentration in calcite bulk crystal and in the hydrated/distorted thin layer present at the crystal surface.

Trace compounds (organics and inorganics) have been shown to affect the growth and dissolution rates of calcite as well as the form of the crystals precipitated (Dobberschütz et al., 2018). Metals such as Mg, Fe and Cu can poison the growth sites as they adsorb on the mineral (Berner, 1975; Reddy and Wang, 1980; Parsiegla and L. Katz, 2000; Nielsen et al., 2016) and this effect increases as the concentration of the incorporated ion increases (Takasaki et al., 1994). For this reason, it would be interesting to systematically study the effect of varying Ni concentrations on calcite precipitation rate and morphology, and calcite Ni isotopic composition.

It would also be of interest to measure the water content in the precipitated calcite. Indeed, according to the present piece of work, the extent of isotope fractionation between the fluid and calcite decreases with increasing growth rate. This behavior can be attributed to the slow dehydration rate of Ni^{2+} compared to that of Ca^{2+}, preventing the cation from losing its hydration sphere when incorporated into fast precipitating calcite. Measurements of the water content of calcite at grown at different rates may provide information on the degree of dehydration attained by the Ni cations during their incorporation into the mineral.

5.2 Suggestions for future research

Based on the good correlation between Ni isotope fractionation and the precipitation rate of calcite in the calcite water system, it can be concluded that Ni incorporated in calcite is likely to be a useful tool for the reconstruction of precipitation rate regimes in natural environments. Nickel isotopes may thus provide information on the values of several geochemical parameters at the time of mineral formation such as, for marine calcites, the ocean saturation state with respect to calcite and P_{CO_2}. If this study represents a first step towards the creation of such a proxy of seawater

composition, additional efforts are however required to have a better understanding of additional factors that affect the isotopic composition of Ni incorporated into calcite.

It is particularly interesting to study the complexation of Ni with organic ligands as Ni strongly complexes with them. In addition, it has been suggested that significant fractionation can occur within species when Ni is complexed with ligands such as Ni- citrate and Ni-crown complex (Fujii et al., 2011; Fujii et al., 2014). The study of Ni fractionation factor in presence of organic groups in the solution for both adsorption and coprecipitation experiments would be a key step to evaluate the use of Ni isotopes in detecting biologic activity in the ocean. In addition, this same strategy can be implemented with coprecipitation experiments; it is possible that a correlation exists concerning the fractionation between Ni calcite and the reactive fluid as a function of pH as is the case of Zn (Mavromatis et al., 2019). By varying the pH of the reactive fluid and thus the speciation of Ni, its possible use as a proxy of pH can be evaluated. As for other ligands, it would be interesting to study the effect that the speciation of Ni in the solution has on the fractionation of Ni during its coprecipitation with calcite since only the free ion can be incorporated, reflecting the isotope fractionation due to speciation in solution.

Further steps should be taken to better approach the isotope fractionation that occurs in natural settings. The seawater system is much more complex and certain changes to the experimental setup would be required to characterize the effects of a solution similar to what would be found in the ocean (ionic strength, competing ions). To study their effect on the Ni isotope fractionation is also important because trace elements in carbonate minerals are usually influenced by more than one variable. For instance, some of the parameters have been shown to affect the isotope composition of the metals incorporated in calcite are temperature (AlKhatib and Eisenhauer, 2017), pH of the solution (Mavromatis et al., 2019), and presence of organic ligands (Mavromatis et al., 2017). The information obtained this way may also lead to the discovery of new potential applications of Ni as a proxy for other paleo variables.

The approach taken during this thesis was to measure the isotopic composition of the trace metal incorporated into calcite, however, it would also be interesting to determine the effects of various chemical exchanges, including Me^{2+}-Ca^{2+} or CO_3^{2-}-SO_4^{2-} substitutions on the isotope fractionation of given metal traces like nickel. For instance, calcite oxygen isotopic composition has been shown to change as a function of precipitation rate (Dietzel et al., 2009) and its Mg content (Mavromatis et al., 2012). By combining the data obtained at different calcite precipitation rates

on metal traces showing opposite dependence of their isotopes fractionation on growth rate, more robust proxies can be created.

Last but not least, the results of both adsorption and coprecipitation studies show that the light isotopes of Ni are associated with the solid during its interactions with calcite. In a seawater setting, this incorporation of light isotopes into calcite could be considered a sink of light Ni isotopes. Considering the large mass of calcite formed annually, the Ni isotope fractionation linked to its interactions with calcite may hence represent a significant contribution to the Ni isotope budget imbalance in the ocean. It is therefore now essential to measure the isotopic composition of Ni incorporated into natural samples to confirm this hypothesis.

Chapitre 5b. Conclusions générales

5.1 Conclusions

L'objectif majeur de cette thèse était de caractériser le fractionnement des isotopes stables du Ni lié à ses interactions avec la calcite. Pour comprendre ces processus de fractionnement, des expériences ont été réalisées pour étudier 1) l'adsorption du Ni à la surface de la calcite en fonction du temps et du pH, et 2) la coprécipitation du Ni avec de la calcite en fonction du taux de précipitation. Les principales conclusions sont résumées dans ce chapitre, et des suggestions pour des recherches futures sont proposées.

Afin d'évaluer l'impact de la spéciation de la solution sur le fractionnement du Ni lors de l'adsorption sur de la calcite, le fractionnement isotopique du Ni a été étudié en fonction du pH de la solution contenant du Ni. Les résultats obtenus montrent que les surfaces de calcite adsorbent préférentiellement les isotopes légers du Ni avec un facteur de fractionnement moyen, $\Delta^{60}Ni_{calcite\text{-}fluide} = -0,49 \pm 0,16$. Ce facteur de fractionnement est indépendant du pH de la solution.

L'impact de l'augmentation du pH de la solution et de la formation subséquente de $NiCO_3°$ et $NiHCO_3^+$ aqueux a été estimé à l'aide de calculs DFT des rapports de fonction de partition réduite de $Ni^{2+}_{(aq)}$ (Fujii et al. 2014). Sur la base des constantes de stabilité récemment publiées de ces espèces (Baeyens et al., 2004), nous avons calculé un enrichissement en isotopes légers de ~0,13 à pH = 8,6 pour $Ni^{2+}_{(aq)}$ et Ni adsorbé, ce qui se situe dans l'incertitude de nos mesures isotopiques. Afin de répondre plus précisément à cette question, cette étude pourrait être étendue/complétée pour inclure des valeurs de pH plus élevées - où un pourcentage plus élevé de Ni en solution aqueuse correspond à NiCO3 ° - et en présence d'autres ligands organiques et inorganiques capables de changer la spéciation du Ni en solution.

La deuxième partie de cette étude a été consacrée à la détermination du fractionnement isotopique lors de la coprécipitation de Ni avec de la calcite en fonction du taux de précipitation, celui-ci étant compris entre $1,22x10^{-7}$ et $2,72x10^{-9}$ mol m^2 s^{-1}. Les données isotopiques indiquent que la calcite incorpore de préférence les isotopes légers du Ni, avec un facteur de fractionnement à l'équilibre égal à -1,0, et que le degré de fractionnement isotopique entre le fluide et la calcite diminue lorsque le taux de précipitation augmente.

A partir des travaux effectués au cours de cette thèse, plusieurs remarques peuvent être faites concernant la croissance des cristaux. Tout d'abord, le fractionnement observé lors des expériences d'adsorption et de coprécipitation a été attribué au changement de la géométrie de

coordination survenant lors de l'adsorption. La distance interatomique Ni-O est légèrement plus longue pour le Ni incorporé dans la calcite que pour les espèces de Ni adsorbées à la surface de la calcite et $Ni(H_2O)_6^{2+}$; cela explique l'enrichissement en isotopes légers du Ni adsorbé et coprécipité et le fractionnement isotopique plus important lors de la coprécipitation de Ni par rapport à l'adsorption. Notons par ailleurs l'absence de corrélation entre le taux de précipitation et le coefficient de partage du Ni entre la calcite et le fluide (DNi), contrairement à ce qui est observé pour les isotopes. Cela provient de la même affinité de Ni^{2+} pour le réseau de fluide et de calcite, comme le révèle le coefficient de partage D_{Ni} égal à 1, qui induit la même concentration de Ni dans le cristal de calcite dans son ensemble et dans la mince couche hydratée / distordue présente à la surface du cristal.

Il a été démontré que les composés à l'état de traces (organiques et inorganiques) affectaient les vitesses de croissance et de dissolution de la calcite ainsi que la forme des cristaux précipités (Dobberschütz et al. 2018). Des métaux tels que le Mg, le Fe et le Cu peuvent perturber les sites de croissance lors de leur adsorption sur le minéral (Berner, 1975; Reddy et Wang, 1980; Parsiegla et L. Katz, 2000; Nielsen et al., 2016) et cet effet augmente lorsque la concentration de ces ions augmente (Takasaki et al. 1994). Pour cette raison, il serait intéressant d'étudier systématiquement l'effet de la variation de la concentration en Ni sur le taux de précipitation et la morphologie de la calcite, ainsi que sur la composition isotopique du Ni de la calcite.

Il serait également intéressant de mesurer le contenu en eau de la calcite précipitée. En effet, il semble que l'ampleur du fractionnement isotopique entre le fluide et la calcite diminue avec l'augmentation du taux de croissance. Ce comportement peut être attribué à la lenteur de déshydratation de Ni^{2+} comparée à celle de Ca^{2+}, empêchant le cation de perdre sa sphère d'hydratation lorsqu'il est incorporé à de la calcite qui précipite rapidement. Des mesures de la teneur en eau de la calcite pour différentes vitesses de croissance pourraient fournir des informations sur le degré de déshydratation atteint par les cations Ni2+ lors de leur incorporation dans le minéral.

5.2 Suggestions pour des recherches futures

Sur la base de la bonne corrélation entre le fractionnement isotopique du nickel et le taux de précipitation de la calcite dans le système eau - calcite, on peut conclure que le Ni incorporé à la calcite sera probablement un outil utile pour la reconstruction des régimes de taux de

précipitation dans les environnements naturels. Les isotopes du nickel peuvent ainsi fournir des informations sur les valeurs de plusieurs paramètres géochimiques au moment de la formation de minéraux, tels que, pour les calcites marines, l'état de saturation de l'océan en ce qui concerne la calcite et la PCO_2. Si cette étude représente un premier pas vers la création d'un tel indicateur indirect de la composition de l'eau de mer, des efforts supplémentaires sont toutefois nécessaires pour mieux comprendre les facteurs supplémentaires qui affectent la composition isotopique du nickel incorporé à la calcite.

Il serait particulièrement intéressant d'étudier la complexation du Ni avec des ligands organiques car le Ni les complexe fortement. Il a été suggéré qu'un fractionnement important peut se produire lorsque le Ni est complexé à des ligands tels que le citrate de Ni et le complexe Ni - crown (Fujii et al. 2011, 2014). L'étude du facteur de fractionnement du nickel en présence de groupes organiques dans la solution pour les expériences d'adsorption et de coprécipitation serait une étape clé pour évaluer le potentiel des isotopes du nickel dans la détection de l'activité biologique dans l'océan. De plus, cette même stratégie peut être mise en œuvre avec des expériences de coprécipitation; il est possible qu'il existe une corrélation qui lie le fractionnement entre la calcite de Ni et le fluide réactif au pH, comme c'est le cas pour le Zn (Mavromatis et al. 2018). En faisant varier le pH du fluide réactif et donc la spéciation du Ni, on peut évaluer son utilisation potentielle en tant que proxy du pH. Pour ce qui est des autres ligands, il serait intéressant d'étudier l'effet de la spéciation de Ni dans la solution sur le fractionnement de Ni lors de sa coprécipitation avec de la calcite puisque seul l'ion libre peut être incorporé, reflétant le fractionnement isotopique dû à la spéciation en solution.

Avant d'appréhender le fractionnement isotopique qui se produit dans des environnements naturels, d'autres étapes sont nécessaires. Le système d'eau de mer est en effet beaucoup plus complexe et certaines modifications de la configuration expérimentale seraient nécessaires pour caractériser les effets d'une solution similaire à celle de l'océan. Il est également important d'étudier leurs effets sur le fractionnement isotopique du nickel, car plusieurs métaux trace dans les minéraux carbonatés sont généralement influencés. Par exemple, il a été démontré que certains des paramètres affectant la composition isotopique des métaux incorporés dans la calcite sont la température (AlKhatib et Eisenhauer 2017), le pH de la solution (Mavromatis et al. 2018) et la présence de ligands organiques (Mavromatis et al. 2017). Les informations ainsi obtenues peuvent

également conduire à la découverte de nouvelles applications potentielles de Ni en tant que proxy pour d'autres variables paléoocéanographiques.

L'approche adoptée au cours de cette thèse consistait à mesurer la composition isotopique du métal trace incorporé à la calcite, mais il serait également intéressant de déterminer les effets de divers échanges chimiques, y compris les substitutions de Me^{2+}-Ca^{2+} ou de CO_3^{2-}-SO_4^{2-} sur le fractionnement isotopique des métaux trace tels que le nickel. Par exemple, il a été démontré que la composition isotopique de la calcite-oxygène évolue en fonction du taux de précipitation (Dietzel et al. 2009) et de la concentration en Mg (Mavromatis et al. 2012). En combinant les données obtenues à différentes vitesses de précipitation pour la calcite et les résultats pour les métaux trace montrant une dépendance inverse de leur fractionnement isotopique en fonction de leur vitesse de croissance, des proxy plus robustes peuvent être créés.

De plus, les résultats des études sur l'adsorption et la coprécipitation montrent que les isotopes légers du Ni sont associés au solide lors de ses interactions avec la calcite. Dans un environnement d'eau de mer, cette incorporation d'isotopes légers dans la calcite pourrait être considérée comme un puits d'isotopes légers de Ni. Compte tenu de l'importante masse de calcite formée chaque année, le fractionnement isotopique du Ni lié à ses interactions avec la calcite peut donc représenter une contribution significative au déséquilibre du bilan isotopique du Ni dans l'océan. Il est donc essentiel de mesurer la composition isotopique du nickel incorporé dans des échantillons naturels pour confirmer cette hypothèse.

Bibliography

Alibert C. and McCulloch M. T. (1997) Strontium/calcium ratios in modern porites corals From the Great Barrier Reef as a proxy for sea surface temperature: Calibration of the thermometer and monitoring of ENSO. *Paleoceanography* 12, 345–363.

AlKhatib M. and Eisenhauer A. (2017) Calcium and strontium isotope fractionation in aqueous solutions as a function of temperature and reaction rate; I. Calcite. *Geochim. Cosmochim. Acta* 209, 296–319.

von Allmen K., Böttcher M. E., Samankassou E. and Nägler T. F. (2010) Barium isotope fractionation in the global barium cycle: First evidence from barium minerals and precipitation experiments. *Chem. Geol.* 277, 70–77.

Anbar A. D. and Rouxel O. (2007) Metal Stable Isotopes in Paleoceanography. *Annu. Rev. Earth Planet. Sci.* 35, 717–746.

Baes C. F. and Mesmer R. S. (1976) The Hydrolysis of Cations. *Berichte der Bunsengesellschaft für Phys. Chemie* 81, 245–246.

Baeyens B., Bradbury M. H. and Hummel W. (2003) Determination of Aqueous Nickel – Carbonate and Nickel – Oxalate Complexation Constants. *J. Solution Chem.* 32, 319–339.

Balan E., Noireaux J., Mavromatis V., Saldi G. D., Montouillout V., Blanchard M., Pietrucci F., Gervais C., Rustad J. R., Schott J. and Gaillardet J. (2018) Theoretical isotopic fractionation between structural boron in carbonates and aqueous boric acid and borate ion. *Geochim. Cosmochim. Acta* 222, 117–129.

Baskaran M. (2011) *Handbook of environmental isotope geochemistry*., Springer.

Beard B. L., Li W., Johnson C. M., Chakraborty S. and Romanek C. S. (2012) Magnesium isotope fractionation during precipitation of inorganic calcite under laboratory conditions. *Earth Planet. Sci. Lett.* 333–334, 304–316.

Beer and Beer A. (1852) Bestimmung der Absorption des rothen Lichts in farbigen Flüssigkeiten. *Ann. der Phys. und Chemie* 86, 78–88.

Belova D. a, Lakshtanov L. Z., Carneiro J. F. and Stipp S. L. S. (2014) Nickel adsorption on chalk and calcite. *J. Contam. Hydrol.* 170, 1–9.

Berner R. A. (1975) The role of magnesium in the crystal growth of calcite and aragonite from sea water. *Geochim. Cosmochim. Acta* 39, 489–504.

Bigeleisen J. (1965) Chemistry of isotopes. *Science.* 147, 463–471.

Bigeleisen J. (1949) The Relative Reaction Velocities of Isotopic Molecules. *J. Chem. Phys.* 17, 675–678.

Blanchard M., Balan E. and Schauble E. A. (2017) Equilibrium Fractionation of Non-traditional Isotopes: a Molecular Modeling Perspective. *Rev. Mineral. Geochemistry* 82, 27–63.

Bogatko S., Claeys P., De Proft F. and Geerlings P. (2013) Li^+ speciation and the use of $^7Li/^6Li$ isotope ratios for ancient climate monitoring. *Chem. Geol.* 357, 1–7.

Böhm F., Eisenhauer A., Tang J., Dietzel M., Krabbenhöft A., Kisakürek B. and Horn C. (2012) Strontium isotope fractionation of planktic foraminifera and inorganic calcite. *Geochim. Cosmochim. Acta* 93, 300–314.

Bourg I. C., Richter F. M., Christensen J. N. and Sposito G. (2010) Isotopic mass dependence of metal cation diffusion coefficients in liquid water. *Geochim. Cosmochim. Acta* 74, 2249–2256.

Brennecka G. A., Wasylenki L. E., Bargar J. R., Weyer S. and Anbar A. D. (2011) Uranium isotope fractionation during adsorption to Mn-oxyhydroxides. *Environ. Sci. Technol.* 45, 1370–1375.

Broecker W. (2012) The Carbon Cycle and Climate Change: Memoirs of my 60 years in Science. *Geochemical Perspect.*, 221–339.

Brunauer S., Emmett P. H. and Teller E. (1938) Adsorption of Gases in Multimolecular Layers. *J. Am. Chem. Soc.* 60, 309–319.

Bryan S. P. and Marchitto T. M. (2010) Testing the utility of paleonutrient proxies Cd/Ca and Zn/Ca in benthic foraminifera from thermocline waters. *Geochemistry, Geophys. Geosystems* 11.

Cameron V. and Vance D. (2014) Heavy nickel isotope compositions in rivers and the oceans. *Geochim. Cosmochim. Acta* 128, 195–211.

Cameron V., Vance D., Archer C. and House C. H. (2009) A biomarker based on the stable isotopes of nickel. *Proc. Natl. Acad. Sci.* 106, 10944–10948.

Caminiti R., Licheri G., Piccaluga G. and Pinna G. (1977) X-ray diffraction and structure of $NiCl_2$ aqueous solutions. *Faraday Discuss. Chem. Soc.* 64, 62.

Van Cappellen P., Charlet L., Stumm W. and Wersin P. (1993) A surface complexation model of the carbonate mineral-aqueous solution interface. *Geochim. Cosmochim. Acta* 57, 3505–3518.

Chang V. T.-C., Williams R. J. P., Makishima A., Belshawl N. S. and O'Nions R. K. (2004) Mg and Ca isotope fractionation during $CaCO_3$ biomineralisation. *Biochem. Biophys. Res. Commun.* 323, 79–85.

Chou L., Garrels R. M. and Wollast R. (1989) Comparative study of the kinetics and mechanisms of dissolution of carbonate minerals. *Chem. Geol.* 78, 269–282.

Clarke F. W. and Wheeler W. C. (1922) The inorganic constituents of marine invertebrates. *USGS Prof. Pap.* 124, 55.

Cléroux C., Cortijo E., Anand P., Labeyrie L., Bassinot F., Caillon N. and Duplessy J.-C. (2008) Mg/Ca and Sr/Ca ratios in planktonic foraminifera: Proxies for upper water column temperature reconstruction. *Paleoceanography* 23.

Colla C. A., Wimpenny J., Yin Q.-Z., Rustad J. R. and Casey W. H. (2013) Calcium-isotope fractionation between solution and solids with six, seven or eight oxygens bound to Ca(II). *Geochim. Cosmochim. Acta* 121, 363–373.

Comans R. N. and Middleburg (1987) J. J. (1987) Sorption of trace metals by calcite: Apphcabiiity of the surface precipitation model. *Geaochim. Cosmochim. Acta* 51, 2587–2591.

Criss R. E. (1999) *Principles of stable isotope distribution*., Oxford University Press.

Curti E. (1999) Coprecipitation of radionuclides with calcite: Estimation of partition coefficients based on a review of laboratory investigations and geochemical data. *Appl. Geochemistry* 14, 433–445.

Curti E. (1977) *Coprecipitation of redionuclides: basic concepts, literature review and applications.*, Villigen.

Davis J. A., Fuller C. C. and Cook A. D. (1987) A model for trace metal sorption processes at the calcite surface: Adsorption of Cd2+ and subsequent solid solution formation. *Geochim. Cosmochim. Acta* 51, 1477–1490.

Davis J. A. and Kent D. B. (1990) Surface Complexation Modeling in Aqueous Geochemistry. *Miner. Interface Geochemistry* 23, 177–260.

deBoer R. B. (1977) Influence of seed crystals on the precipitation of calcite and aragonite. *Am. J. Sci.* 277, 38–60.

DePaolo D. J. (2011) Surface kinetic model for isotopic and trace element fractionation during precipitation of calcite from aqueous solutions. *Geochim. Cosmochim. Acta* 75, 1039–1056.

Dickson A. G. and Goyet C. (1994) Handbook of methods for the analysis of the various parameters of the carbon dioxide system in sea water. Version 2. *Epic. Diego, ORNL/CDIAC-74*.

Dietzel M., Tang J., Leis A. and Köhler S. J. (2009) Oxygen isotopic fractionation during inorganic calcite precipitation ― Effects of temperature, precipitation rate and pH. *Chem. Geol.* 268, 107–115.

Dobberschütz S., Nielsen M. R., Sand K. K., Civioc R., Bovet N., Stipp S. L. S. and Andersson M. P. (2018) The mechanisms of crystal growth inhibition by organic and inorganic inhibitors. *Nat. Commun.* 9, 1578.

Donat J. R., Lao K. A. and Bruland K. W. (1994) Speciation of dissolved copper and nickel in South San Francisco Bay: a multi-method approach. *Anal. Chim. Acta* 284, 547–571.

Dong S. and Wasylenki L. E. (2016) Zinc isotope fractionation during adsorption to calcite at high and low ionic strength. *Chem. Geol.* 447, 70–78.

Dromgoole E. L. and Walter L. M. (1990) Iron and manganese incorporation into calcite: Effects of growth kinetics, temperature and solution chemistry. *Chem. Geol.* 81, 311–336.

Eiler J. M., Bergquist B., Bourg I., Cartigny P., Farquhar J., Gagnon A., Guo W., Halevy I., Hofmann A., Larson T. E., Levin N., Schauble E. A. and Stolper D. (2014) Frontiers of stable isotope geoscience. *Chem. Geol.* 372, 119–143.

Elzinga E. J. and Reeder R. J. (2002) X-ray absorption spectroscopy study of $Cu^{2+}$and Zn^{2+}adsorption complexes at the calcite surface: Implications for site-specific metal incorporation preferences during calcite crystal growth. *Geochim. Cosmochim. Acta* 66, 3943–3954.

Emrich K., Ehhalt D. H. and Vogel J. C. (1970) Carbon isotope fractionation during the

precipitation of calcium carbonate. *Earth Planet. Sci. Lett.* 8, 363–371.

Estrade N., Cloquet C., Echevarria G., Sterckeman T., Deng T., Tang Y. T. and Morel J. L. (2015) Weathering and vegetation controls on nickel isotope fractionation in surface ultramafic environments (Albania). *Earth Planet. Sci. Lett.* 423, 24–35.

Fantle M. S. and DePaolo D. J. (2007) Ca isotopes in carbonate sediment and pore fluid from ODP Site 807A: The Ca^{2+}(aq)–calcite equilibrium fractionation factor and calcite recrystallization rates in Pleistocene sediments. *Geochim. Cosmochim. Acta* 71, 2524–2546.

Fantle M. S. and Tipper E. T. (2014) Calcium isotopes in the global biogeochemical Ca cycle: Implications for development of a Ca isotope proxy. *Earth-Science Rev.* 129, 148–177.

Fenter P., Geissbühler P., DiMasi E., Srajer G., Sorensen L. B. and Sturchio N. C. (2000) Surface speciation of calcite observed in situ by high-resolution X-ray reflectivity. *Geochim. Cosmochim. Acta* 64, 1221–1228.

Fenter P., Teng H., Geissbühler P., Hanchar J., Nagy K. and Sturchio N. (2000) Atomic-scale structure of the orthoclase (001)–water interface measured with high-resolution X-ray reflectivity. *Geochim. Cosmochim. Acta* 64, 3663–3673.

Flannery J. A. and Poore R. Z. (2013) Sr/Ca Proxy Sea-Surface Temperature Reconstructions from Modern and Holocene *Montastraea faveolata* Specimens from the Dry Tortugas National Park, Florida, U.S.A. *J. Coast. Res.* 63, 20–31.

Freund D., Rybacki E. and Dresen G. (2001) Effect of impurities on grain growth in synthetic calcite aggregates. *Phys. Chem. Miner.* 28, 737–745.

Fujii T., Moynier F., Abe M., Nemoto K. and Albarède F. (2013) Copper isotope fractionation between aqueous compounds relevant to low temperature geochemistry and biology. *Geochim. Cosmochim. Acta*, 29–44.

Fujii T., Moynier F., Blichert-Toft J. and Albarède F. (2014) Density functional theory estimation of isotope fractionation of Fe, Ni, Cu, and Zn among species relevant to geochemical and biological environments. *Geochim. Cosmochim. Acta* 140, 553–576.

Fujii T., Moynier F., Dauphas N. and Abe M. (2011) Theoretical and experimental investigation of nickel isotopic fractionation in species relevant to modern and ancient oceans. *Geochim. Cosmochim. Acta* 75, 469–482.

Gall L., Williams H. M., Halliday A. N. and Kerr A. C. (2017) Nickel isotopic composition of the mantle. *Geochim. Cosmochim. Acta* 199, 196–209.

Gall L., Williams H. M., Siebert C., Halliday A. N., Herrington R. J. and Hein J. R. (2013) Nickel isotopic compositions of ferromanganese crusts and the constancy of deep ocean inputs and continental weathering effects over the Cenozoic. *Earth Planet. Sci. Lett.* 375, 148–155.

Galy A., Bar-Matthews M., Halicz L. and O'Nions R. K. (2002) Mg isotopic composition of carbonate: insight from speleothem formation. *Earth Planet. Sci. Lett.* 201, 105–115.

Gaskova O. L., Bukaty M. B., Shironosova G. P. and Kabannik V. G. (2009) Thermodynamic model for sorption of bivalent heavy metals on calcite in natural-technogenic environments. *Russ. Geol. Geophys.* 50, 87–95.

Ghizellaoui S. and Euvrard M. (2008) Assessing the effect of zinc on the crystallization of calcium carbonate. *Desalination* 220, 394–402.

Goldberg E. D. (1954) Marine Geochemistry 1. Chemical Scavengers of the Sea. *J. Geol.* 62, 249–265.

Goldstein S. L. L. and Hemming S. R. R. (2013) *Long-lived Isotopic Tracers in Oceanography, Paleoceanography, and Ice-sheet Dynamics*. 2nd ed., Elsevier Ltd.

Gomes P. C., Fontes M. P. F., da Silva A. G., de S. Mendonça E. and Netto A. R. (2001) Selectivity Sequence and Competitive Adsorption of Heavy Metals by Brazilian Soils. *Soil Sci. Soc. Am. J.* 65, 1115.

Grossman E. L. and Ku T.-L. (1986) Oxygen and carbon isotope fractionation in biogenic aragonite: Temperature effects. *Chem. Geol. Isot. Geosci. Sect.* 59, 59–74.

Gueguen B. (2013) Contribution of nickel isotope geochemistry to the study of oceanic metalliferous deposits. .

Gueguen B., Rouxel O., Ponzevera E., Bekker A. and Fouquet Y. (2013) Nickel Isotope Variations in Terrestrial Silicate Rocks and Geological Reference Materials Measured by MC-ICP-MS. *Geostand. Geoanalytical Res.* 37, 297–317.

Gueguen B., Sorensen J. V., Lalonde S. V., Peña J., Toner B. M. and Rouxel O. (2018) Variable Ni isotope fractionation between Fe-oxyhydroxides and implications for the use of Ni isotopes as geochemical tracers. *Chem. Geol.* 481, 38–52.

Hall J. M. and Chan L.-H. H. (2004) Ba/Ca in benthic foraminifera: Thermocline and middepth circulation in the North Atlantic during the last glaciation. *Paleoceanography* 19, 1–13.

Helm L. and Merbach A. E. (1999) Water exchange on metal ions: Experiments and simulations. *Coord. Chem. Rev.* 187, 151–181.

Henderson L. M. and Kracek F. C. (1927) The fractional precipitation of barium and radium chromates. *J. Am. Chem. Soc.* 49, 738–749.

Hippler D., Buhl D., Witbaard R., Richter D. K. and Immenhauser A. (2009) Towards a better understanding of magnesium-isotope ratios from marine skeletal carbonates. *Geochim. Cosmochim. Acta* 73, 6134–6146.

Hoffmann U. and Stipp S. L. S. (2001) The behavior of Ni^{2+} on calcite surfaces. *Geochim. Cosmochim. Acta* 65, 4131–4139.

Hofmann A., Bekker A., Dirks P., Gueguen B., Rumble D. and Rouxel O. J. (2014) Comparing orthomagmatic and hydrothermal mineralization models for komatiite-hosted nickel deposits in Zimbabwe using multiple-sulfur, iron, and nickel isotope data. *Miner. Depos.* 49, 75–100.

Hofmann A. E., Bourg I. C. and DePaolo D. J. (2012) Ion desolvation as a mechanism for kinetic isotope fractionation in aqueous systems. *Proc. Natl. Acad. Sci.* 109, 18689–18694.

Hohl H., Sigg L. and Stumm W. (1980) Characterization of surface chemical properties of oxides in natural waters. *Part. Water* 189, 1–31.

Huang F., Wu Z., Huang S. and Wu F. (2014) First-principles calculations of equilibrium silicon isotope fractionation among mantle minerals. *Geochim. Cosmochim. Acta* 140, 509–520.

Jeandel C. and Oelkers E. H. (2015) The influence of terrigenous particulate material dissolution on ocean chemistry and global element cycles. *Chem. Geol.* 395, 50–66.

Jenkins W. J. (2003) Tracers of Ocean Mixing. *Treatise on Geochemistry*, 223–246.

Jenne E. A., American Chemical Society and Society for Environmental Geochemistry and Health (1979) *Chemical Modeling in Aqueous Systems: Speciation, Sorption, Solubility, and Kinetics: Based on a Symposium Cosponsored by the Society of [sic] Environmental Geochemistry and Health and the ACS Division of Environmental Chemistry at the 176th Meeting of th.*, American Chemical Society.

Jiskra M., Wiederhold J. G., Bourdon B. and Kretzschmar R. (2012) Solution speciation controls mercury isotope fractionation of Hg(II) sorption to goethite. *Environ. Sci. Technol.* 46, 6654–6662.

Joswiak M. N., Doherty M. F. and Peters B. (2018) Ion dissolution mechanism and kinetics at kink sites on NaCl surfaces. *Proc. Natl. Acad. Sci. U. S. A.* 115, 656–661.

Juillot F., Maréchal C., Ponthieu M., Cacaly S., Morin G., Benedetti M., Hazemann J. L., Proux O. and Guyot F. (2008) Zn isotopic fractionation caused by sorption on goethite and 2-Lines ferrihydrite. *Geochim. Cosmochim. Acta* 72, 4886–4900.

Katz A. (1973) The interaction of magnesium with calcite during crystal growth at 25–90°C and one atmosphere. *Geochim. Cosmochim. Acta* 37, 1563–1586.

Kitano Y., Okumura M. and Idogaki M. (1980) Abnormal behaviors of copper (II) and zinc ions in parent solution at the early stage of calcite formation. *Geochem. J.* 14, 167–175.

Kornicker W. A., Morse J. W. and Damasceno R. N. (1985) The chemistry of Co^{2+} interaction with calcite and aragonite surfaces. *Chem. Geol.* 53, 229–236.

Krabbenhöft A., Eisenhauer A., Böhm F., Vollstaedt H., Fietzke J., Liebetrau V., Augustin N., Peucker-Ehrenbrink B., Müller M. N., Horn C., Hansen B. T., Nolte N. and Wallmann K. (2010) Constraining the marine strontium budget with natural strontium isotope fractionations ($^{87}Sr/^{86}Sr^*$, $\delta^{88}Sr/^{86}Sr$) of carbonates, hydrothermal solutions and river waters. *Geochim. Cosmochim. Acta* 74, 4097–4109.

Lafuente B., Downs R. T., Yang H. and Stone N. (2016) The power of databases: The RRUFF project. In *Highlights in Mineralogical Crystallography* pp. 1–29.

Lakshtanov L. Z. and Stipp S. L. S. (2007) Experimental study of nickel(II) interaction with calcite: Adsorption and coprecipitation. *Geochim. Cosmochim. Acta* 71, 3686–3697.

Lamana R. T. (2010) Nickel sorption on calcite surface: a macroscopic experimental study, Master Thesis. McGill University, Montréal, Canada.

Lea D. W. (2013) Elemental and Isotopic Proxies of Past Ocean Temperatures. *Treatise Geochemistry Second Ed.* 8, 373–397.

Lea D. W. and Boyle E. A. (1990) Foraminiferal reconstruction of barium distributions in water masses of the glacial oceans. *Paleoceanography* 5, 719–742.

Lemarchand D., Wasserburg G. J. and Papanastassiou D. A. (2004) Rate-controlled calcium isotope fractionation in synthetic calcite. *Geochim. Cosmochim. Acta* 68, 4665–4678.

Li H., Schoonmaker J. E., Li Y.-H. and Schoonmaker J. E. (2003) Chemical composition and mineralogy of marine sediments. *Treatise on Geochemistry* 7, 1–35.

Lorens R. (1978) A study of biological and physical controls on the trace metal content of calcite and aragonite.

Lorens R. B. (1981) Sr, Cd, Mn and Co distribution coefficients in calcite as a function of calcite precipitation rate. *Geochim. Cosmochim. Acta* 45, 553–561.

Mackenzie F. T. and Lerman A. (2006) Isotopic Fractionation of Carbon: Inorganic and Biological Processes, in:Carbon in the Geobiosphere — Earth's Outer Shell —.Springer Netherlands.

Magini M., Paschina G. and Piccaluga G. (1982) Ni–Cl bonding in concentrated Ni(II) aqueous solutions at high Cl^-/Ni^{2+} ratios. An x-ray diffraction investigation. *J. Chem. Phys.* 76, 1116–1121.

Marchitto T. M. (2011) *Zinc and cadmium in benthic foraminifera as tracers of ocean paleochemistry*., Massachusetts Institute of Technology.

Marriott C. S., Henderson G. M., Belshaw N. S. and Tudhope A. W. (2004) Temperature dependence of δ^7Li, δ^{44}Ca and Li/Ca during growth of calcium carbonate. *Earth Planet. Sci. Lett.* 222, 615–624.

Marshall J. F. and McCulloch M. T. (2002) An assessment of the Sr/Ca ratio in shallow water hermatypic corals as a proxy for sea surface temperature. *Geochim. Cosmochim. Acta* 66, 3263–3280.

Mavromatis V., Gautier Q., Bosc O. and Schott J. (2013) Kinetics of Mg partition and Mg stable isotope fractionation during its incorporation in calcite. *Geochim. Cosmochim. Acta* 114, 188–203.

Mavromatis V., González A. G. A. G., Dietzel M. and Schott J. (2019) Zinc isotope fractionation during the inorganic precipitation of calcite – Towards a new pH proxy. *Geochim. Cosmochim. Acta* 244, 99–112.

Mavromatis V., Immenhauser A., Buhl D., Purgstaller B., Baldermann A. and Dietzel M. (2017) Effect of organic ligands on Mg partitioning and Mg isotope fractionation during low-temperature precipitation of calcite in the absence of growth rate effects. *Geochim. Cosmochim. Acta* 207, 139–153.

Mavromatis V., Montouillout V., Noireaux J., Gaillardet J. and Schott J. (2015) Characterization of boron incorporation and speciation in calcite and aragonite from co-precipitation experiments under controlled pH, temperature and precipitation rate. *Geochim. Cosmochim. Acta* 150, 299–313.

Mavromatis V., Schmidt M., Botz R., Comas-Bru L. and Oelkers E. H. (2012) Experimental quantification of the effect of Mg on calcite–aqueous fluid oxygen isotope fractionation. *Chem. Geol.* 310–311, 97–105.

McBride M. B. (1980) Chemisorption of Cd^{2+} on Calcite Surfaces1. *Soil Sci. Soc. Am. J.* 44, 26.

McKinney, C.R., McCrea, J.M., Epstein, S., Allen, H.A., Urey H. C. (1950) Improvements in mass spectrometers for the measurement of small differences in isotope abundance ratios. *Rev. Sci. Instrum.* 21(8), 724–730.

Meldrum F. C. and Cölfen H. (2008) Controlling Mineral Morphologies and Structures in Biological and Synthetic Systems. *Chem. Rev.* 108, 4332–4432.

Meyer H. J. (1984) The influence of impurities on the growth rate of calcite. *J. Cryst. Growth* 66, 639–646.

Milliman J. D. and Droxler A. W. (1996) Neritic and pelagic carbonate sedimentation in the marine environment: ignorance is not bliss. *Geol. Rundschau* 85, 496–504.

Mix A. C., Morey A. E., Pisias N. G. and Hostetler S. W. (1999) Foraminiferal faunal estimates of paleotemperature: Circumventing the No-analog problem yields cool Ice Age tropics. *Paleoceanography* 14, 350–359.

Möller P. and Sastri C. S. (1974) Estimation of the Number of Surface Layers of Calcite Involved in *Ca* - ^{45} *Ca* Isotopic Exchange with Solution. *Zeitschrift für Phys. Chemie* 89, 80–87.

Morse J. W., Arvidson R. S. and Lüttge A. (2007) Calcium Carbonate Formation and Dissolution. *Chem. Rev.* 107, 342–381.

Morse J. W. and Mackenzie F. T. (1990) *Geochemistry of Sedimentary Carbonates*., Elsevier.

Mucci A. (1983) The solubility of calcite and aragonite in seawater at various salinities, temperatures, and one atmosphere total pressure. *Am. J. Sci.* 283, 780–799.

Mucci A. and Morse J. W. (1985) Auger spectroscopy determination of the surface-most adsorbed layer composition on aragonite, calcite, dolomite, and magnesite in synthetic seawater. *Am. J. Sci.* 285, 306–317.

Mucci A. and Morse J. W. (1983) The incorporation of Mg^{2+} and Sr^{2+} into calcite overgrowths: influences of growth rate and solution composition. *Geochim. Cosmochim. Acta* 47, 217–233.

Munsel D., Kramar U., Dissard D., Nehrke G., Berner Z., Bijma J., Reichart G. J. and Neumann T. (2010) Heavy metal incorporation in foraminiferal calcite: Results from multi-element enrichment culture experiments with Ammonia tepida. *Biogeosciences* 7, 2339–2350.

Nielsen A. E. (1984) Electrolyte crystal growth mechanisms. *J. Cryst. Growth* 67, 289–310.

Nielsen L. C., DePaolo D. J. and De Yoreo J. J. (2012) Self-consistent ion-by-ion growth model for kinetic isotopic fractionation during calcite precipitation. *Geochim. Cosmochim. Acta* 86, 166–181.

Nielsen M. R., Sand K. K., Rodriguez-Blanco J. D., Bovet N., Generosi J., Dalby K. N. and Stipp S. L. S. (2016) Inhibition of Calcite Growth: Combined Effects of Mg^{2+} and SO_4^{2-}. *Cryst. Growth Des.* 16, 6199–6207.

O'Neil J. R. (1986) Theoretical and experimental aspects of isotopic fractionation. *Rev. Mineral.* 16, 1–40.

Parkhurst, D. L. and Appelo C. A. J. (2013) Description of input and examples for PHREEQC version 3 - A computer program for speciation, batch-reaction, onedimensional transport, and inverse geochemical calculations. *U.S. Geol. Surv. Tech. methods, Model. Tech. groundwater.*

Parkhurst D. L. and Appelo C. A. J. (1999) *User's guide to PHREEQC - a computer program for speciation, batch reaction, one-dimentional transport, and inverse geochemical calcualtions, Water-Resources Investigations Report*.,

Parsiegla K. I. and L. Katz J. (2000) Calcite growth inhibition by copper(II): II. Effect of solution composition. *J. Cryst. Growth* 213, 368–380.

Peacock C. L. and Sherman D. M. (2007) Sorption of Ni by birnessite: Equilibrium controls on Ni in seawater. *Chem. Geol.* 238, 94–106.

Pearce C. R., Parkinson I. J., Gaillardet J., Chetelat B. and Burton K. W. (2015) Characterising the stable (δ88/86Sr) and radiogenic (87Sr/86Sr) isotopic composition of strontium in rainwater. *Chem. Geol.* 409, 54–60.

Pertlik F. (1986) Structures of hydrothermally synthesized cobalt(II) carbonate and nickel(II) carbonate. *Acta Cryst.* 42, 4–5.

Pingitore N. E. and Eastman M. P. (1984) The experimental partitioning of Ba2+ into calcite. *Chem. Geol.* 45, 113–120.

Plummer L. N. and Busenberg E. (1982) The solubilities of calcite, aragonite and vaterite in CO_2-H_2O solutions between 0 and 90°C, and an evaluation of the aqueous model for the system $CaCO_3$-CO_2-H_2O. *Geochim. Cosmochim. Acta* 46, 1011–1040.

Pogge von Strandmann P. A. E. (2008) Precise magnesium isotope measurements in core top planktic and benthic foraminifera. *Geochemistry, Geophys. Geosystems* 9.

Pokrovsky O. S., Galy A., Schott J., Pokrovski G. S. and Mantoura S. (2014) Germanium isotope fractionation during Ge adsorption on goethite and its coprecipitation with Fe oxy(hydr)oxides. *Geochim. Cosmochim. Acta* 131, 138–149.

Pokrovsky O. S., Mielczarski J. A., Barres O. and Schott J. (2000) Surface Speciation Models of Calcite and Dolomite/Aqueous Solution Interfaces and Their Spectroscopic Evaluation. *Langmuir* 16, 2677–2688.

Pokrovsky O. S. and Schott J. (2002) Surface chemistry and dissolution kinetics of divalent metal carbonates. *Environ. Sci. Technol.*

Pokrovsky O. S., Schott J. and Mielczarski J. A. (2002a) Surface speciation of dolomite and calcite in aqueous solutions. In *Encyclopedia of surface and colloid science*

Pokrovsky O. S., Schott J. and Ponts T. (2002b) Surface complexation modelling of the dissolution kinetics of Mg- bearing carbonate minerals. *Pokrov. OS, Mielczarski JA, Barres O, Schott J Surf. Speciat. Model. Calcite Dolomite/Aqueous Solut. Interfaces Their Spectrosc. Eval. Langmuir 162677–2688. doi 10.1021/la980905e*, 1198–1199.

Pokrovsky O. S., Schott J. and Thomas F. (1999) Dolomite surface speciation and reactivity in aquatic systems. *Geochim. Cosmochim. Acta* 63, 3133–3143.

Porter S. J., Selby D. and Cameron V. (2014) Characterising the nickel isotopic composition of organic-rich marine sediments. *Chem. Geol.* 387, 12–21.

Quitté G. and Oberli F. (2006) Quantitative extraction and high precision isotope measurements of nickel by MC-ICPMS. *J. Anal. At. Spectrom.* 21, 1249–1255.

Raiteri P. and Gale J. D. (2010) Water Is the Key to Nonclassical Nucleation of Amorphous Calcium Carbonate. *J. Am. Chem. Soc.* 132, 17623–17634.

Ratié G., Jouvin D., Garnier J., Rouxel O., Miska S., Guimarães E., Cruz Vieira L., Sivry Y.,

Zelano I., Montarges-Pelletier E., Thil F. and Quantin C. (2015) Nickel isotope fractionation during tropical weathering of ultramafic rocks. *Chem. Geol.* 402, 68–76.

Reddy M. M. and Nancollas G. H. (1971) The crystallization of calcium carbonate: I. Isotopic exchange and kinetics. *J. Colloid Interface Sci.* 36, 166–172.

Reddy M. M. and Wang K. K. (1980) Crystallization of calcium carbonate in the presence of metal ions: I. Inhibition by magnesium ion at pH 8.8 and 25°C. *J. Cryst. Growth* 50, 470–480.

Reeder R. J. (1990) Crystal chemistry of the rhombohedral carbonates. *Rev. Miner.* 11, 1–47.

Reeder R. J., Lamble G. M. and Northrup P. A. (1999) XAFS study of the coordination and local relaxation around Co^{2+}, ZN^{2+}, Pb^{2+}, and Ba^{2+} trace elements in calcite. *Am. Miner.* 84, 1049–1060.

Reeder R. J. and Ribbe P. H. (1983) Crystal chemistry of the rhombohedral carbonates. In *Carbonates: Mineralogy and Chemistry* pp. 1–47.

Rimstidt J. D., Balog A. and Webb J. (1998) Distribution of trace elements between carbonate minerals and aqueous solutions. *Geochim. Cosmochim. Acta* 62, 1851–1863.

Rodler A., Sánchez-Pastor N., Fernández-Díaz L. and Frei R. (2015) Fractionation behavior of chromium isotopes during coprecipitation with calcium carbonate: Implications for their use as paleoclimatic proxy. *Geochim. Cosmochim. Acta* 164, 221–235.

Román-Ross G., Cuello G. J., Turrillas X., Fernández-Martínez A. and Charlet L. (2006) Arsenite sorption and co-precipitation with calcite. *Chem. Geol.* 233, 328–336.

Romanek C. S., Grossman E. L. and Morse J. W. (1992) Carbon isotopic fractionation in synthetic aragonite and calcite: Effects of temperature and precipitation rate. *Geochim. Cosmochim. Acta* 56, 419–430.

Sabine C. L., Feely R. A., Gruber N., Key R. M., Lee K., Bullister J. L., Wanninkhof R., Wong C. S., Wallace D. W. R., Tilbrook B., Millero F. J., Peng T. H., Kozyr A., Ono T. and Rios A. F. (2004) The oceanic sink for anthropogenic CO_2. *Science.*

Saenger C. and Wang Z. (2014) Magnesium isotope fractionation in biogenic and abiogenic carbonates: implications for paleoenvironmental proxies. *Quat. Sci. Rev.* 90, 1–21.

Saito M. A., Moffett J. W. and DiTullio G. R. (2004) Cobalt and nickel in the Peru upwelling region: A major flux of labile cobalt utilized as a micronutrient. *Global Biogeochem. Cycles* 18.

Sandstrom D. R. (1979) Ni^{2+} coordination in aqueous $NiCl_2$ solutions: Study of the extended x-ray absorption fine structure. *J. Chem. Phys.* 71, 2381–2386.

Sanyal A., Hemming N. G., Broecker W. S., Lea D. W., Spero H. J. and Hanson G. N. (1996) Oceanic *p*H control on the boron isotopic composition of foraminifera: Evidence from culture experiments. *Paleoceanography* 11, 513–517.

Saulnier S., Rollion-Bard C., Vigier N. and Chaussidon M. (2012) Mg isotope fractionation during calcite precipitation: An experimental study. *Geochim. Cosmochim. Acta* 91, 75–91.

Schauble E. A. (2004) Applying Stable Isotope Fractionation Theory to New Systems. *Rev. Mineral. Geochemistry* 55, 65–111.

Schlegel M. L., Nagy K. L., Fenter P. and Sturchio N. C. (2002) Structures of quartz (100)- and (101)-water interfaces determined by x-ray reflectivity and atomic force microscopy of natural growth surfaces. *Geochim. Cosmochim. Acta* 66, 3037–3054.

Schott J., Mavromatis V., Fujii T., Pearce C. R. and Oelkers E. H. (2016) The control of carbonate mineral Mg isotope composition by aqueous speciation: Theoretical and experimental modeling. *Chem. Geol.*

Schott J., Mavromatis V., González-González A. and Oelkers E. H. (2014) Kinetic and Thermodynamic Controls of Divalent Metals Isotope Composition in Carbonate: Experimental Investigations and Applications. *Procedia Earth Planet. Sci.*

Sclater F. R., Boyle E. and Edmond J. M. (1976) On the marine geochemistry of nickel. *Earth Planet. Sci. Lett.* 31, 119–128.

Sohrin Y. and Bruland K. W. (2011) Global status of trace elements in the ocean. *TrAC Trends Anal. Chem.* 30, 1291–1307.

Spivak-Birndorf L. J., Wang S. J., Bish D. L. and Wasylenki L. E. (2018) Nickel isotope fractionation during continental weathering. *Chem. Geol.* 476, 316–326.

Sposito G. (2009) *Distinguishing Adsorption from Surface Precipitation*. ed. A. C. Society,

Stipp S. L. S., Eggleston C. M. and Nielsen B. S. (1994) Calcite surface structure observed at microtopographic and molecular scales with atomic force microscopy (AFM). *Geochim. Cosmochim. Acta* 58, 3023–3033.

Stipp S. L. S. and Hochella M. F. (1991) Structure and bonding at the calcite surface as observed with X-ray photoelectron spectroscopy (XPS) and (LEED). *Geochim. Cosmochim. Acta* 55, 1723–1736.

Struempler A. W. (1973) Adsorption characteristics of silver, lead, cadmium, zinc, and nickel on borosilicate glass, polyethylene, and polypropylene container surfaces. *Anal. Chem* 45, 2251–2254.

Stumm W M. J. (1996) *Aquatic Chemistry: Chemical Equilibria and Rates in Natural Waters*., Wiley, New York.

Tahervand S. and Jalali M. (2017) Sorption and desorption of potentially toxic metals (Cd, Cu, Ni and Zn) by soil amended with bentonite, calcite and zeolite as a function of pH. *J. Geochemical Explor.*

Takasaki S., Parsiegla K. I. and Katz J. L. (1994) Calcite growth and the inhibiting effect of iron(III). *J. Cryst. Growth* 143, 261–268.

Tang J., Köhler S. J. and Dietzel M. (2008) Sr^{2+}/Ca^{2+} and $^{44}Ca/^{40}Ca$ fractionation during inorganic calcite formation: I. Sr incorporation. *Geochim. Cosmochim. Acta* 72, 3718–3732.

Tesoriero A. J. and Pankow J. F. (1996) Solid solution partitioning of Sr^{2+}, $Ba2^{+}$, and Cd^{2+} to calcite. *Geochim. Cosmochim. Acta* 60, 1053–1063.

Tipper E., Galy A.., Gaillardet J., Bickle M., Elderfield H. and Carder E. (2006) The magnesium isotope budget of the modern ocean: Constraints from riverine magnesium isotope ratios. *Earth Planet. Sci. Lett.* 250, 241–253.

Tipple B. J., Meyers S. R. and Pagani M. (2010) Carbon isotope ratio of Cenozoic CO_2 : A comparative evaluation of available geochemical proxies. *Paleoceanography* 25.

Urey H. C. (1947) The thermodynamic properties of isotopic substances. *J. Chem. Soc.*, 562–581.

Vance D., Archer C., Little S. H., Köbberich M. and de Souza G. F. (2017) The oceanic cycles of the transition metals and their isotopes. *Acta Geochim.* 36, 359–362.

Vance D., Little S. H., Archer C., Cameron V., Andersen M. B., Rijkenberg M. J. A. and Lyons T. W. (2016) The oceanic budgets of nickel and zinc isotopes: The importance of sulfdic environments as illustrated by the Black Sea. *Phil.Trans.R.Soc.A* 374.

Villegas-Jiménez A., Mucci A. and Paquette J. (2009) Proton/calcium ion exchange behavior of calcite. *Phys. Chem. Chem. Phys.* 11, 8895.

Voigt M., Mavromatis V. and Oelkers E. H. (2017) The experimental determination of REE partition coefficients in the water-calcite system. *Chem. Geol.* 462, 30–43.

Wang J., Rustad J. R. and Casey W. H. (2007) Calculation of water-exchange rates on aqueous polynuclear clusters and at oxide-water interfaces. *Inorg. Chem.* 46, 2962–2964.

Wang Y. and Xu H. (2001) Prediction of trace metal partitioning between minerals and aqueous solutions: a linear free energy correlation approach. *Geochim. Cosmochim. Acta* 65, 1529–1543.

Wasylenki L. E., Dove P. M. and De Yoreo J. J. (2005) Effects of temperature and transport conditions on calcite growth in the presence of Mg^{2+}: Implications for paleothermometry. *Geochim. Cosmochim. Acta* 69, 4227–4236.

Wasylenki L. E., Howe H. D., Spivak-Birndorf L. J. and Bish D. L. (2015) Ni isotope fractionation during sorption to ferrihydrite: Implications for Ni in banded iron formations. *Chem. Geol.* 400, 56–64.

Wasylenki L. E., Swihart J. W. and Romaniello S. J. (2014) Cadmium isotope fractionation during adsorption to Mn oxyhydroxide at low and high ionic strength. *Geochim. Cosmochim. Acta* 140, 212–226.

Wasylenki L. E., Weeks C. L., Bargar J. R., Spiro T. G., Hein J. R. and Anbar A. D. (2011) The molecular mechanism of Mo isotope fractionation during adsorption to birnessite. *Geochim. Cosmochim. Acta* 75, 5019–5031.

Watkins J. M., DePaolo D. J. and Watson E. B. (2017) Kinetic Fractionation of Non-Traditional Stable Isotopes by Diffusion and Crystal Growth Reactions. *Rev. Mineral. Geochemistry*.

Watkins J. M. and Watson E. B. (2017) Non-Traditional Stable Isotopes by Diffusion and Crystal Growth Reactions. 82, 85–125.

Watson E. B. (2004) A conceptual model for near-surface kinetic controls on the trace-element and stable isotope composition of abiogenic calcite crystals. *Geochim. Cosmochim. Acta* 68, 1473–1488.

Webb G. E. and Kamber B. S. (2000) Rare earth elements in Holocene reefal microbialites: a new shallow seawater proxy. *Geochim. Cosmochim. Acta* 64, 1557–1565.

Wiederhold J. G. (2015) Metal stable isotope signatures as tracers in environmental geochemistry.

Environ. Sci. Technol.

Wilkinson, B. H. and Algeo T. J. (1989) Sedimentary carbonate record of calciummagnesium cycling. *Am. J. Sci.* 289, 1158–1194.

Wollast R. (1990) *Rate and mechanism of dissolution of carbonates in the system $CaCO_3$ –$MgCO_3$.*, Wiley.

De Yoreo J. J., Gilbert P. U. P. A., Sommerdijk N. A. J. M., Penn R. L., Whitelam S., Joester D., Zhang H., Rimer J. D., Navrotsky A., Banfield J. F., Wallace A. F., Michel F. M., Meldrum F. C., Cölfen H. and Dove P. M. (2015) Crystallization by particle attachment in synthetic, biogenic, and geologic environments. *Science.* 349.

De Yoreo J. J. and Vekilov P. G. (2003) Principles of Crystal Nucleation and Growth. *Rev. Mineral. Geochemistry* 54, 57–93.

De Yoreo J. J., Zepeda-Ruiz L. A., Friddle R. W., Qiu S. R., Wasylenki L. E., Chernov A. A., Gilmer G. H. and Dove P. M. (2009) Rethinking Classical Crystal Growth Models through Molecular Scale Insights: Consequences of Kink-Limited Kinetics. *Cryst. Growth Des.* 9, 5135–5144.

Yuan W., Saldi G. D., Chen J., Vetuschi Zuccolini M., Birck J.-L., Liu Y. and Schott J. (2018) Gallium isotope fractionation during Ga adsorption on calcite and goethite. *Geochim. Cosmochim. Acta* 223, 350–363.

Zachara J. M., Cowan C. E. and Resch C. T. (1991) Sorption of divalent metals on calcite. *Geochim. Cosmochim. Acta* 55, 1549–1562.

Zachara J. M., Kittrick J. A. and Harsh J. B. (1988) The mechanism of Zn^{2+} adsorption on calcite. *Geochim. Cosmochim. Acta* 52, 2281–2291.

Zeebe R. E. (2005) Stable boron isotope fractionation between dissolved $B(OH)_3$ and $B(OH)_4^-$. *Geochim. Cosmochim. Acta* 69, 2753–2766.

Zeebe R. E. and Wolf-Gladrow D. A. *CO_2 in seawater : equilibrium, kinetics, isotopes*., Elsevier Science

Zhao M.-Y. and Zheng Y.-F. (2014) Marine carbonate records of terrigenous input into Paleotethyan seawater: Geochemical constraints from Carboniferous limestones. *Geochim. Cosmochim. Acta* 141, 508–531.

Zhong S. and Mucci A. (1995) Partitioning of rare earth elements (REEs) between calcite and seawater solutions at 25°C and 1 atm, and high dissolved REE concentrations. *Geochim. Cosmochim. Acta* 59, 443–453.

Annex

A version of this paper was submitted to *Geochimica et Cosmochimica Acta* on the 24th September 2018 as a manuscript titled "Experimental determination of Ni isotope fractionation during Ni adsorption from an aqueous fluid onto calcite surfaces" and is authored by Cristina Castillo Alvarez, Ghylaine Quitté, Jacques Schott and Eric H. Oelkers.

EXPERIMENTAL DETERMINATION OF NI ISOTOPE FRACTIONATION DURING NI ADSORPTION FROM AN AQUEOUS FLUID ONTO CALCITE SURFACES

Cristina Castillo Alvarez [a], Ghylaine Quitté [b], Jacques Schott [a] and Eric H. Oelkers [a]

[a] GET, CNRS-Université de Toulouse, UMR 5563, 31400 Toulouse, France, [b] IRAP, Université de Toulouse, CNRS, UPS, CNES, UMR 5277, 31400 Toulouse, FRANCE

ABSTRACT

The fractionation of Ni isotopes during Ni adsorption from aqueous fluids onto calcite surfaces was measured at 25 ^{o}C and as a function of pH from 7.7 to 8.9. Experiments showed that the percent Ni adsorbed and the degree of Ni isotope fractionation attained constant values in less than 24 hours after the calcite was exposed to the Ni bearing solution. The percentage of Ni adsorbed from the fluid onto the calcite surfaces increased from 9 to 67% as the pH increased over this range. Calcite preferentially incorporates light Ni isotopes during adsorption, resulting in a fractionation factor between adsorbed and aqueous ($\Delta^{60}Ni_{calcite\text{-}fluid}$) of -0.49 ± 0.16‰. This fractionation factor is independent of pH over the experimental range of pH. The preferential incorporation of light Ni isotopes into calcite likely results from the change in coordination environment between absorbed and aqueous nickel, Ni-O length in the Ni-CO_3 bond formed by Ni at calcite surface being greater than in the Ni^{2+} aquo ion. The recognition of the preferential uptake of isotopically light Ni by calcite surfaces may help resolve the current calculated imbalance of the Ni isotope budget in the global oceans.

1. INTRODUCTION

The interpretation of the Ni isotopic signatures in the marine record is facilitated by a detailed understanding of the mechanisms and extent of Ni isotope fractionation during natural processes. Towards this goal, equilibrium isotope fractionation between Ni adsorbed onto calcite

surfaces and its coexisting aqueous fluids was measured as a function of pH at 25 ^{o}C. The purpose of this paper is to report the results of this experimental study and to use these results to better assess the Ni isotopic compositions of various natural Ni reservoirs.

The marine budgets of transition metals and their isotopes help constrain size and importance of natural sources and sinks on a global scale. The global marine Ni budget is controlled by the input of dissolved Ni from river water, dissolution in the oceans of riverine and atmospheric transported particulate material, Ni scavenging by marine minerals sedimentation, and geothermal activity (Sclater et al., 1976; Jeandel and Oelkers, 2015). Based on isotopic mass balance considerations from these sources it has been concluded that another source of isotopically heavy Ni or another sink of isotopically light Ni is missing in these mass balance calculations (Gall et al., 2013; Gueguen et al., 2013; Cameron and Vance, 2014; Porter et al., 2014). A number of processes have been suggested as the possible light Ni sink. As adsorption of Ni onto Fe/Mn oxide surfaces is a major sink in the ocean (Peacock and Sherman, 2007), this process has been proposed to bridge this imbalance. Indeed, experimental work by Wasylenki et al. (2015) shows that Ni sorption onto ferrihydrite surfaces favors the incorporation of light Ni, leaving an isotopically heavier Ni in aqueous solution behind. This possible solution to the currently perceived marine Ni imbalance, however, has been questioned by Gall et al. (2013) based on the analysis of the Ni isotopic compositions of modern marine precipitated ferrihydrite. An alternative sink to potentially resolve this imbalance is the scavenging of Ni by sulfides associated with anoxic or suboxic marine sediments enriched in organic matter (Gueguen et al., 2013; Eiler et al., 2014). The present study considers the possibility that Ni adsorption onto calcite surfaces may also contribute to this imbalance in the global marine Ni budget.

Nickel isotope fractionation has received attention due to its potential use as tracer of biochemical processes (Cameron et al., 2009). Nickel exhibits a nutrient-like behavior, with its dissolved concentration ranging from 2 nmol/kg at the ocean surface to 12 nmol/kg at greater depths (Sohrin and Bruland, 2011). Interest in Ni isotope fractionation stems in part from results of ab-initio calculations performed by (Fujii et al., 2011) who reported that aqueous Ni-organic complexes exhibit a unique degree of Ni isotope fractionation. Indeed, laboratory experiments have documented significant Ni isotope fractionation during its incorporation into methanogens (Cameron et al., 2009) and uptake by plants (Estrade et al., 2015).

Nickel adsorption onto calcite surfaces is also of interest due to its unique adsorption behavior. Ni adsorbs on calcite by rearranging the solid surface through the formation of Ni-carbonate surface complexes (Stipp et al., 1994; Hoffmann and Stipp, 2001) that remain on the surface as partly hydrated exchangeable ions (Zachara et al., 1991). The single-ion hydration energies of the metal sorbates is also a good approximation for the sorption reversibility of metals (Zachara et al. 1991). The high hydration energy of Ni prevents its dehydration on the calcite surface, which is a required step for its incorporation into the bulk mineral. Nevertheless nickel's electron configuration leads its hydrated complexes on calcite surfaces to be more stable than those of other divalent metal complexes (Hoffmann and Stipp, 2001). The degree to which these unique Ni adsorption properties affect its isotopic fractionation will be assessed with the aid of this experimental study.

2. MATERIALS AND METHODS

Experiments were performed to quantify the equilibrium Ni stable isotope fractionation between aqueous Ni and Ni adsorbed on the calcite surface. Three series of experiments were conducted. First, Ni was adsorbed onto calcite surface at constant pH and aqueous Ni concentration as a function of time to assess the kinetics of this reaction. Second, Ni was adsorbed onto calcite surfaces at constant pH and various aqueous Ni concentrations. Third, Ni was adsorbed onto calcite surfaces at constant aqueous Ni concentrations and various pH. In all instances the concentration of Ni in the aqueous solution was kept below the solubility of gaspeite ($NiCO_3$) to avoid its precipitation during the experiments.

2.1 starting materials

Synthetic high purity Merck MESURE® calcite was used for all experiments. Prior to its use in the experiments, this calcite was first washed in distilled acetone, then pretreated according to the method described by Reddy and Nancollas (1971). The quality of the resulting calcite was assessed by X-ray diffraction using an INEL CPS-120 diffractometer with Co Kα-radiation having a detection limit of ~5%. The acquired diffraction patterns were compared to the characteristic

profile for calcite taken from the RRUFF database (Lafuente et al., 2016). This comparison confirmed the solid to be pure calcite. A surface area of 0.31±0.03 m^2/g was determined by triple-point krypton adsorption according to the BET method (Brunauer et al., 1938), using a Quantachrome Autosorb-1MP instrument. Scanning Electron Microscope (SEM) images were obtained of this initial calcite using a JEOL JSM 6700F spectrometer at the Raimond Castaing center for microcharacterization in Toulouse, France. Resulting images are displayed in Fig. 1. They show the rhombohedral morphology of the calcite crystals, as well as intergrowth and agglomeration. These SEM images were also used to determine the average length of the calcite crystal to be about 6µm.

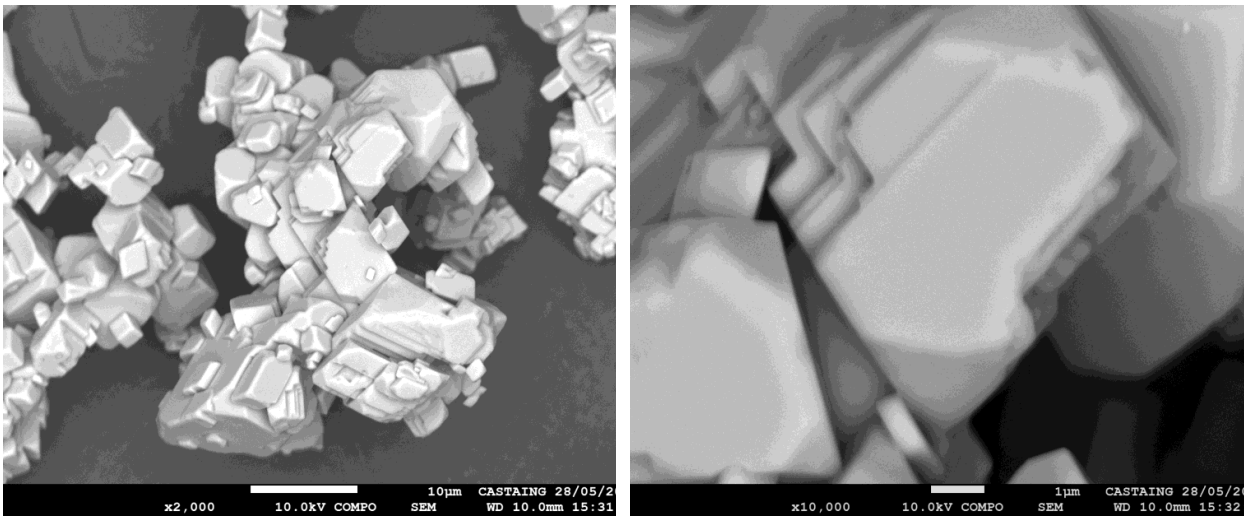

Figure 1. SEM images of the synthetic calcite used in the present study. The scale bar in the left image is 10 µm long, whereas the scale bar in the right image is 1 µm long.

The initial aqueous fluids used in the experiments were pre-equilibrated with the same calcite used in the experiments. These pre-equilibrated fluids were prepared by adding approximately 2 g of calcite to an aqueous solution having a total ionic strength of 0.01 mol/kg. The solution was prepared using reagent grade NaCl, HCl, NaOH and 18.2 MΩ Milli-Q water obtained from a Millipore system. The pH of the aqueous solutions was then adjusted to a value from 7.6 to 8.8 for the pH dependent experiments, or to 8.3 for the time dependent and adsorption isotherm experiments by adding either HCl or NaOH. This fluid remained in contact with the

calcite for up to 3 weeks until the measured pH was constant. The pre-equilibrated fluid was separated from the calcite by filtration using a Merck Millipore 0.22 μm teflon syringe filter prior to its use. The aqueous Ni stock solutions added to these fluids for subsequent adsorption experiments were created by dissolving Sigma-Aldrich, 99.99 %, trace metal basis $Ni(NO_3)_2$ to 18.2 M**Ω** water to obtain a 6 ppm Ni solution.

All adsorption experiments were performed in 50 ml screw top polycarbonate centrifuge tubes. Each experiment was initiated by placing a known quantity of calcite powder and a Ni free aqueous solution pre-equilibrated with calcite into the tube. Each reactor was closed and mixed using a rotator for 24 hours. After this time a selected quantity of an aqueous Ni stock solution was added to the initial calcite-aqueous fluid mixture, prior to reclosing the tube. This mixture was then returned to the rotator. After a given time period (from 0.5 to 168 hrs for the time dependent series, 24 hrs for the Ni adsorption isotherm, and 72 hours for the pH dependent experiments), a tube was removed from the rotator and the reactor with its content was centrifuged for 15 minutes at 4500 rpm on an Eppendorf 5804 centrifuge. The tube was then opened and the solids were separated from the fluid phase using a 0.2 micron Teflon Merck Millipore filter. The collected fluids were separated into three subsamples: one of the subsamples was used to measure pH immediately after sampling, while the other two samples were acidified, one with ultrapure HNO_3 and the other with ultrapure HCl for further analysis. Before starting the Ni sorption runs on calcite several tests were conducted to ensure that no nickel could be adsorbed on the walls of the polycarbonate tubes from solutions at the pHs investigated in this study. No measurable loss of Ni from the starting solution was observed after a period of 1 day during which the tubes were continuously shaken.

2.2 Chemical analyses

Nickel concentrations of the initial stock solutions and collected final fluid samples of each experiment were determined using an Atomic Absorption Spectrometer Perkin Elmer AAnalyst 600 together with a graphite furnace. Concentrations were obtained from measured absorbance using a calibration curve generated from standards having concentrations ranging from 10-100 ppb. New standards were prepared fresh and new calibration curves were made each day the analyses were performed. A 0.05M NH_4Cl matrix modifier was used during the measurements. The uncertainties on these analyses, based upon duplicated measurements are estimated to be ± 2%.

The pH of fluid samples was measured immediately after sampling using a standard Mettler Toledo glass pH electrode. This electrode was calibrated before every measurement using Thermo Fisher pH=4.006, 6.865 and 9.183 buffer solutions at 25°C. The uncertainties on these pH measurements are estimated to be ±0.03 pH units.

2.3 Ni isotope analysis

2.3.1 Isotope notation

Isotope compositions in this paper are presented in delta notation, δ^{60}Ni, corresponding to ratio of ^{60}Ni relative to ^{58}Ni normalized to the Aldrich ICP standard. The isotopic offset between this metal on the solid and the fluid phase ($\triangle\ ^{60}\mathrm{Ni}_{\ solid-fluid}$) is defined by

$$\triangle\ ^{60}\mathrm{Ni}_{\ solid-fluid} = \delta^{60}\mathrm{Ni}_{solid} - \delta^{60}\mathrm{Ni}_{fluid} \quad (1)$$

Assuming that the loss of Ni from the solution was solely caused by Ni sorption on calcite, the average isotopic composition of sorbed Ni during a closed system adsorption experiment can be calculated from the initial and final Ni chemical and isotopic compositions of the fluid and mass balance considerations taking account of (Criss, 1999)

$$\delta^{60}\mathrm{Ni}_{total} m_{\mathrm{Ni},total} = \delta^{60}\mathrm{Ni}_{solid} m_{\mathrm{Ni},solid} + \delta^{60}\mathrm{Ni}_{fluid} m_{\mathrm{Ni},fluid} \quad (2)$$

where $m_{\mathrm{Ni},solid}$ and $m_{\mathrm{Ni},fluid}$ refer to the mass of Ni adsorbed onto the calcite and present in the aqueous fluid phase, respectively. Note that $\delta^{60}\mathrm{Ni}_{total}$ and $m_{\mathrm{Ni},total}$ are constant during a closed system reactor experiment.

2.3.2 Sample purification

Prior to the measurement of Ni isotopic ratios by mass spectrometry, Ni was separated using an approach based on Quitté and Oberli (2006). This separation procedure was performed under a laminar flow hood using trace metal grade NH_4OH and H_2O_2, and doubly distilled HNO_3 and HCl. The overall purification of the samples consisted of five separation steps:

1) The first step began by evaporating the sample to dryness in Savillex Teflon containers. The resulting residue was dissolved in 2 ml of 9 M aqueous HCl. An ion exchange column

was prepared by adding 1.8 mL of pre-cleaned, Bio-Rad 100–200 mesh AG1-X8 anion resin to a 10-mL polypropylene column. The resin was cleaned with alternating 6N HCl and 18.2 MΩ H_2O and then conditioned by passing 10 mL of 9M HCl through the column. The 2 ml sample was then passed through the column to remove Fe from the sample. Nickel eluted immediately. A further 4 ml of 9N HCl was added to the column to ensure the complete recovery of Ni.

2) The second step aimed at removing Zn from the sample. It began by evaporating the Ni elution cut collected from the first step to dryness and re-dissolving it into 2 ml of 2 M HCl. This sample was passed through the same ion exchange column as in the first step described above, but conditioned this time by passing 10 mL of a 2M HCl through the column. The sample was loaded on the column in 2mL 2M HCl, once again Ni eluted immediately, and a further 4 ml of 2M HCl was passed through the column to ensure the complete recovery of Ni.

3) The third step separated major matrix elements. It began by evaporating the Ni elution sample collected from step 2 to dryness then redissolving it into 5 ml of 1 M HCl and 1 ml of 1M ammonium citrate. The ammonium citrate solution was prepared by mixing a citric acid solution and a trace grade NH_4OH solution. Once its pH has been adjusted to 8-9 using NH_4OH, the sample was then loaded onto a column filled with 2 ml of Triskem Nickel specific resin (based on dimethylglyoxime, DMG). Prior to its use, this resin was cleaned with water and ammonium citrate and conditioned with 5 ml of 0.2M of ammonium citrate whose pH was adjusted to 8-9. After the sample was loaded onto the resin in the column, it was washed with 20 ml of 0.2 M ammonium citrate (adjusted pH=8-9) to remove matrix elements. Nickel was then recovered from the column by passing 12 ml of 3M HNO_3. Three drops of perchloric acid were added to the Ni fraction to get rid of the DMG-Ni complex and the sample was evaporated to dryness. The sample was then taken up in 1mL of concentrated HNO_3 and 1mL of ultrapure H_2O_2 and heated for a few hours to remove potential organics and ensure a complete release of Ni from the DMG-Ni complex. The sample was then evaporated again. If necessary, this oxidation procedure was repeated twice.

4) The fourth step is a purification step. The cleaned residue was dissolved into 0.2mL of 18.2 MΩ H_2O and passed through a column containing 0.12 mL of Bio-Rad AG50W-X8 resin (200–400 mesh), previously cleaned with H_2O and 6M HCl for 2 cycles, then conditioned with water. The matrix elements were washed with 2.5 mL of 0.2M HCl, then Ni was recovered in 0.5 mL of 3M HCl.

Table 1 Summary of the purification procedure used to prepare fluid samples for Ni isotope analysis by mass spectrometry.

	reagent	volume (mL)
Col. 1		
resin	AG1-X8	2
conditioning	2M HCl	10
load	2M HCl *	2
Ni elution	2M HCl	4
Col. 2		
resin	AG1-X8	2
conditioning	9M HCl	10
load	9M HCl *	2
Ni elution	9M HCl	4
Col. 3		
resin	Nickel specific	2
conditioning	0.2M $(NH_4)_3C_6H_8O_7$	12
load	1M $(NH_4)_3C_6H_8O_7$ +1M HCl	1+5
clean matrix	0.2M $(NH_4)_3C_6H_8O_7$	20
Ni elution	3M HNO_3	12
Col. 4		
resin	AG50W-X8	0.15
conditioning	H_2O	0.7
load	H_2O	0.2
clean matrix	0.2M HCl	2.5
Ni elution	3M HCl	0.5
Col. 5		
resin	AG1-X8	2
conditioning	6M HCl	10
load	2M HCl *	2
Ni elution	2M HCl	4

* Ni starts eluting during this step

5) The final step removed any remaining Fe from the sample (including Fe released by the resin), and followed closely the protocol of step 1 or 2, replacing 9M or 2M HCl by 6M HCl. A summary of these steps is provided in Table 1.

2.3.3 Mass spectrometry

The sample recovered from step 5 was dried and the residue retained for analysis. This residue was finally dissolved in 0.1M HCl for isotope analysis. Nickel isotope measurements were performed at the OMP analytical platform in Toulouse France, using a Thermo-Finnigan Neptune multi-collector inductively coupled plasma mass spectrometer (MC-ICPMS). Samples were measured in medium resolution mode, using the sample-standard bracketing technique and Cu doping to correct for mass bias. The concentration of the measured samples varied between 50 and 200 ppb, and the Cu concentration was kept at half that of Ni. Samples were measured in 2 cycles. During the first cycle, stable Ni isotope masses were measured (58, 60, 61, 62 and 64) along with masses 57 and 66, which are used to correct for possible isobaric interference from ^{58}Fe and ^{64}Zn, respectively. During the second cycle, Cu isotopes were measured together with Ni isotopes and used to correct for instrumental mass bias.

A sigma Aldrich Ni standard was processed through the whole chemical separation procedure with every set of experimental samples to ensure that no fractionation occurred during the Ni separation process. The original composition of this standard is plotted next to the average composition of processed standards in figure 2. No isotope fractionation is observed for the processed standards relative to the corresponding unprocessed standards, confirming that the chemical procedure is well suited to study the natural mass dependent isotope fractionation characteristic of our experimental samples. The 2SD (standard deviations) of δ^{60}Ni was calculated based on multiple (typically 3) measurements of each solution and ranged between 0.01 and 0.11‰.

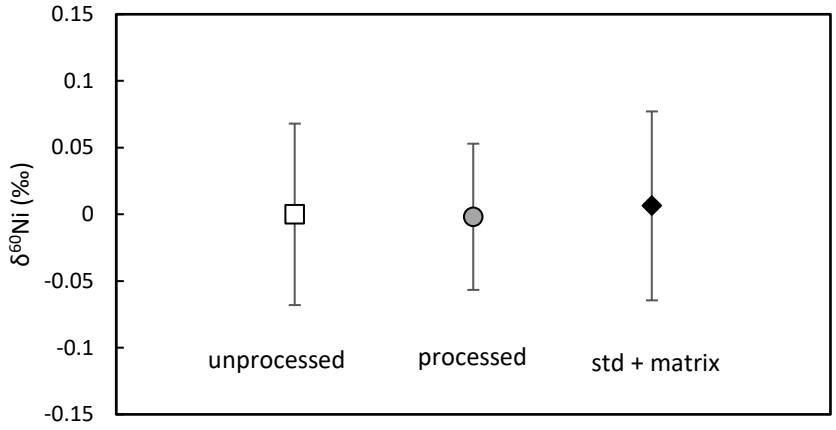

Figure 2. Ni isotopic composition of processed and unprocessed standards used to validate the analytical procedure. The open square represents the isotope composition of the unprocessed standard, the filled circle shows the composition of the processed standard, and the filled diamond shows the composition of a standard-doped processed experimental matrix.

2.4 Geochemical Calculations

All thermodynamic calculations, including aqueous fluid speciation calculations and mineral solubility calculations were performed using PHREEQC (Parkhurst and Appelo, 1999) together with its minteq.v4 database.

3. RESULTS

In total, 28 individual batch experiments were performed in the three series. The conditions and measured fluid compositions of these experiments are summarized in Table 2. The first experimental series was designed to assess if Ni adsorption onto calcite surfaces, and its associated fraction are time dependent. The results of this series are shown in Figure 3 for reaction times from 3 to 168 hrs. It can be seen that the extent of Ni adsorption keeps constant from the very first sampling after 3 hrs. In contrast isotopic steady-state is reached only after ~30 hrs, and the isotopic composition of sorbed Ni becomes very slightly lighter with time which may reflect some incorporation of Ni in the calcite lattice.

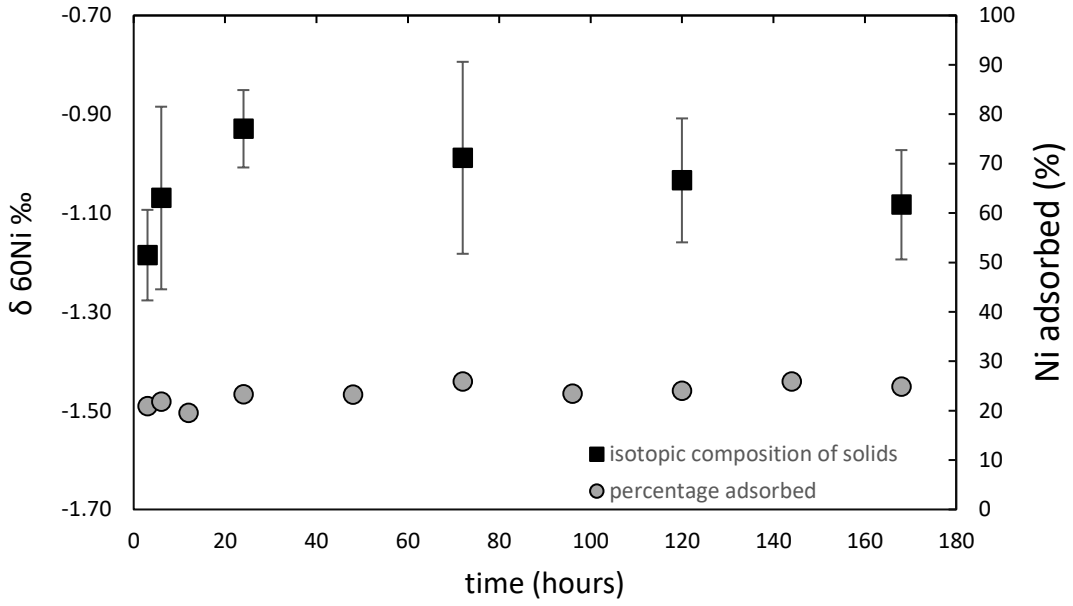

Figure 3 Percent of Ni adsorbed on calcite surfaces and the Ni isotopic composition of this adsorbed Ni as a function of elapsed time at 25 ºC and pH 8.3. The percent Ni adsorbed is shown as filled circles and their values are given in the right hand scale, whereas the corresponding Ni isotope composition of the solids is shown as filled squares, these values are given by the left axis. The isotope composition of the solids was obtained from the measured aqueous Ni isotopic composition using mass balance considerations. The uncertainties on the measured adsorption extent is approximated by the symbol size.

A second experimental series was designed to assess the partition coefficient of Ni onto the calcite surfaces. This series was run at a pH of 8.3 and aqueous Ni concentrations varied from 60 to 120 ppb. The Ni concentrations in this experimental series was limited on one hand by the analytical detection limits for Ni and on the other hand by the requirement to keep this fluid undersaturated with respect to gaspeite ($NiCO_3$). A linear correlation between the concentration of aqueous Ni and adsorbed Ni was observed (see Fig. 4) consistent with adsorption being the predominant mechanism for Ni loss from solution. The apparent partition coefficient of Ni at pH=8.3 was calculated to be

$$K_d = (m_{Ni\text{-}ads}/m_{solid})/(m_{Ni\text{-}aq}/m_{solution}) = 0.011.$$

Note that Ni isotope compositions were not determined for the samples collected from this experimental series.

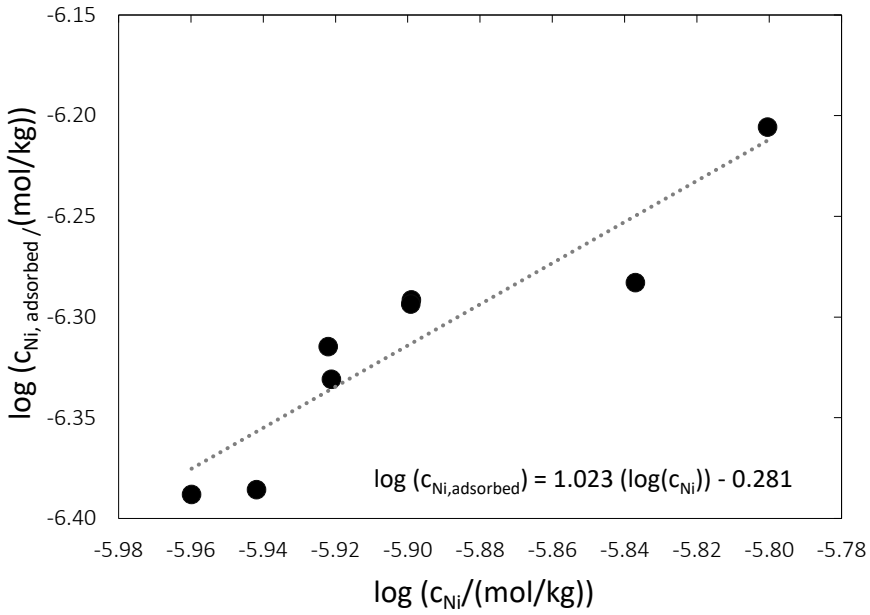

Figure 4 Variation of the Ni concentration adsorbed on calcite surfaces as a function of the aqueous Ni concentration at 25 °C. The line shown through the data points corresponds to a least squares fit of the data; the equation of this line is provided on the figure.

A third experimental series determined the amount of Ni adsorbed onto calcite surfaces as a function of pH from 7.6 to 8.8. The results, shown in Fig. 5, illustrate the increase in the percent of Ni adsorbed from 8.7 to 67 % as the pH increased over this range. The Ni isotope composition of the fluids and solids recovered from this experimental series, as well as those recovered from the first experimental series are plotted as a function of the fraction of Ni adsorbed on calcite in Fig 6. Note that whereas the Ni isotope compositions of the fluids in this figure were directly determined from measurements, those of the solids were determined from the measured fluid compositions and mass balance constraints. It can be seen that all experiments show a preferential sorption of Ni lighter isotopes on calcite surface leaving the experimental solutions heavier than the initial Ni stock solution. The offset between the fluid and adsorbed Ni compositions is almost independent of the percentage of Ni adsorbed which indicates that Ni isotope fractionation during adsorption

on calcite surface occurs at equilibrium. The extent of Ni isotope fractionation between calcite surface and the fluid is plotted as a function of pH in Figure 6b. It can be seen that the fractionation factor between solid and solution, $\Delta^{60}Ni_{calcite\text{-}fluid}$ = -0.49±16‰ does not vary significantly as the pH increases from 7.7 to 8.6. Note that Ni isotopic fractionation very slightly increases (by about 0.05‰) at the lowest Ni surface coverage which may reflect some Ni surface precipitation for high Ni surface coverage. However, one should note the large uncertainty affecting the data for the lowest extents of Ni sorption.

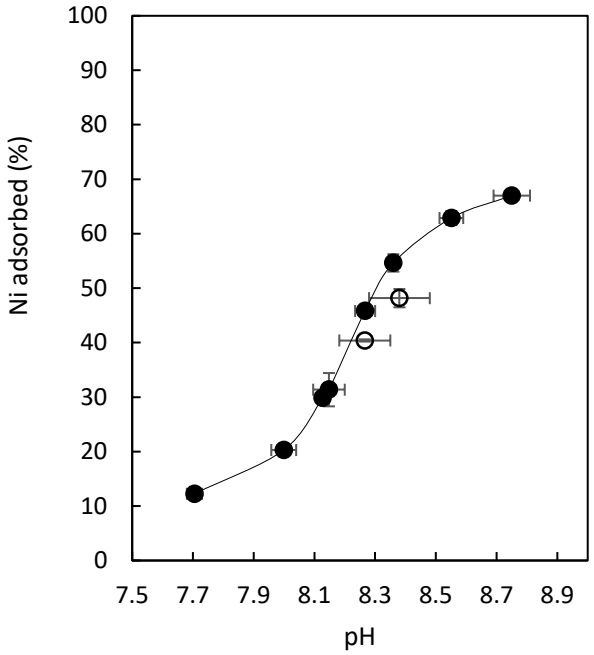

Figure 5. The percent Ni adsorbed from the aqueous solution onto calcite surfaces as a function of pH at 25 °C. The filled symbols correspond to experiments where the isotopic compositions of Ni were determined, whereas these were not determined for experiments shown as open symbols.

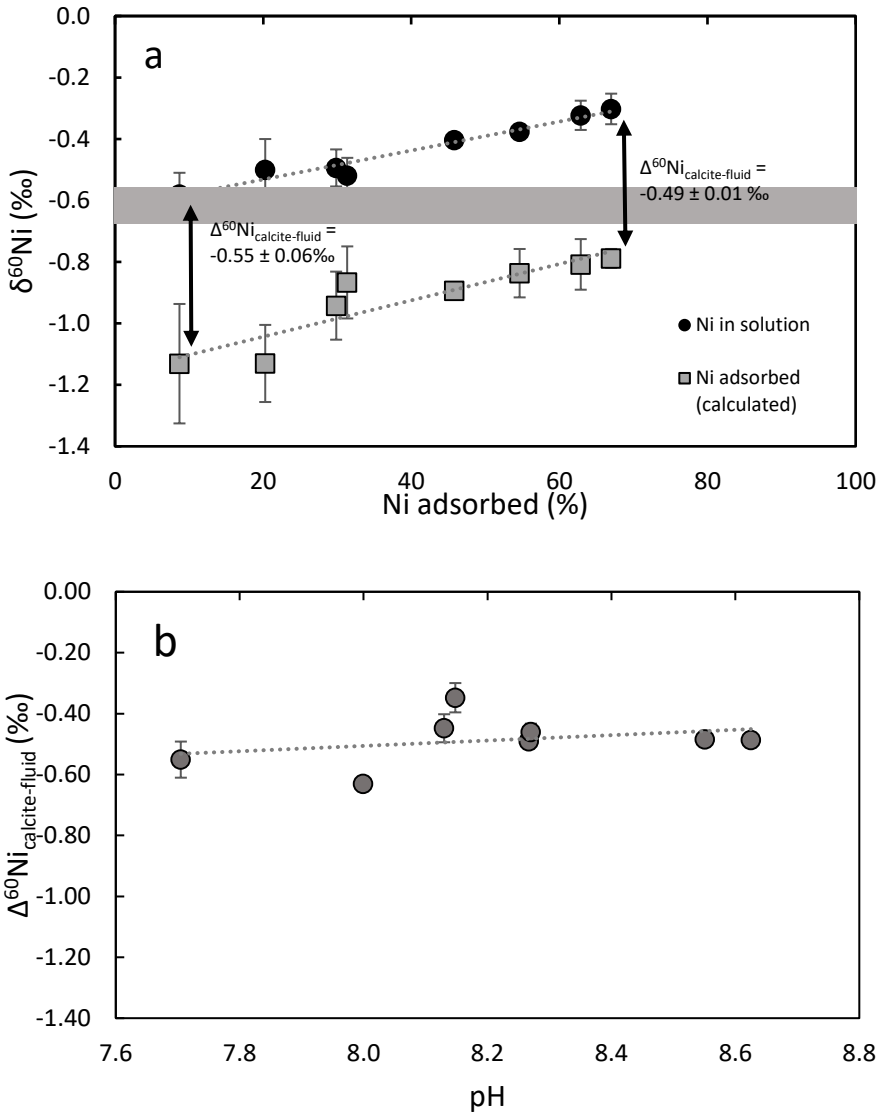

Figure 6 a) Ni isotope composition of the adsorbed and aqueous Ni as a function of percentage of Ni adsorbed and b) the Ni fractionation factor between calcite and fluid ($\Delta^{60}Ni_{calcite\text{-}fluid}$) as a function of pH. In figure 6a, the circles represent the Ni isotope compositions of the aqueous solutions, which were directly measured. The squares represent the isotopic compositions of the Ni adsorbed onto calcite surfaces, which were obtained from mass balance calculations – see text. The gray band shows the initial composition of the solution.

Table 2: Summary of measured total aqueous Ni concentrations, and the Ni isotopic compositions of the aqueous fluid and calcite measured from samples collected from time dependent experimental series and the pH dependent experimental series Samples collected from the time dependent series are labeled with the prefix K, whereas the pH dependent series are labeled with the prefix P. [a] *The isotopic composition of the solid was determined using mass balance calculations*

label	pH	Experiment duration (hours)	Total Ni. (ng)	Final aqueous Ni (ng)	$\delta^{60/58}$Ni (fluid) ‰	2 σ	$\delta^{60/58}$Ni (solid)[a] ‰	2 σ	$\Delta^{60/58}$Ni solid-fluid ‰	2 σ
K01	8.3	3	2998	2370	-0.48	0.04	-1.19	0.09	-0.70	0.05
K02	8.2	6	3005	2349	-0.50	0.08	-1.07	0.18	-0.56	0.10
K03	8.3	12	3014	2424			-3.21			
K04	8.2	24	3008	2307	-0.54	0.03	-0.93	0.08	-0.39	0.04
K05	8.3	48	2980	2288			-2.70			
K06	8.2	72	2977	2207	-0.50	0.10	-0.99	0.19	-0.49	0.11
K07	8.2	96	2976	2279			-2.68			
K08	8.2	120	2973	2257	-0.50	0.06	-1.03	0.13	-0.53	0.07
K09	8.2	144	2972	2198			-2.43			
K10	8.2	168	2973	2234	-0.48	0.06	-1.08	0.11	-0.61	0.06
P01	7.7	72	3108	2825	-0.58	0.02	-1.13	0.12	-0.55	0.06
P02	8	72	3111	2502	-0.50	0.01	-1.13	0.02	-0.63	0.01
P03	8.1	72	3117	2221	-0.49	0.05	-0.94	0.08	-0.45	0.05
P04	8.2	72	3120	2178						
P05	8.1	72	3111	1734	-0.52	0.05	-0.87	0.08	-0.35	0.05
P06	8.3	72	3113	1473	-0.40	0.03	-0.89	0.03	-0.49	0.02
P07	8.4	72	3109	1890						
P08	8.3	72	3115	1669	-0.38	0.04	-0.84	0.03	-0.46	0.03
P09	8.6	72	3118	1231	-0.32	0.02	-0.81	0.01	-0.49	0.01
P10	8.6	72	3111	1095	-0.30	0.01	-0.79	0.01	-0.49	0.01

4. DISCUSSION

4.1 Comparison of measured Ni adsorption with previous studies.

The nickel sorption isotherm, plotted on a log-log scale in Fig. 4, exhibits a linear trend with a slope close to 1, which is the same trend described by previous experiments (Zachara et al., 1991; Lakshtanov and Stipp, 2007; Belova et al., 2014). This behavior indicates that the partitioning of Ni within solid and liquid phases does not depend on the Ni concentration The apparent partition coefficient deduced from the data reported in Figure 4, $K_{Ni} = 0.011$ at pH = 8.3 is in good agreement with the value extracted from Zachara et al. (1991) at the same pH ($K_{Ni} = 0.012$). The maximum of Ni adsorption in the experiments presented above is reached after a few hours, which is consistent with previous work on Ni (Zachara et al., 1991) and other divalent cations (McBride, 1980; Zachara et al., 1988). Our experiments show no variation in the amount of Ni adsorbed at the calcite surface as time progresses; a similar behavior was observed for Ni adsorption on ferrihydrates and goethite (Wasylenki et al. 2015) and Zn on calcite (Dong and Wasylenki, 2016).

Nickel adsorption onto calcite surfaces increases with pH to pH ~ 9 which is in accord with the previous studies (Zachara et al., 1991; Belova et al., 2014; Tahervand and Jalali, 2017).This is associated with the buildup of a negative charge on calcite surface. Within the framework of calcite surface complexation models (Van Cappellen et al., 1993; Pokrovsky et al., 1999; Pokrovsky et al., 2000), Ni could be adsorbed according to the following reaction (Pokrovsky et al., 2002b):

$$>CO_3^- + Ni^{2+} = >CO_3Ni^+ \quad (3)$$

where $>CO_3^-$ and $>CO_3Ni^+$stand for the deprotonated carbonate site and the Ni surface complex formed on the carbonate site, respectively. The increase of $>CO_3^-$ concentration with increasing pH to pH ~ 9 accounts for the corresponding increase of the extent of Ni sorption.

4.2 Interpretation of Ni isotope fractionation during its adsorption onto calcite surfaces.

A number of past studies have measured Ni fractionation as it adsorbs onto mineral surfaces. Wasylenki et al. (2015) determined $\Delta^{60}Ni_{ferrihydrite\text{-}fluid}$ during 25 ºC adsorption

experiments to be -0.35 ± 0.10‰. Similarly Gueguen et al. (2018) reported an identical $\Delta^{60}Ni_{ferrihydrite\text{-}fluid}$ = -0.35 ± 0.08‰ from corresponding experiments. Spivak-Birndorf et al. (2018) reported that nickel isotope fractionation from aqueous solution onto montmorillonite resulted in a $\Delta^{60}Ni_{montrormillinite\text{-}fluid}$ = -0.11 ± 0.09‰. The adsorption of Ni from aqueous solution onto goethite was reported to yield the greatest fractionation with $\Delta^{60}Ni_{goethite\text{-}fluid}$ = -0.77 ± 0.23‰ (Gueguen et al. 2018). These relatively small fractionation factors are consistent with that generated for the adsorption of Ni onto calcite in the present study, $\Delta^{60}Ni_{calcite\text{-}fluid}$ = -0.49 ± 0.16‰ (2SD).

This study shows that calcite preferably adsorbs light Ni isotopes. In contrast, calcite preferentially absorbs heavy Zn, with $\Delta^{66}Zn_{adsorbed\text{-}solution}$ averaging 0.41 ± 0.18‰ and 0.73 ± 0.08‰ in 0.1 and 0.7 M aqueous NaCl solutions, respectively (Dong and Wasylenki, 2016). This preferential uptake of heavy Zn was interpreted to stem from a change in coordination between the aqueous six-fold $Zn(H_2O)_6^{2+}$ complex and Zn adsorbed on the calcite surface, which has a four-fold coordination (Dong and Wasylenki, 2016). This tetrahedral coordination of Zn on the calcite surface was confirmed through EXAFS analysis (Elzinga and Reeder, 2002). Similarly changes in the coordination geometry of metal cations as they adsorb onto mineral surfaces has been shown to cause isotopic fractionation (e.g. for Ga isotopes on calcite and goethite surfaces, Yuan et al., 2018)). This behavior of Zn contrasts with that of Ni, which likely does not change coordination number as it adsorbs to calcite surfaces from aqueous solution. In cases where coordination number does not change upon adsorption, small distortions of bond angles and lengths can also drive isotopic fractionation (Juillot et al., 2008; Brennecka et al., 2011; Wasylenki et al., 2014; Wasylenki et al., 2015; Gueguen et al., 2018).

Several experimental and theoretical studies have been carried out to determine the Ni-O bond length in aqueous $Ni(H_2O)_6^{2+}$. Experimentally measured bond lengths range between 2.05-2.07 Å (XRD, (Caminiti et al., 1977; Magini et al., 1982)and 2.07 Å (EXAFS, Sandstrom, 1979). These values are in good agreement with DFT (Density Functional Theory) calculations for the cluster $Ni(H_2O)_{18}^{2+}$ (2.073 Å, Fujii et al., 2011). They are slightly shorter than Ni-O bond length in gaspeite ($NiCO_3$) as determined by XRD (2.076 Å, Pertlik, 1986). This suggests that the replacement in nickel environment, during its adsorption at calcite surface, of a H_2O by a carbonate group should result in a slight increase of the Ni-O bond length and induce an enrichment in light isotope of the Ni surface complex formed.

Previous studies have reported that the isotopic fractionation of metals between a fluid and a mineral phase also depends on the aqueous speciation of this metal (Balan et al., 2018; Fujii et al., 2011, 2014; Mavromatis et al., 2018; Schott et al., 2016). As our experiments were performed at pHs ranging from 7.7 to 8.6, Ni aqueous speciation was impacted by the formation with increasing pH of $NiHCO_3^+$ and $NiCO_3°$ at the expense of the Ni^{2+} aquo ion. Based on the thermodynamic constants for Ni aqueous species from the minteq.v4 database, Ni^{2+} accounts for 92% of total dissolved Ni at pH 7.7 but for only 48% at pH 8.6. At the same time, if $NiHCO_3^+$ and $NiCO_3°$ concentrations are negligible at pH 7.7, they represent at pH 8.6 respectively 8 and 41% of dissolved nickel. Based on Fujii et al. (2011, 2014), DFT calculations of reduced partition function ratios among Ni aqueous species, the equilibrium fractionation factor at 25°C between aqueous Ni^{2+} and $NiCO_3°$ ($\Delta^{60}Ni_{Ni+2\text{-}NiCO3°}$) is equal to -0.557‰ and that between Ni^{2+} and $NiHCO_3^+$ ($\Delta^{60}Ni_{Ni+2\text{-}NiHCO3+}$) is -0.355‰. As such the nickel carbonate and bicarbonate complexes present in solution at pH 8.6 should make $Ni^{2+}_{(aq)}$ and adsorbed Ni ~0.26‰ lighter than at pH 7.7. The data of the present study do not show this slight enrichment of adsorbed Ni in light isotopes (^{58}Ni) when solution pH increases from 7.7 to 8.6. However, it should be noted that according to the stability constants values of $NiCO_3°$ and $NiHCO_3^+$ recently published by Baeyens et al. (2003), Ni^{2+} would account at pH 8.6 for 69% of total dissolved Ni, and $NiCO_3°$ and $NiHCO_3^+$ for only 25 and 2%, respectively. The subsequent enrichment of Ni^{2+}(aq) and adsorbed Ni in light isotope would be of ~0.13‰ which is within the uncertainty attached to our isotopic measurements.

4.3 Implications for natural systems.

A number of previous works have concluded that our current understanding of the Ni isotopic balance in the oceans requires the identification of either another source of isotopically heavy Ni or another sink of isotopically light Ni. Various processes have been suggested as the possible light Ni sink including adsorption of Ni on ferrihydrates and incorporation into sedimentary sulfides (Gueguen et al., 2013; Wasylenki et al., 2015; Vance et al., 2016). The present study considered the possibility that Ni adsorption onto calcite surfaces may also contribute to resolving this imbalance in the global marine Ni budget. This study shows that light Ni is preferentially adsorbed onto calcite at $\Delta^{60}Ni_{calcite\text{-}solution}$= -0.49 ± 0.16‰. Although the mass of Ni removed from the ocean by adsorption onto calcite may be too small to completely resolve the

currently perceived Ni isotope imbalance, considering the large mass of calcite formed annually, it may be a significant contributor to resolving this imbalance.

5. CONCLUSIONS

Experiments in the present study were performed to determine the degree of Ni isotope fractionation imparted by the adsorption of Ni from an aqueous solution onto calcite surfaces. The major results include:

1) No variation of the isotope composition of Ni adsorbed onto calcite was observed with time.

2) Calcite surfaces preferentially adsorb isotopic light Ni with an average fractionation factor, $\Delta^{60}Ni_{calcite\text{-}fluid}$ = -0.49 ± 0.16‰. The fractionation factor is independent of the amount of adsorbed nickel indicating an equilibrium isotope exchange process.

3) Ni does not change coordination number as it adsorbs to calcite surfaces from aqueous solution, however, the Ni-O interatomic distance is slightly longer for Ni incorporated in calcite as it is for $Ni(H_2O)_6^{2+}$. This change in coordination geometry is likely the mechanism driving the fractionation of Ni isotopes during their incorporation on calcite.

4) A preferred adsorption of light Ni isotopes onto calcite from seawater could help resolve, at least in part, the current perceived Ni isotope budget imbalance in the ocean.

ACKNOWLEDGEMENTS

The research was supported by ISONOSE a People Programme (Marie Curie Actions) of the European Unions' Seventh Framework Programme FP7/2017-2013/ under REA grant agreement n° [608069]. We thank Alain Castillo for BET measurements, Carole Causserand and Manuel Henry from the Géosciences Environement Toulouse for their assistance in the laboratories. We would also like to thank Martin Voigt, Giuseppe Saldi, and Pascale Benezeth for helpful discussions.

REFERENCES

Baeyens, B., Bradbury, M.H., Hummel, W., 2003. Determination of Aqueous Nickel – Carbonate and Nickel – Oxalate Complexation Constants. J. Solution Chem. 32, 319–339.

Balan, E., Noireaux, J., Mavromatis, V., Saldi, G.D., Montouillout, V., Blanchard, M., Pietrucci, F., Gervais, C., Rustad, J.R., Schott, J., Gaillardet, J., 2018. Theoretical isotopic fractionation between structural boron in carbonates and aqueous boric acid and borate ion. Geochim. Cosmochim. Acta 222, 117–129. https://doi.org/10.1016/J.GCA.2017.10.017

Belova, D. a, Lakshtanov, L.Z., Carneiro, J.F., Stipp, S.L.S., 2014. Nickel adsorption on chalk and calcite. J. Contam. Hydrol. 170, 1–9. https://doi.org/10.1016/j.jconhyd.2014.09.007

Brennecka, G.A., Wasylenki, L.E., Bargar, J.R., Weyer, S., Anbar, A.D., 2011. Uranium isotope fractionation during adsorption to Mn-oxyhydroxides. Environ. Sci. Technol. 45, 1370–1375. https://doi.org/10.1021/es103061v

Brunauer, S., Emmett, P.H., Teller, E., 1938. Adsorption of Gases in Multimolecular Layers. J. Am. Chem. Soc. 60, 309–319. https://doi.org/10.1021/ja01269a023

Cameron, V., Vance, D., 2014. Heavy nickel isotope compositions in rivers and the oceans. Geochim. Cosmochim. Acta 128, 195–211. https://doi.org/10.1016/j.gca.2013.12.007

Cameron, V., Vance, D., Archer, C., House, C.H., 2009. A biomarker based on the stable isotopes of nickel. Proc. Natl. Acad. Sci. 106, 10944–10948. https://doi.org/10.1073/pnas.0900726106

Caminiti, R., Licheri, G., Piccaluga, G., Pinna, G., 1977. X-ray diffraction and structure of NiCl2 aqueous solutions. Faraday Discuss. Chem. Soc. 64, 62. https://doi.org/10.1039/dc9776400062

Criss, R.E., 1999. Principles of stable isotope distribution. Oxford University Press.

Dong, S., Wasylenki, L.E., 2016. Zinc isotope fractionation during adsorption to calcite at high and low ionic strength. Chem. Geol. 447, 70–78. https://doi.org/10.1016/j.chemgeo.2016.10.031

Eiler, J.M., Bergquist, B., Bourg, I., Cartigny, P., Farquhar, J., Gagnon, A., Guo, W., Halevy, I., Hofmann, A., Larson, T.E., Levin, N., Schauble, E.A., Stolper, D., 2014. Frontiers of stable isotope geoscience. Chem. Geol. 372, 119–143. https://doi.org/10.1016/j.chemgeo.2014.02.006

Elzinga, E.J., Reeder, R.J., 2002. X-ray absorption spectroscopy study of Cu2+and Zn2+adsorption complexes at the calcite surface: Implications for site-specific metal incorporation

preferences during calcite crystal growth. Geochim. Cosmochim. Acta 66, 3943–3954. https://doi.org/10.1016/S0016-7037(02)00971-7

Estrade, N., Cloquet, C., Echevarria, G., Sterckeman, T., Deng, T., Tang, Y.T., Morel, J.L., 2015. Weathering and vegetation controls on nickel isotope fractionation in surface ultramafic environments (Albania). Earth Planet. Sci. Lett. 423, 24–35. https://doi.org/10.1016/j.epsl.2015.04.018

Fujii, T., Moynier, F., Blichert-Toft, J., Albarède, F., 2014. Density functional theory estimation of isotope fractionation of Fe, Ni, Cu, and Zn among species relevant to geochemical and biological environments. Geochim. Cosmochim. Acta 140, 553–576. https://doi.org/10.1016/j.gca.2014.05.051

Fujii, T., Moynier, F., Dauphas, N., Abe, M., 2011. Theoretical and experimental investigation of nickel isotopic fractionation in species relevant to modern and ancient oceans. Geochim. Cosmochim. Acta 75, 469–482. https://doi.org/10.1016/j.gca.2010.11.003

Gall, L., Williams, H.M., Siebert, C., Halliday, A.N., Herrington, R.J., Hein, J.R., 2013. Nickel isotopic compositions of ferromanganese crusts and the constancy of deep ocean inputs and continental weathering effects over the Cenozoic. Earth Planet. Sci. Lett. 375, 148–155. https://doi.org/10.1016/j.epsl.2013.05.019

Gueguen, B., Rouxel, O., Ponzevera, E., Bekker, A., Fouquet, Y., 2013. Nickel Isotope Variations in Terrestrial Silicate Rocks and Geological Reference Materials Measured by MC-ICP-MS. Geostand. Geoanalytical Res. 37, 297–317. https://doi.org/10.1111/j.1751-908X.2013.00209.x

Gueguen, B., Sorensen, J. V., Lalonde, S. V., Peña, J., Toner, B.M., Rouxel, O., 2018. Variable Ni isotope fractionation between Fe-oxyhydroxides and implications for the use of Ni isotopes as geochemical tracers. Chem. Geol. 481, 38–52. https://doi.org/10.1016/j.chemgeo.2018.01.023

Hoffmann, U., Stipp, S.L.S., 2001. The behavior of Ni 2 on calcite surfaces. Geochim. Cosmochim. Acta 65, 4131–4139. https://doi.org/10.1016/S0016-7037(01)00691-3

Jeandel, C., Oelkers, E.H., 2015. The influence of terrigenous particulate material dissolution on ocean chemistry and global element cycles. Chem. Geol. 395, 50–66. https://doi.org/10.1016/j.chemgeo.2014.12.001

Juillot, F., Maréchal, C., Ponthieu, M., Cacaly, S., Morin, G., Benedetti, M., Hazemann, J.L., Proux, O., Guyot, F., 2008. Zn isotopic fractionation caused by sorption on goethite and 2-Lines ferrihydrite. Geochim. Cosmochim. Acta 72, 4886–4900. https://doi.org/10.1016/j.gca.2008.07.007

Lafuente, B., Downs, R.T., Yang, H., Stone, N., 2016. The power of databases: The RRUFF project, in: Highlights in Mineralogical Crystallography. pp. 1–29. https://doi.org/10.1515/9783110417104-003

Lakshtanov, L.Z., Stipp, S.L.S., 2007. Experimental study of nickel(II) interaction with calcite: Adsorption and coprecipitation. Geochim. Cosmochim. Acta 71, 3686–3697. https://doi.org/10.1016/j.gca.2007.04.006

Magini, M., Paschina, G., Piccaluga, G., 1982. Ni–Cl bonding in concentrated Ni(II) aqueous solutions at high Cl − /Ni 2+ ratios. An x-ray diffraction investigation. J. Chem. Phys. 76, 1116–1121. https://doi.org/10.1063/1.443079

McBride, M.B., 1980. Chemisorption of Cd2+ on Calcite Surfaces1. Soil Sci. Soc. Am. J. 44, 26. https://doi.org/10.2136/sssaj1980.03615995004400010006x

Parkhurst, D.L., Appelo, C.A.J., 1999. User's guide to PHREEQC - a computer program for speciation, batch reaction, one-dimentional transport, and inverse geochemical calcualtions, Water-Resources Investigations Report, Water-Resources Investigations Report. https://doi.org/10.3133/WRI994259

Peacock, C.L., Sherman, D.M., 2007. Sorption of Ni by birnessite: Equilibrium controls on Ni in seawater. Chem. Geol. 238, 94–106. https://doi.org/10.1016/j.chemgeo.2006.10.019

Pertlik, F., 1986. Structures of hydrothermally synthesized cobalt(II) carbonate and nickel(II) carbonate. Acta Cryst. 42, 4–5.

Pokrovsky, O.S., Mielczarski, J.A., Barres, O., Schott, J., 2000. Surface Speciation Models of Calcite and Dolomite/Aqueous Solution Interfaces and Their Spectroscopic Evaluation. Langmuir 16, 2677–2688. https://doi.org/10.1021/la980905e

Pokrovsky, O.S., Schott, J., Ponts, T., 2002. Surface complexation modelling of the dissolution kinetics of Mg- bearing carbonate minerals. Pokrov. OS, Mielczarski JA, Barres O, Schott J Surf. Speciat. Model. Calcite Dolomite/Aqueous Solut. Interfaces Their Spectrosc. Eval. Langmuir 162677–2688. doi 10.1021/la980905e 1198–1199.

Pokrovsky, O.S., Schott, J., Thomas, F., 1999. Dolomite surface speciation and reactivity in aquatic systems. Geochim. Cosmochim. Acta 63, 3133–3143. https://doi.org/10.1016/S0016-7037(99)00240-9

Porter, S.J., Selby, D., Cameron, V., 2014. Characterising the nickel isotopic composition of organic-rich marine sediments. Chem. Geol. 387, 12–21. https://doi.org/10.1016/j.chemgeo.2014.07.017

Quitté, G., Oberli, F., 2006. Quantitative extraction and high precision isotope measurements of nickel by MC-ICPMS. J. Anal. At. Spectrom. 21, 1249–1255. https://doi.org/10.1039/b607569j

Reddy, M.M., Nancollas, G.H., 1971. The crystallization of calcium carbonate: I. Isotopic exchange and kinetics. J. Colloid Interface Sci. 36, 166–172. https://doi.org/10.1016/0021-9797(71)90161-5

Sandstrom, D.R., 1979. Ni 2+ coordination in aqueous NiCl 2 solutions: Study of the extended x-ray absorption fine structure. J. Chem. Phys. 71, 2381–2386. https://doi.org/10.1063/1.438643

Schott, J., Mavromatis, V., Fujii, T., Pearce, C.R., Oelkers, E.H., 2016. The control of carbonate mineral Mg isotope composition by aqueous speciation: Theoretical and experimental modeling. Chem. Geol. https://doi.org/10.1016/j.chemgeo.2016.03.011

Sclater, F.R., Boyle, E., Edmond, J.M., 1976. On the marine geochemistry of nickel. Earth Planet. Sci. Lett. 31, 119–128. https://doi.org/10.1016/0012-821X(76)90103-5

Sohrin, Y., Bruland, K.W., 2011. Global status of trace elements in the ocean. TrAC Trends Anal. Chem. 30, 1291–1307. https://doi.org/10.1016/J.TRAC.2011.03.006

Spivak-Birndorf, L.J., Wang, S.J., Bish, D.L., Wasylenki, L.E., 2018. Nickel isotope fractionation during continental weathering. Chem. Geol. 476, 316–326. https://doi.org/10.1016/j.chemgeo.2017.11.028

Stipp, S.L.S., Eggleston, C.M., Nielsen, B.S., 1994. Calcite surface structure observed at microtopographic and molecular scales with atomic force microscopy (AFM). Geochim. Cosmochim. Acta 58, 3023–3033. https://doi.org/10.1016/0016-7037(94)90176-7

Tahervand, S., Jalali, M., 2017. Sorption and desorption of potentially toxic metals (Cd, Cu, Ni and Zn) by soil amended with bentonite, calcite and zeolite as a function of pH. J. Geochemical Explor. https://doi.org/10.1016/j.gexplo.2017.07.005

Van Cappellen, P., Charlet, L., Stumm, W., Wersin, P., 1993. A surface complexation model of the carbonate mineral-aqueous solution interface. Geochim. Cosmochim. Acta 57, 3505–3518. https://doi.org/10.1016/0016-7037(93)90135-J

Vance, D., Little, S.H., Archer, C., Cameron, V., Andersen, M.B., Rijkenberg, M.J.A., Lyons, T.W., 2016. The oceanic budgets of nickel and zinc isotopes: The importance of sulfdic environments as illustrated by the Black Sea. Phil.Trans.R.Soc.A 374. https://doi.org/10.1098/rsta.2015.0294

Mavromatis,V., Gonzalez, A.G., Dietzel, M., Schott, J., 2018. Zinc isotope fractionation during the inorganic precipitation of calcite – Towards a new pH proxy. Geochim. Cosmochim. Acta.

Wasylenki, L.E., Howe, H.D., Spivak-Birndorf, L.J., Bish, D.L., 2015. Ni isotope fractionation during sorption to ferrihydrite: Implications for Ni in banded iron formations. Chem. Geol. 400, 56–64. https://doi.org/10.1016/j.chemgeo.2015.02.007

Wasylenki, L.E., Swihart, J.W., Romaniello, S.J., 2014. Cadmium isotope fractionation during adsorption to Mn oxyhydroxide at low and high ionic strength. Geochim. Cosmochim. Acta 140, 212–226. https://doi.org/10.1016/J.GCA.2014.05.007

Yuan, W., Saldi, G.D., Chen, J., Vetuschi Zuccolini, M., Birck, J.-L., Liu, Y., Schott, J., 2018. Gallium isotope fractionation during Ga adsorption on calcite and goethite. Geochim. Cosmochim. Acta 223, 350–363. https://doi.org/10.1016/J.GCA.2017.12.008

Zachara, J.M., Cowan, C.E., Resch, C.T., 1991. Sorption of divalent metals on calcite. Geochim. Cosmochim. Acta 55, 1549–1562. https://doi.org/10.1016/0016-7037(91)90127-Q

Zachara, J.M., Kittrick, J.A., Harsh, J.B., 1988. The mechanism of Zn2+ adsorption on calcite. Geochim. Cosmochim. Acta 52, 2281–2291. https://doi.org/10.1016/0016-7037(88)90130-5